REMARKS

Claims 40, 43, 44, 48, 50, 51, and 56-64 were acted upon in the aforesaid Office Action. Claims 50, 51, 57 and 58 have been canceled, leaving claims 40, 43, 44, 48, 56 and 59-64 for further consideration.

Claims 40, 43, 44, 48, 56 and 59-64 stand rejected as failing to comply with written description requirements. More specifically, Claim 40 was deemed lacking in a sufficient number of representative species to demonstrate that the patentee possessed the full scope of the claimed innovation.

Claims 40 and 48 have been amended to include specifics, such as scaffold structure porosity (as stated in the specification as filed, page 41, lines 2 and 3), a specific lay-down pattern (as stated in the specification as filed, page 40, line 9), pore morphology (as stated in the specification as filed, page 40, lines 14 and 15), and the extrusion filament material formation specifics (as stated in the specification as filed, page 34, lines 14-16).

The remaining claims depend from either Claim 40 or Claim 48.

The Examiner has held that claims 40, 43, 44, 48, 56, and 59 to 64 are unpatentable over Richter et al. (US 6,280,478) (hereafter referred to as the '478 patent), Cima et al. (US 5,518,680) (hereafter referred to as the '680 patent) and Jang (US 6,129,872) (hereafter referred to as the '872 patent), as evidenced by Kuslich (US 5,549,679) (hereafter referred to as the '679 patent).

The Examiner has acknowledged at page 6, paragraph (c) of the aforesaid Office Action that there is no disclosure or suggestion in the '478 patent of the specific lay down patterns recited in claims 40 and 48 of the present application. Further, contrary to the Examiner's opinion that the '680 patent and the '872 patent suggest that the lay down patterns of scaffold structures can be modified based on the patient's needs and that a person of ordinary skill in the art would be motivated to have a scaffold having lay-down patterns forming triangular pores or five-sided polygonal pores, the inventor submits that although the '680 patent discloses that it is possible to produce devices for tissue regeneration having a specifically tailored microstructure of interconnected pores and channels (column 13, lines 6 to 10 of the '680 patent), there is no suggestion in the '680 patent which would lead and/or motivate a person of ordinary skill in the art to prepare a structure specifically having lay-down patterns forming triangular pores or five-sided polygonal pores, or having an orientation of layers of 0°/60°/120° or 0°/72°/144°/36°/108°, as set forth in claims 40 and 48. In particular, it is submitted that the suitability of the morphology and size of the pore for tissue regeneration is dependent on several factors such as (i) shape of pore; (ii) size of pore; (iii) depth of pore; and (iv) repeatable patterns of the pore. The permutations of such factors are infinite and hence create a huge amount of possibilities. Although it is disclosed in the '680 patent that it is possible to produce devices for tissue regeneration having a specifically tailored microstructure of interconnected pores

and channels, the final decision can only be made through careful consideration of the following factors: (i) the mechanical properties required for the final structure; (ii) the surface morphology of the individual struts; (iii) shapes and sizes of cells intended to be regenerated; (iv) resorption kinectics; (v) waste products and energy transfer, etc. Accordingly, it would be evident to a person of ordinary skill in the art that any decision to select or arrive at a suitable apparatus without experimental evidence or, at the very least, any simulation modelling would be on a basis of chance rather than an informed decision. It would therefore not be obvious to a person of ordinary skill in the art given the general teaching in the '680 patent and the '872 patent to arrive at the apparatus as recited in claims 40 and 48 of the present application.

Further, and as explained above, the '680 patent only teaches a person of ordinary skill in the art devices having a general shape. In contrast, the present application discloses an apparatus comprising a scaffold structure having a specific microarchitecture, as in claims 40 and 48 of the present application.

The '872 patent at column 16, lines 44 to 50 only describes how the CAD model simulates a structure. This does not actually teach a structure having lay-down patterns forming triangular pores or five-sided polygonal pores. In particular, the inventor of the present application submits that the CAD model employs the use of unstructured triangulated surfaces (facets) represented by the unit normal and vertices using a 3D-Cartesian

system. This data is represented in the STL format native to most CAD software. The triangle facets describe the normal of the plane surface of the shape it is representing through a coordinate system (as seen in Figure 1a). The eventual 3D shape is made up of these triangles that are joined together defining the surface topology of the 3D shape (Figure 1b). Computer Aided Manufacturing (CAM) or Solid Freeform Fabrication (SFF), such as that described in the '872 patent, requires this necessary triangulated geometry to be imported as a STL file output. The eventual 3D structure is built up in layers which are known as slices from the file output (see Figure 2). From the STL file format, the slicing soft gathers information on how to build up the slice. This is described in the '872 patent at column 1, lines 37-40 in the stereolithography method. The building up of the volume shape through the slices from the CAD program does not specify or teach the layering pattern in which case most programs would determine the "best pathway" for generation of the solid 3D form based on factors such as slice perimeter and material. The process of addition or subtraction of these layers to form the eventual structure is described but does not take into account the eventual lay down pattern. An analogy of this is represented by a solid block and a block filled with holes of different shapes (see Figure 3). The shape of both boxes is determined by the STL format as represented by the triangle facets. The morphology is determined by the slicing software/cam files which decide "the best pathway" following the perimeters of the slices created by the addition of slices one layer at a time. These triangle facets do not describe the

surface morphology of the final fabricated part, but rather topology of the 3D shape only. They also do not teach a structure with the specific lay-down patterns forming triangular or five-sided polygonal pores. On the contrary, they are only data representation in the STL file format to describe the eventual 3D shape. In view of the above, even though the '872 patent teaches the STL file format describing a CAD model's surface topology as a single surface represented by triangular facets, it would not appear to be obvious to a person of ordinary skill in the art referring to the teachings of the '872 patent, to arrive at an apparatus having a lay-down pattern forming triangular pores.

The Applicants also submit that a structure having lay-down patterns forming triangular pores or five-sided polygonal pores, as described in claims 40 an 48, or having an orientation of layers of 0°/60°/120° or 0°/72°/144°/36°/108°, as described in claims 40 and 48, would be more suitable for tissue engineering applications, as such structures allow the flow transport of nutrients and wastes, and have the capacity to deliver a high volume of cells. This is disclosed at page 41, lines 6 to 16 of the application as originally filed. Further, cells are able to recognise the surroundings and therefore encourage the development of a vascular network which is able to regulate the transport of nutrients and waste in the structure. This is disclosed at page 46, lines 10 to 20 of the application as originally filed. In fact, an apparatus comprising a scaffold structure having such orientations as recited in claims 40 and 48 of the present application are advantageous since such

orientations have shown to allow bone cells to attach and proliferate. An example of a cell attached in the pore of a structure having a pattern of 0°/60°/120° is shown in **Exhibit 1**.

Further, the inventors have also conducted further studies on the properties and response of the apparatus of claims 40 and 48 of the present application. Some of these results have been published in well-respected journals in the field of tissue engineering. Summaries of some of the articles are provided below:

a) Mechanical properties and cell cultural response of polycaprolactone scaffolds designed and fabricated via fused deposition modeling - J Biomed Mat Res, 2001, 55(2):203-216.

The results of this study show that human fibroblasts colonize on the struts and bars of FDM-fabricated PCL scaffolds having a lay-down pattern forming triangular and five-sided polygonal pores, respectively, and form a cell-to-cell and cell-to-extracellular-matrix interconnective network throughout the entire 3D honeycomb-like architecture. Qualitative data of a human osteoblast-like cell culture demonstrate the good biocompatibility of PCL for hard-tissue formation. The proliferation of human osteoblasts cells and vascularisation showed that the PCL scaffold is non-cytotoxic. The formation of actin-supported sheetlike protrusions known as lamellipodia up to a period

of 3 weeks throughout the entire PCL 3D scaffold architecture further demonstrated its biocompatibility.

b) Scaffold Design and *in Vitro* Study of Ostepchondral Co-culture in a Three-Dimensional Porous Polycaprolactone Scaffold Fabricated by Fused Deposition Modeling - Tissue Engineering, 2003, 9 (Supplement 1):S103-S112.

Scaffolds having a lay-down pattern forming triangular pores and having an orientation of layers of 0°/60°/120° were used. Two cell types were used in this study - marrow stromal cells and chondrocytes. Both cell types proliferated, migrated, linked in their scaffold compartments, and integrated at the interface. Osteoblasts and chondrocytes produced different extracellular matrices in each scaffold compartment. Mineralized nodules deposited in the osteogenic cell seeded compartment. High osteocalcin was detected in precultured osteogenic cell supernatant and high alkaline phosphatase was detected in the coculture supernatant of osteochondral constructs. The remarkable cubic distribution of the osteoblasts and chondrocytes as well as the rich formation of extracellular matrices of both cell types were attributed to the large surface area and the three-dimensional spatial architecture provided by the interconnected porous structure of the 3D PCL scaffold design. This study has demonstrated the biocompatibility as evidenced by extensive cell proliferation in the PCL scaffold.

c) Fused deposition modeling of novel scaffold architectures for tissue engineering applications - Biomaterials, 2002, 23:1169-1185.

A PCL scaffold having a lay-down pattern forming triangular pores and having an orientation of layers of 0°/60°/120° and another scaffold having a lay-down pattern forming square pores and having an orientation of layers of 0°/90° were used. These scaffolds showed fully interconnected channel networks, and highly controllable porosity and channel size. Examination of the mechanical deformation indicated that the porous PCL scaffolds demonstrated stress-strain behavior highly similar to that of a typical porous material undergoing compression. The efficacy of the FDM technique for scaffold design and fabrication had been proven in this research.

d) Induction of Ectopic Bone Formation by Using Human Periosteal Cells in Combination With a Novel Scaffold Technology - Cell Transplantation, 2002, vol 11(2):125-138.

PCL scaffolds having lay-down patterns forming triangular pores or five-sided polygonal pores, and having an orientation of layers of 0°/60°/120° or 0°/72°/144°/36°/108° were used in this study. Immunohistochemical analysis confirmed the osteoblastic phenotype of the seeded cells. Formation of focal adhesions and stress fibers could be

observed in both scaffold architectures. Three-dimensional cell proliferation was observed after 2 weeks of culturing with centripetal growth pattern inside the pore network. The deposition of calcified extracellular matrix was observed after 3 weeks of culturing. In vivo, endochondral bone formation with osteoid production was detectable via von Kossa and Osteocalcin staining after 6 and 17 weeks. Histology and SEM revealed that the entire scaffold/bone grafts were penetrated by a vascular network. This study showed the potential of bone tissue engineering by using human periosteal cells in combination with the PCL scaffolds.

Each of the above articles is enclosed as **Exhibits 2, 3, 4** and **5**, respectively.

The Applicants would also like to bring to the Examiner's attention an article (*In Vivo* Mesenchymal Cell Recruitment by a Scaffold Loaded with Transforming Growth Factor β1 and the Potential for *in Situ* Chondrogenesis - Tissue Engineering, 2002, vol 8(3):469-482) which was authored by an Applicant of the present application, and which appeared in the journal entitled "Tissue Engineering". A copy of the journal article is enclosed as **Exhibit 6**. The scaffold used in the study was a PCL scaffold having lay-down patterns forming triangular pores and having an orientation of layers of 0°/60°/120°, such as that recited in claim 40 of the present application. The cover of the issue of Tissue Engineering in which the article appeared was a scanning

electron micrograph of freeze-fractured surfaces of a PCL scaffold showing completely interconnected triangular pores. The cover is enclosed as **Exhibit 7** and a copy of the table of contents showing the cover illustration credit is enclosed as **Exhibit 8**. This further exhibits that the apparatus of claim 40 has been regarded as commercially successful in the field. If the Examiner's opinion that the apparatus of claims 40 and 48 is obvious to a person of ordinary skill in the art is indeed true, the apparatus of claim 40 would not have achieved such commercial success and recognition in the field. Accordingly, the Applicants submit that the apparatus of claims 40 and 48, and their dependent claims, are indeed patentable and not obvious to a person of ordinary skill in the art.

In view of the amendments entered herein and the comments set forth above, it is believed that claims 40, 43, 44, 48, 56 and 59-64 are in condition for allowance, which is most respectfully requested.

In the event that any fees may be required in this matter, please charge the same to Deposit Account No. 16-0221.

Respectfully submitted,

Scott R. Foster
Registration No. 20,570
Pandiscio & Pandiscio, P.C.
470 Totten Pond Road
Waltham, MA 02451-1914
Tel. (781) 290-0060

KC/NUS8DIVI.AMD3

EXHIBIT 1

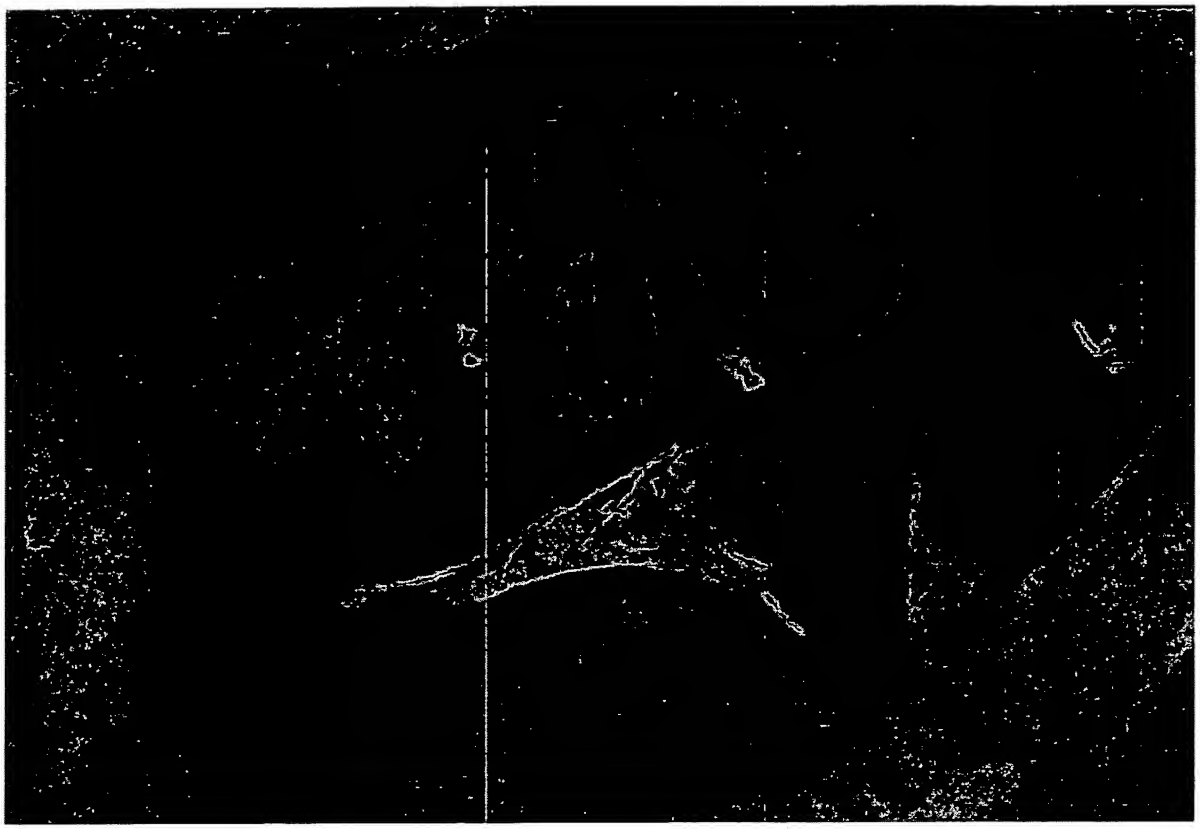

EXHIBIT 2

Mechanical properties and cell cultural response of polycaprolactone scaffolds designed and fabricated via fused deposition modeling

Dietmar W. Hutmacher,[1,2] Thorsten Schantz,[1] Iwan Zein,[3] Kee Woei Ng,[1] Swee Hin Teoh,[1] Kim Cheng Tan[4]
[1]*Laboratory for Biomedical Engineering, National University of Singapore, 10 Kent Ridge Crescent, Singapore 119260*
[2]*Department of Orthopedic Surgery, National University of Singapore, 10 Kent Ridge Crescent, Singapore 119260*
[3]*Centre for Biomedical Materials Applications and Technology, National University of Singapore, 10 Kent Ridge Crescent, Singapore 119260*
[4]*Temasek Engineering School, Temasek Polytechnic, 21 Tampines Avenue 1, Singapore 529757*

Received 24 July 2000; revised 2 November 2000; accepted 2 November 2000

Abstract: A number of different processing techniques have been developed to design and fabricate three-dimensional (3D) scaffolds for tissue-engineering applications. The imperfection of the current techniques has encouraged the use of a rapid prototyping technology known as *fused deposition modeling* (FDM). Our results show that FDM allows the design and fabrication of highly reproducible bioresorbable 3D scaffolds with a fully interconnected pore network. The mechanical properties and *in vitro* biocompatibility of polycaprolactone scaffolds with a porosity of 61 ± 1% and two matrix architectures were studied. The honeycomb-like pores had a size falling within the range of 360 × 430 × 620 μm. The scaffolds with a 0/60/120° lay-down pattern had a compressive stiffness and a 1% offset yield strength in air of 41.9 ± 3.5 and 3.1 ± 0.1 MPa, respectively, and a compressive stiffness and a 1% offset yield strength in simulated physiological conditions (a saline solution at 37 °C) of 29.4 ± 4.0 and 2.3 ± 0.2 MPa, respectively. In comparison, the scaffolds with a 0/72/144/36/108° lay-down pattern had a compressive stiffness and a 1% offset yield strength in air of 20.2 ± 1.7 and 2.4 ± 0.1 MPa, respectively, and a compressive stiffness and a 1% offset yield strength in simulated physiological conditions (a saline solution at 37 °C) of 21.5 ± 2.9 and 2.0 ± 0.2 MPa, respectively. Statistical analysis confirmed that the five-angle scaffolds had significantly lower stiffness and 1% offset yield strengths under compression loading than those with a three-angle pattern under both testing conditions ($p \leq 0.05$). The obtained stress–strain curves for both scaffold architectures demonstrate the typical behavior of a honeycomb structure undergoing deformation. *In vitro* studies were conducted with primary human fibroblasts and periosteal cells. Light, environmental scanning electron, and confocal laser microscopy as well as immunohistochemistry showed cell proliferation and extracellular matrix production on the polycaprolactone surface in the 1st culturing week. Over a period of 3–4 weeks in a culture, the fully interconnected scaffold architecture was completely 3D-filled by cellular tissue. Our cell culture study shows that fibroblasts and osteoblast-like cells can proliferate, differentiate, and produce a cellular tissue in an entirely interconnected 3D polycaprolactone matrix. J Biomed Mater Res 55: 203–216, 2001

Key words: tissue engineering; design and fabrication of three-dimensional scaffolds; polycaprolactone

INTRODUCTION

Tissue-engineering techniques generally require the use of a porous, bioresorbable scaffold, which serves as a three-dimensional (3D) template for initial cell attachment and subsequent tissue formation, both *in vitro* and *in vivo*. The ability of the scaffold to be metabolized by the body allows it to be gradually replaced by new cells to form functional tissues. Ideally, a scaffold should have the following characteristics:

Correspondence to: D. W. Hutmacher; e-mail: mpedwh@nus.edu.sq

(1) be highly porous with an interconnected pore network for cell growth and flow transport of nutrients and metabolic waste;
(2) be biocompatible and bioresorbable with controllable degradation and resorption rates to match tissue replacement;
(3) have suitable surface chemistry for cell attachment, proliferation, and differentiation; and
(4) have mechanical properties to match those of the tissues at the site of implantation.[1]

Many different processing techniques have been developed to design and fabricate 3D scaffolds for tissue-engineered implants.[2] These conventional techniques include fiber bonding, solvent casting, particulate

leaching, membrane lamination, melt molding, temperature-induced phase separation (TIPS), gas foaming, and three-dimensional printing (3DP). A wide range of scaffold characteristics, such as porosity and pore size, have been reported with such fabrication techniques. However, no single technique with a computer-controlled process has allowed researchers to design and fabricate scaffolds with a completely interconnected pore network, a highly regular and reproducible scaffold morphology, and a microstructure that varies across the scaffold matrix and is solvent-free.[3] These are essential scaffold features to facilitate cell proliferation and differentiation, extracellular matrix synthesis, and flow transport of nutrients and wastes. *In vivo*, the scaffold structure should protect the inside of the pore network proliferating cells and their extracellular matrix from being mechanically overloaded for a sufficient period of time.[3] This is especially critical for load-bearing tissues such as bone and cartilage.

The imperfection of the current techniques has encouraged our research group to apply a rapid prototyping (RP) technology known as *fused deposition modeling* (FDM), which offers the potential to design and fabricate highly reproducible, bioresorbable 3D scaffolds with a fully interconnected pore network. The FDM method is an RP technique that builds a physical model by depositing layers of thermoplastic material one at a time.[4] Figure 1 shows a schematic representation of the FDM process. The FDM method involves the melt extrusion of filament materials through a heated nozzle and deposition as thin solid layers on a platform (Fig. 1). The nozzle is positioned on the surface of a build platform at the start of fabrication. It is part of the extruder head (FDM head), which also encloses a liquefier to melt the filament material fed through two counter-rotating rollers. Figure 2 shows how each layer is made of raster roads deposited in the x and y directions. A fill gap can be programmed between the roads to provide horizontal channels. Subsequent layers are deposited with the x–y direction of deposition, the raster angle, programmed to provide different lay-down patterns. Usually, FDM is used to fabricate solid models. For the purpose of fabricating porous structures, a positive value is applied to the raster fill gap to impart a channel within a build layer. Arranged in a regular manner, the channels are

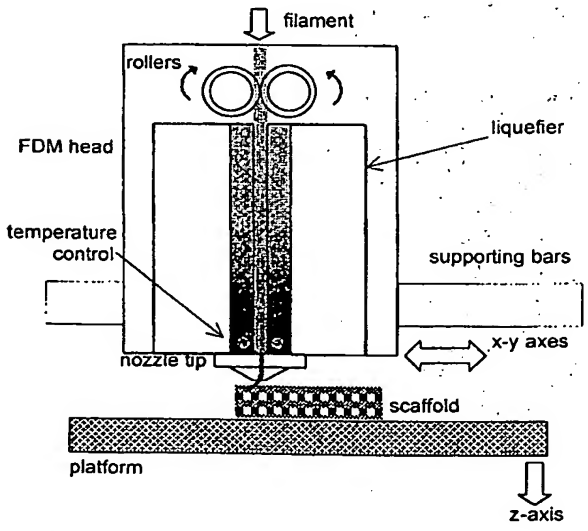

Figure 1. Schematic diagram of the FDM process.

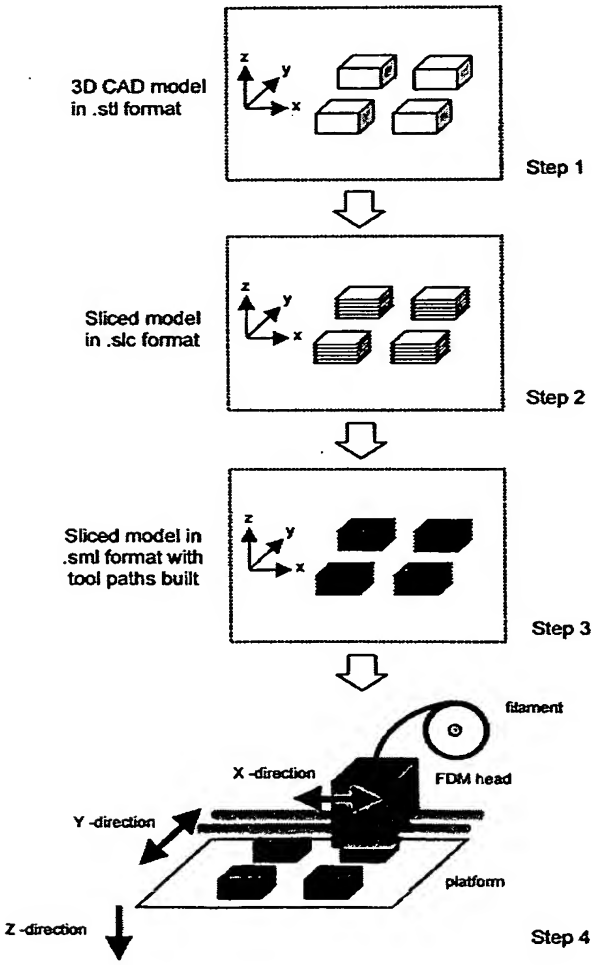

Figure 2. Sequence of the data preparation for FDM model fabrication. Step 1: Importing of computer-aided design (CAD) data in STL (stereolithography) format into QS. Step 2: Slicing of the CAD model into horizontal layers and conversion into SLC format. Step 3: Creation of a deposition path for each layer and conversion into SML format for downloading to the FDM machine. Step 4: FDM-fabrication process with a filament modeling material to build the actual physical part in an additive manner layer by layer.

interconnected even in three dimensions. The layer-by-layer fabrication allows the design of a pore morphology that varies across the scaffold structure.[5]

Polycaprolactone (PCL) is a semicrystalline, bioresorbable polymer belonging to the aliphatic polyester family. It was selected over other aliphatic polyesters for FDM because of its favorable properties for thermoplastic processing. It has a low glass-transition temperature of –60 °C, a melting point of 60 °C, and a high decomposition temperature of 350 °C with a wide range of temperatures that allow extrusion.[6] Extensive *in vitro* and *in vivo* biocompatibility and efficacy studies have been performed, resulting in U.S. Food and Drug Administration approval of a number of medical and drug delivery devices.[7–10] At present, PCL is regarded as a soft- and hard-tissue-compatible bioresorbable material.[6] This article describes how FDM was used to fabricate PCL scaffolds of various microarchitectures. It also details how these scaffolds were characterized, qualitatively and quantitatively, with light and scanning electron microscopy (SEM), mechanical testing, gas permeation chromatography, differential scanning calorimetry (DSC), and gel permeation chromatography (GPC). The efficacy of such PCL scaffolds from a biocompatibility point of view was studied in human fibroblast and osteoblast cell cultures.

MATERIALS AND METHODS

Filament fabrication

Pellets of PCL (catalog no. 44,074-4) from Aldrich Chemical Co., Inc. (Milwaukee, WI) were used for this study. This semicrystalline bioresorbable polymer has an average number-average molecular weight (M_n) of 80,000 (GPC) with a melt index of 1.0 g/10 min (ASTM D1238-73). It has a melting point of 60 °C (DSC). The polymer pellets were kept in a desiccator prior to usage. Filament fabrication was performed with a fiber-spinning machine (Alex James & Associates Inc., Greensville, SC). PCL pellets were melted at 190 °C in a cylinder with an external heating jacket. After a hold time of 15 min, the temperature was lowered to 140 °C, and the polymer melt was extruded through spinnerets with a die exit diameter of 0.064 in. (1.63 mm). Each batch of PCL pellets weighed 30 ± 1 g. The piston speed was set at 10 mm/min. The extrudate was quenched in chilled water placed 40 mm below the die exit. The combination of temperature, piston speed, and height drop to water quenching settings produced a filament diameter of 1.70 ± 0.10 mm. The PCL filaments were fabricated to have a consistent diameter to fit the drive wheels of the FDM system. The filaments were vacuum-dried and kept in a desiccator prior to usage.

Scaffold design and fabrication

Scaffold specimens were fabricated with PCL filaments with a FDM 3D Modeler RP system from Stratasys Inc. (Eden Prairie, MN). Blocks of 32.0 (length) × 25.5 (width) × 13.5 mm (height) with a 61% porosity were created directly in Stratasys QuickSlice (QS) software. The head speed, fill gap, and raster angle for every layer were programmed through the QS software and saved in the SLC (Slice) file format. Figure 3 shows the effect of these parameters on the geometry of the scaffold structures. Lay-down patterns of 0/60/120° and 0/72/144/36/108° were used to give a honeycomb-like pattern of triangular and polygonal pores, respectively.

The two-dimensional slice data were converted into the QS SML (Stratasys Machine Language) file format, which automatically generated the build paths based on the input parameters for each slice layer. The SML data were sent to the FDM machine to fabricate the scaffold specimens with a T16 tip. The liquefier temperature was set at 120 °C, and the envelope temperature remained at 25 ± 2 °C (ambient temperature) throughout the fabrication process. After manufacture, the four specimens of each configuration were cut with an ultrasharp blade into slightly smaller blocks with the dimensions 28.0 (length) × 21.0 (width) × 13.5 mm (height). One of these new blocks each was used to measure

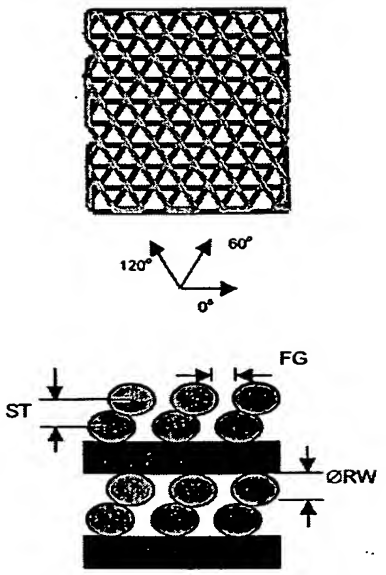

FDM Build Parameters	Scaffold Characteristics
Road width of rasters (RW)	Wall thickness
Fill gap between rasters (FG)	Vertical-channel width
Slice thickness (ST)	Horizontal-channel width
Raster angle	3D micro-architecture

Figure 3. Scaffold characteristics resulting from the setting of different FDM build parameters for a 0/60/120° lay-down pattern. *Road width* (RW) is defined as the diameter of the circular cross section of laid filament, *fill gap* (FG) is the edge-to-edge horizontal distance between adjacent filaments, *slice thickness* (ST) is the vertical distance between the filament center of adjacent layers, and *layer gap* (LG) is the edge-to-edge vertical distance between layers of the same filament alignment.

the porosity of the design, and then all four specimens were each divided into 12 small scaffold specimens (6.5 × 6.5 × 13.5 mm) for microscopic characterization and compression testing, as described in the following sections.

Porosity calculation

The ratio of the apparent volume to the true volume of the scaffolds was used to calculate the porosity of each design configuration. An ultrapycnometer (Quantachrome Ultrapycnometer 1000, Quantachrome Corp., Boynton Beach, FL) was used to measure the volume of the PCL scaffolds (6.5 × 6.5 × 13.5 mm) at 25 °C in pure argon; three measurements were made on each specimen, and the mean was used in the porosity calculations. For cellular solids with pore sizes bigger then 100 μm, ultrapycnometer porosimetry tends to underestimate the true porosity. Therefore, the porosity was also calculated by the following method: (1) measuring the weight and volume of each sample, (2) calculating from these measurements the apparent density of the PCL scaffolds $p^* = m\ (g)/V\ (cm^3)$, and (3) using the formula porosity $= \varepsilon = 1 - \rho^*/\rho \times 100\%$ ($\rho_{PCL} = 1145\ g/cm^3$).

Microscopic characterization

One each of the scaffold specimens measuring 6.5 × 6.5 × 13.5 mm was used to measure the pore size and morphology of the scaffold on SEM photographs. The specimens were freeze-fractured after being dipped in liquid nitrogen for 30 min. Fracture surfaces were then gold-sputtered with a JEOL fine coater JFC-1200 at 10 mA for 12 s. These were studied with a JEOL scanning electron microscope (JSM-5800LV) operating at 15 kV.

GPC

The polymer molecular weight distribution was determined by a gel permeation chromatograph equipped with a differential refractor (Waters, model 410, Milford, MA) and an absorbance detector refractor (Waters, model 2690). The samples were dissolved in tetrahydrofuran and eluted in a series of configurations through a Styragel column refractor (Waters) at a flow rate of 1 mL min^{-1}. Polystyrene standards (Polysciences, Warrington, PA) were used to obtain a calibration curve.

DSC

A thermal analysis differential scanning calorimeter (TA Instruments, DSC 2910, New Castle, DE) was used to analyze the thermal transition of the PCL samples during melting to measure the crystallinity fraction. PCL samples were extracted at stages of filament and scaffold fabrication and were represented by the raw PCL pellet, melt-extruded PCL filament. and the extruded roads from FDM. Samples of 7.0–7.7 mg were heated at a rate of 5 °C/min from 25 to 70 °C in aluminum pans with nitrogen as a purge gas. The crystallinity fractions were based on an enthalpy of fusion value of 139.5 J/g for 100% crystalline PCL, as reported.[5]

Mechanical testing

To determine the effect of the physiological environment on the compressive properties of PCL scaffolds, scaffolds were tested under the following two conditions: (1) in a phosphate-buffered saline (PBS) solution preconditioned in PBS for 1 day or (2) at ambient conditions. Six samples (6.5 × 6.5 × 13.5 mm) of each design configuration were tested on an Instron 4502 uniaxial testing system and a 1-kN load cell (Canton, MA) according to the guidelines set in the ASTM F451-99a standard specification for acrylic bone cement. This is the latest edition of the standard used by a number of groups recently.[11–14] The specimens were compressed at a rate of 1 mm/min up to a strain level of approximately 0.7 mm/mm. Young's modulus (MPa) was calculated from the stress–strain curve as the slope of the initial linear portion of the curve, with any toe region due to the initial settling of the specimen neglected. Compressive strength at yield was defined as the intersection of the stress–strain curve with the modulus slope at an offset of 1.0% strain. For the mechanical properties measured, a Student's t test was performed in comparing means from two independent sample groups. A significance level of 0.05 was used in all the statistical tests performed. MiniTab statistics software version 12.2 (MiniTab Inc., State College, PA) was used for statistical analysis.

Cell culture experiments

To investigate the efficacy of the PCL scaffolds for tissue-engineering applications, we studied two different mammalian cell types. One day prior to cell seeding, the 3D scaffolds were sterilized in 70% ethanol overnight. The ethanol was removed by centrifugation three times in changes of PBS for 15 min with 1000 rpm.

Fibroblast cultures and seeding

Human fibroblasts were harvested from the anterior cruciate ligament of a 34-year-old male patient The fibroblasts were isolated via enzyme digestion by incubation at 37 °C in 5% CO_2 for 12 h with a collagenase–trypsin solution (Sigma, St. Louis, MO). After the fourth passage, cultures were trypsinized, and cell viability was examined via trypan blue (Sigma) exclusion. The cell pellets obtained after centrifugation of the trypsinized cell suspensions were resuspended in 300 μL of DMEM, and 450,000 cells in 30 μL were carefully seeded onto 16 scaffolds with a micropipette. The seeded

scaffolds were left untouched for 2 h to allow for protein secretion and cell attachment. A culture medium (2 mL) was then added to each well so that the scaffolds would be fully submerged. The specimens were then placed for 4 weeks in a self-sterilizable incubator (WTB Binder, Tuttlingen, Germany) at 37 °C in 5% CO_2, 95% air, and 99% relative humidity.

Osteoprogenitor cell cultures and seeding

Primary human osteoprogenitor cells were isolated under sterile conditions by stripping periosteum from the skull of a patient, who underwent craniofacial surgery. Monolayer cell culture flasks were filled with 3 to 5 small pieces and Dulbecos Modified Eagle medium (Gibco, Grand Island NY, USA) with 10% fetal bovine serum, 1% penicillin, and 1% streptomycin and 1% amphoterecin. 50.0mgL ascorbic acid was added to promote the osteoblastic phenotype. Then the flasks were placed in a self-sterilizable incubator (WTB Binder, Tuttlingen, Germany) at 37 °C in 5% CO_2, 95% air, and 99% relative humidity. After the monolayer culture grew to confluence and exhibited nodule formation, the osteoblast-like cells were harvested with a 0.05% trypsinethylendiamine tetra-acetic acid (EDTA) solution, split, resuspended in the culture medium, and filled into new culture flasks. The culture medium was replaced every 3rd or 4th day. Alkaline phosphatase and osteocalcin staining verified the osteoblastic phenotype. After confluent monolayers were achieved by the fourth passage, the cells were enzymatically lifted from the flask with 0.25% trypsin/EDTA (Hyclone, Utah) and counted with a hemocytometer. The cell mortality was less than 5%, as shown by trypan blue staining, and maintained a stable cell metabolism. Cell pellets were resuspended, and aliquots of 15 μmL containing 50,000 cells were seeded onto the top of PCL scaffolds measuring 6 × 6 × 2 mm. Subsequently, the seeded scaffolds were placed into an incubator to allow the cells to build adhesion plaques on the polymer surface. After 2 h, 1 mL of complete medium was added into each well. Cell-scaffold constructs were then cultured for a period of 3 weeks.

Phase contrast light and environmental scanning electron microscopy (ESEM)

The establishment of the fibroblast and osteoblast-like phenotype, intercellular connections, and extracellular matrix production were examined daily by phase-contrast light microscopy for 3 and 4 weeks, respectively. The adhesion of the cells and their distribution were studied via ESEM. Specimens were fixed in 2.5% gluteraldehyde (Merck, Germany) for at least 4 h at 4 °C. They were then dehydrated in a graded ethanol series of 30, 50, 90, and 100% for 5 min at each grade, dried, and examined with a JEOL JSM-5800LV SEM at 15 kV.

Confocal laser microscopy (CLM) and immunohistochemistry

We prepared cell/scaffold constructs for CLM by staining viable cells green with the fluorescent dye fluorescein diacetate (FDA; Molecular Probes Inc., Oregon). The 3D cultures were incubated at 37 °C with 2 μg/mL FDA in PBS for 15 min. After being rinsed twice in PBS, each sample was then placed in a 1 mg/mL propidium iodide (PI) solution (Molecular Probes) for 2 min at room temperature to stain dead cells red. The samples were then rinsed twice in PBS and viewed under a confocal laser microscope (Olympus IX70-HLSH100 Fluoview). Depth projection images were constructed from up to 25 horizontal image sections through the cultures.

Samples were first fixed in 3.7% formaldehyde at room temperature for 30 min. After two 5-min rinsings with PBS, 200 μg/mL RNAse A was added and left for 30 min at room temperature. Phalloidin (A12379 Alexa Fluo 488 phalloidin, Molecular Probes) was then added at a 1/200 dilution for 45 min at room temperature and in darkness. Samples were subsequently counterstained with a 5 μg/mL PI solution, dried, and mounted for viewing under a fluorescence microscope.

RESULTS

Porosity calculation and microscopic characterization

Ultrapycnometer measurements revealed a porosity of 55 and 56% for PCL scaffolds with lay-down patterns of 0/60/120° (Fig. 4) and 0/72/144/36/108° (Fig. 5), respectively. In comparison, porosimetry calculation via the apparent density resulted in a 61% ± 1 for both scaffold architectures. The pore morphologies measured, based on SEM micrographs, fell within the ranges of 380 × 430 × 590 and 360 × 410 × 620 μm, respectively. The structures of the scaffolds designed and fabricated with the FDM method were highly similar to the honeycomb of the bee, with its regular array of identical pores, when viewed in the z direction of the fabrication process. The main difference lies in the morphology of the pores: the bee's honeycomb comprises hexagonal pores surrounded by solid faces/walls that nest together to fill a plane, but the FDM scaffold structure is built from intercrossing filaments stacked in horizontal planes and comprises pores surrounded by solid edges/struts. Even though the pores of the bee's honeycomb are usually hexagonal in section, they can also be triangles, squares, or other polygonal shapes in manmade honeycombs.[15] Conclusively, the mechanics of honeycombs lends great understanding to how the FDM scaffolds behave under loading forces.[16]

DSC and GPC

The crystallinity fraction of PCL was not observed to rise significantly when the polymer was processed

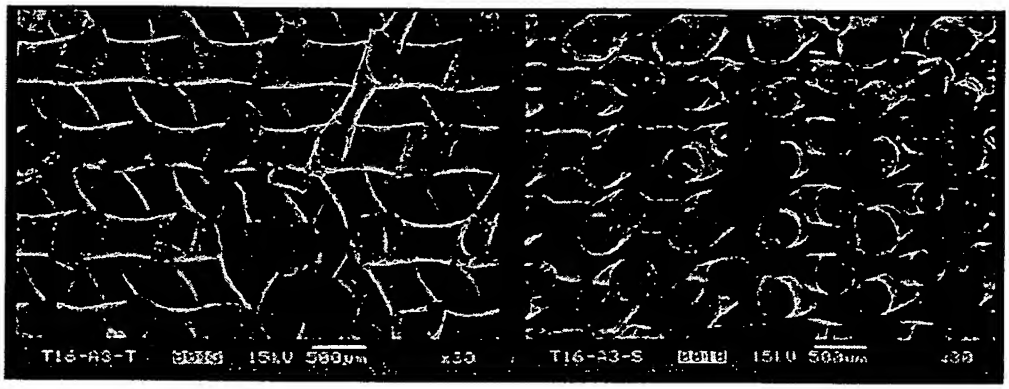

Figure 4. Freeze-fractured surfaces of a PCL scaffold with a 0/60/120° lay-down pattern and a porosity of 61% (side view and top view). The view of the PCL scaffold in the –z direction of the FDM build process shows a completely interconnected honeycomb pattern with triangular pores.

into filaments via the melt-extrusion process and subsequently through the FDM process. The values ranged between 56 and 58%. The shear forces on the polymer melt during the filament extrusion as well as FDM processes did not cause the percentage of crystallites to change significantly. Table I shows the results of DSC and GPC. PCL as a semicrystalline polymer shows a well-defined melting profile. All samples were completely melted above 60 °C. Potential degradation of PCL by the melt processing methods, filament extrusion and FDM, was characterized by the measurement of the molecular weight. The filament extrusion and FDM processing did not result in a significant change in the molecular weight.

Compression testing

Figure 6 shows the typical stress–strain curve for three-angle and five-angle scaffold specimens tested in air and a simulated physiological environment. These curves demonstrate the typical behavior of a honeycomb undergoing deformation. It comprises three distinct regions: a linear–elastic region followed by a plateau of roughly constant stress leading into a final region of steeply rising stress. Figure 7 shows the results obtained from compression testing of the scaffolds with lay-down patterns of 0/60/120° and 0/72/144/36/108°. Statistical analysis of the results was used to compare the stiffness and compressive 1% offset yield strength. A Student's *t* test for independent variables was used to check for differences between results obtained from the two different designs after normality, which is a prerequisite for using the *t* test, had been established with an Andersen–Darling test. The scaffolds with a 0/60/120° lay-down pattern had compressive stiffness and 1% offset yield strength in air of 41.9 ± 3.5 and 3.1 ± 0.1 MPa, respectively, and in simulated physiological conditions (a saline solution at 37 °C), the values were 29.4 ± 4.0 and 2.3 ± 0.2 MPa, respectively. In comparison, the scaffolds with a

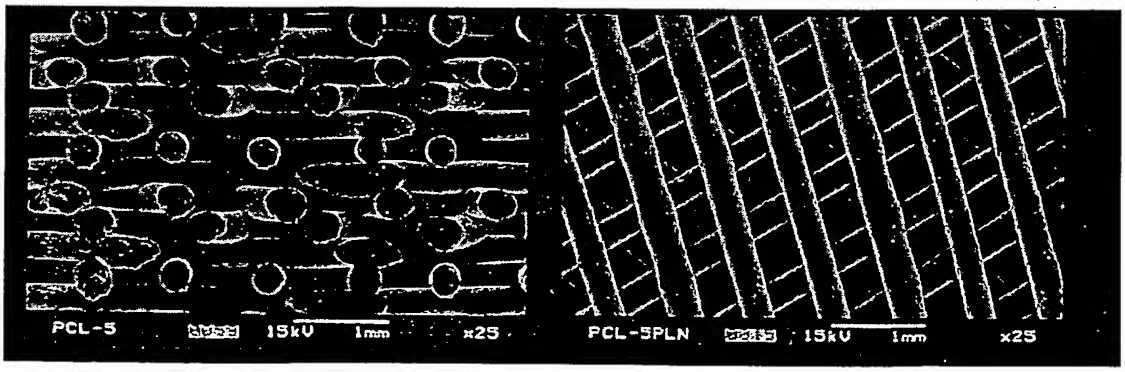

Figure 5. Freeze-fractured surfaces of PCL scaffolds with a 0/72/144/36/108° lay-down pattern and a porosity of 61 ± 1% (side view and top view). The view of the PCL scaffold in the –z direction of the FDM build process shows a completely interconnected honeycomb pattern with polygonal pores.

TABLE I
Molecular Weight Distribution and DSC Results for the Different PCL Specimens

PCL Sample	M_n	M_w	Polydispersity (M_w/M_n)	Crystallinity Fraction (%)
Raw pellet	78,542	139,923	1.781500	55.9
Raw filament	82,245	141,359	1.718753	58.0
PCL scaffold	87,343	146,739	1.680030	57.3

0/72/144/36/108° lay-down pattern had compressive stiffness and 1% offset yield strength in air of 20.2 ± 1.7 and 2.4 ± 0.1 MPa, respectively, and in simulated physiological conditions (a saline solution at 37 °C), the values were 21.5 ± 2.9 and 2.0 ± 0.2 MPa, respectively. Statistical analysis confirmed that the five-angle scaffolds had significantly lower stiffness and 1% offset yield strengths under compression loading than those with a three-angle pattern under both testing conditions ($p \leq 0.05$).

Fibroblast seeding and culture

The cells started attaching onto PCL scaffold surfaces 2 h after seeding. The cells that adhered to the PCL matrix initially were spherical in shape. After 2 to 3 days in the culture, the fibroblasts migrated and developed an interconnecting network of cells (Figs. 8 and 9). In the 1st culturing week, the cells used the rods and struts as templates for their proliferation, and a multilayered cell lawn could be detected in the SEM [Fig. 10(a)]. By day 8, fibroblasts were seen throughout the entire scaffold with a strong presence of extracellular matrix. On week 2, the fibroblast started to bridge the walls of the fully interconnected

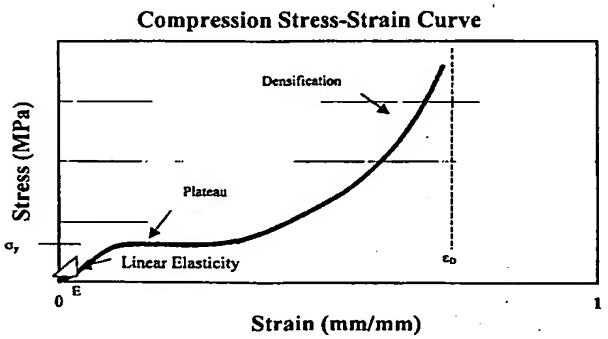

Figure 6. Typical stress–strain curves of FDM scaffolds under compression loading. The secant modulus of such specimens was measured as the gradient of the stress–strain curve at a strain level of 10%. The offset yield strength is defined at a 1% strain. As strain increases, the 3D pores of the scaffolds are crushed and undergo a densification process. When the rods and struts are crushed, the stress level rises quickly.

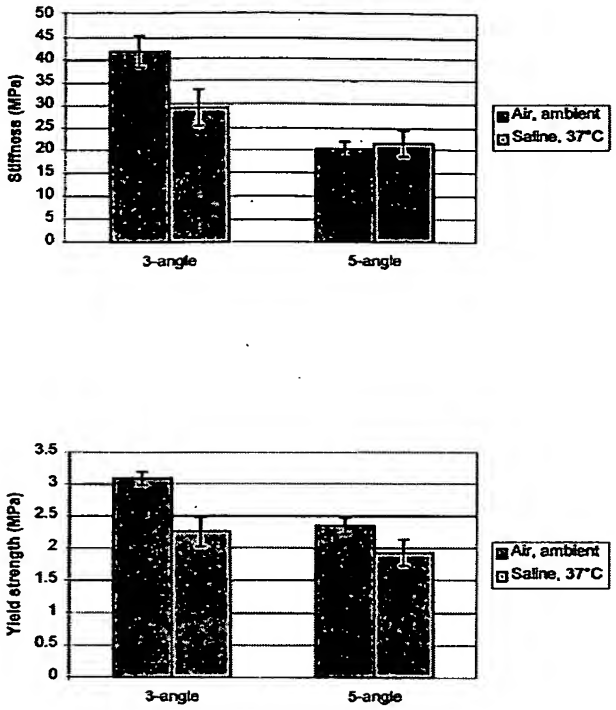

Figure 7. Compressive modulus, yield strength, and yield strain for PCL scaffolds in air and a simulated physiological environment

pore network via 3D extracellular matrix production [Fig. 10(b)]. From this point on, the cell-to-cell contact points and the extracellular matrix and culture media acted as a template. In general, the cells started the 3D growth process at the junctions of the bars and struts. By this phenomenon, the cells were able to three-dimensionally bridge distances up to 10 times the size of a cell. After the cells had grown over the entire surfaces of the rods and struts, they started filling up the pores in a circular manner. In week 4, the complete 3D scaffold architecture was taken up by cell/tissue formation (Figs. 8 and 9).

Seeding and culture of osteoblast-like cells

Osteoblast-like cells started attaching 2 h after seeding. Cells actively colonized the surface of the PCL matrix after only 4 days in the culture (Figs. 11 and 12). Osteoblast-like cells showed a 3D phenotype and established their tentacle-like enlargements of the plasma membrane known as filipodia. In the first 3 to 5 days, cells were arranged in a swirling pattern, and individual cells had a long, thin, spindle-shaped morphology. Microscopically, it was observed that the cells had attached and spread on the PCL bars and

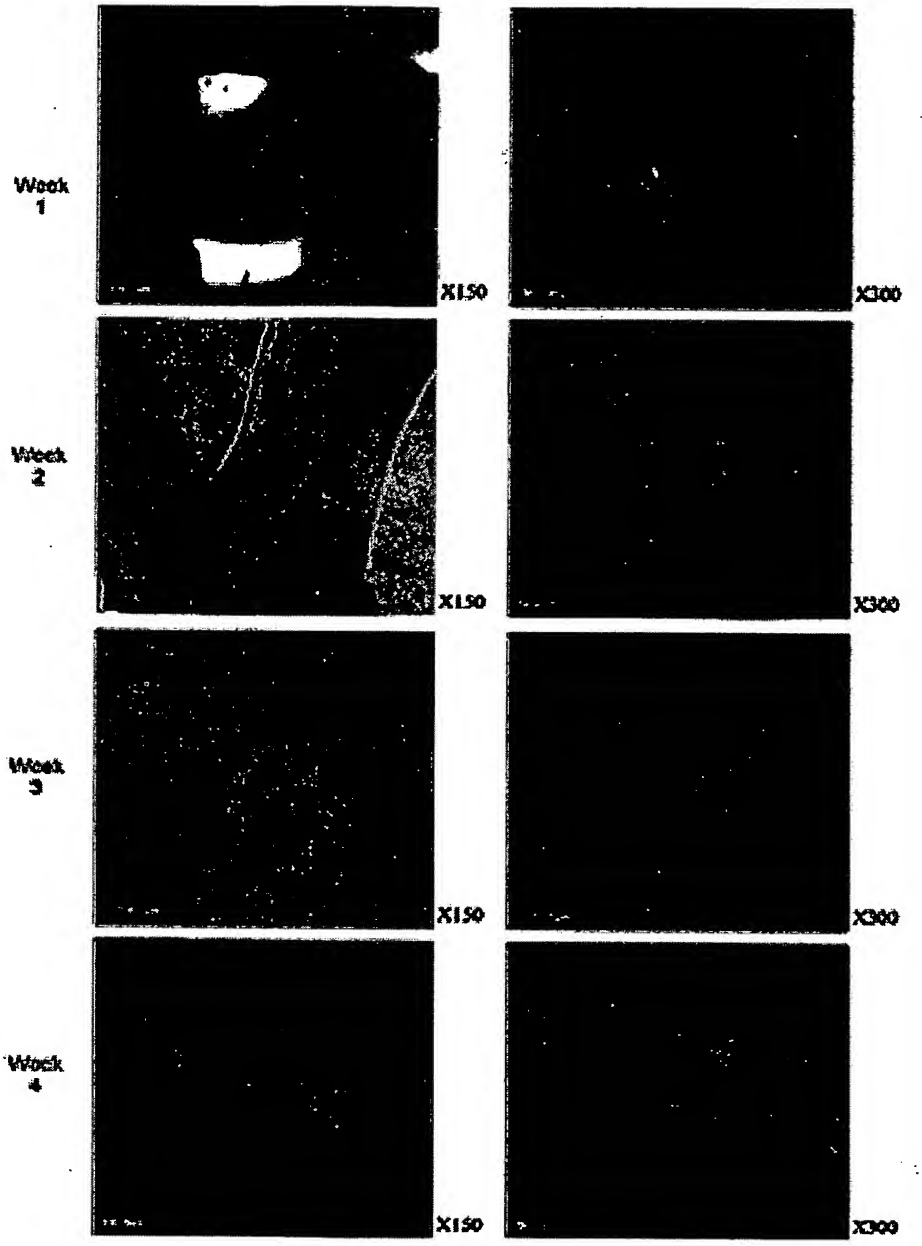

Figure 8. CLM images taken after 1, 2, 3, and 4 weeks in the culture (left row, 0/60/120° lay-down pattern, and right row, 0/72/144/36/108° lay-down pattern). [Color figure can be viewed in the online issue, which is available at www.interscience.wiley.com.]

cross sections, presenting a star-shaped morphology (Figs. 11 and 12). At the interconnected pores, cells appeared to grow along the rods and span across the pore architecture. Over the 3-week period, a centripetal cell ingrowth within the pores could be observed, with the extracellular matrix acting as a guiding structure for the cells. Phallodin staining and SEM revealed a netlike growth structure (Fig. 13). On the basis of these described qualitative data, a significant difference of the proliferation patterns of the two different scaffold architectures could not be observed. In another study, a quantitative comparison of cell attachment and proliferation on the surface of PCL scaffolds with six different matrix architectures, a cell proliferation assay was performed. The data revealed that a scaffold with a 0/60/120° lay-down pattern had a higher proliferation rate in the first 2 weeks, whereas the scaffolds with a 0/72/144/36/108° lay-down

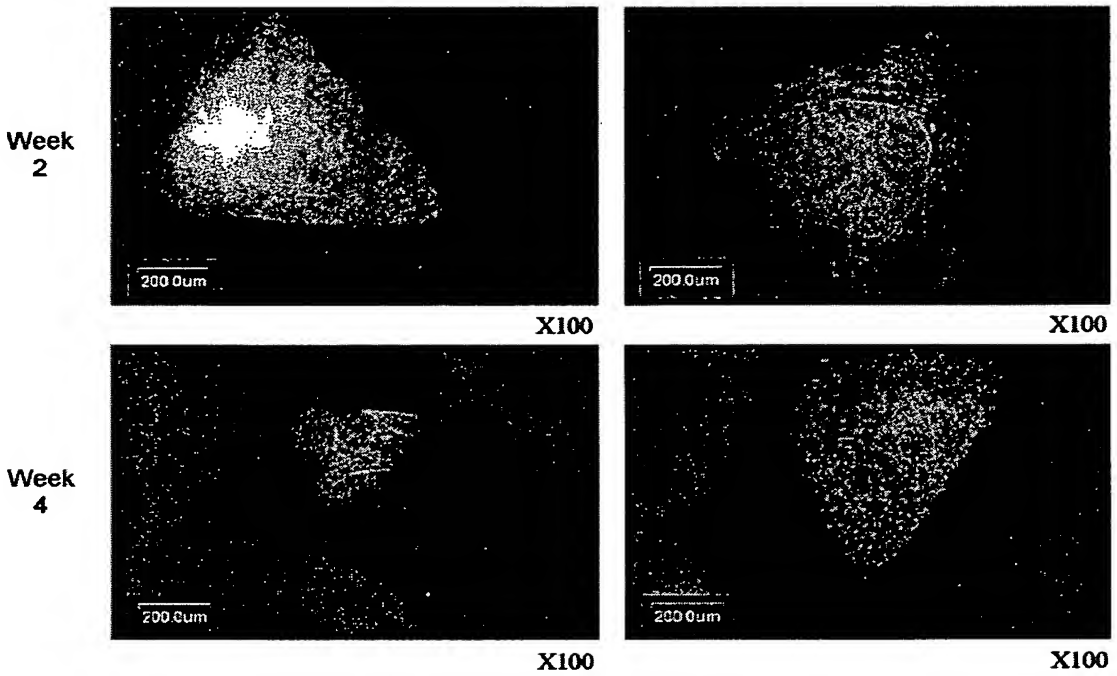

Figure 9. Phase contrast images taken on weeks 2 and 4 (left row, 0/60/120° lay-down pattern, and right row, 0/72/144/36/108° lay-down pattern).

overtook the three-angle matrix architecture in weeks 3 and 4 (unpublished data).

DISCUSSION

Almost all tissue-engineering concepts require the use of some form of porous scaffold, which serves as a template for cell proliferation and ultimately tissue formation.[17] Through our investigations, we found that the FDM method allows the computer-controlled and highly reproducible fabrication of bioresorbable scaffolds with controlled porosity and pore size over a physiologically relevant range, which permits the tailoring of scaffold properties for particular tissue requirements.

The conventional techniques of scaffold fabrication, solvent casting/salt leaching, gas foaming/salt leaching, vacuum drying, fiber bonding, and TIPS, produce structures that are generally classified as foams and have been reviewed.[3] There are numerous drawbacks of applying those scaffolds for tissue-engineering applications. The pores are not fully interconnected be-

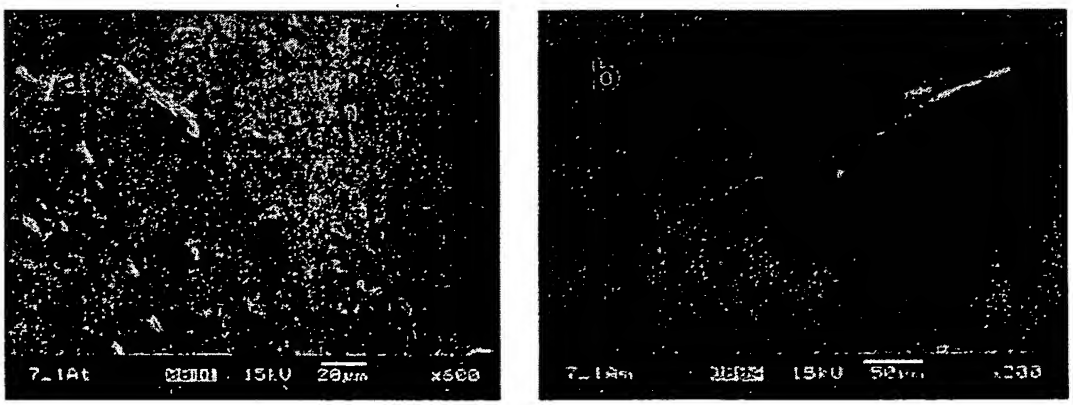

Figure 10. (a) The scanning electron micrograph of a specimen after 2 weeks of culturing shows multiple fibroblast layers colonizing the rod of a PCL scaffold. (b) In week 4, bridging through a pore can be seen.

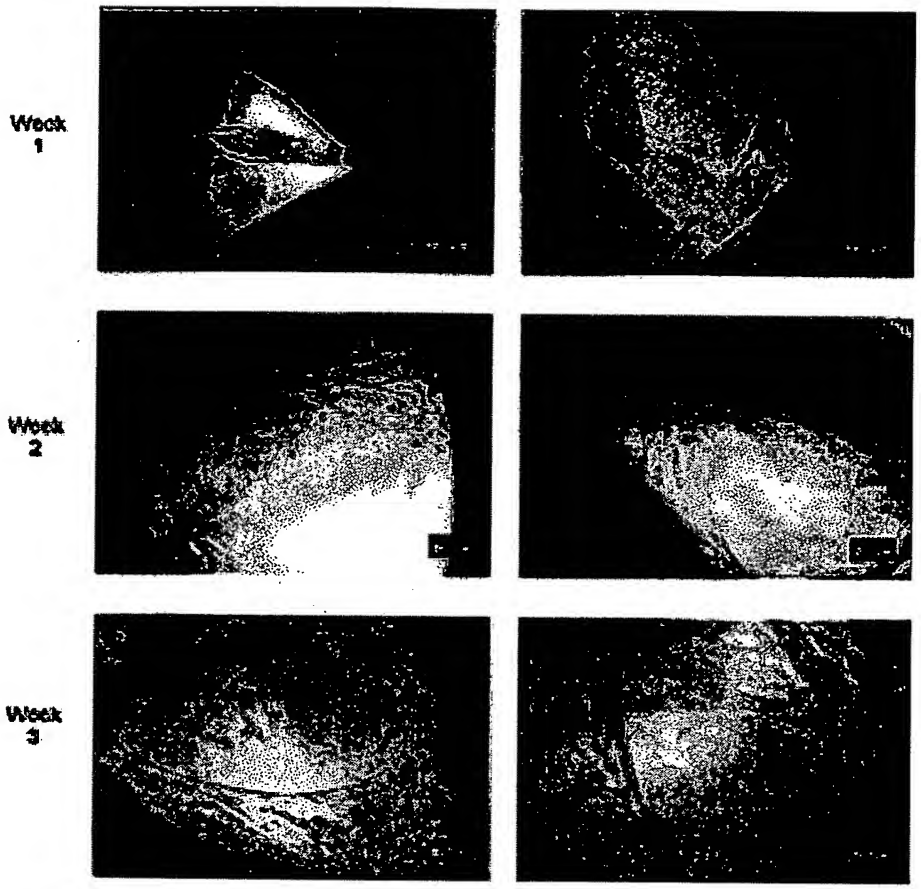

Figure 11. Phase light contrast microscopy images (original magnification ×100) of osteoprogenitor cells cultured for up to 3 weeks. The PCL scaffold exhibited good biocompatibility evident in the increasing cell proliferation and cell activity. Microscopically, it was observed that the cells had attached and spread on the PCL bars and cross sections, presenting a star-shaped morphology. At the junction of the scaffold columns and bars, cells appeared to connect structures and bridging across the 3D pores. Over the 3-week period, a centripetal cell ingrowth within the pores could be observed with the extracellular matrix acting as a guiding structure for the cells (left row, 0/60/120° lay-down pattern, and right row, 0/72/144/36/108° lay-down pattern). [Color figure can be viewed in the online issue, which is available at www.interscience.wiley.com.]

cause of the formation of skin layers during solvent evaporation. The pore size varies, as it is difficult to ensure that the porogens are well-dispersed and not agglomerated to form bigger particles. The thickness and length of the pore walls and edges vary, depending on the solvent evaporation rate. The scaffolds cannot be made with thick sections, as deeply embedded porogens become too distant from the surface and residual porogens may be left in the final structure. The use of organic solvents requires careful and complete removal of residual solvents prior to clinical usage.

In addition, none of the conventional scaffold fabrication techniques not allow the fabrication of a 3D scaffold with a varying multiple-layer design (Fig. 14). Such a matrix architecture is advantageous in instances where tissue engineers want to grow a bitissue or multiple-tissue interface, for example, an articular cartilage/bone transplant (Fig. 15). RP machines, such as FDM and 3DP, that build a physical model by depositing layers of a material one at a time allow such a design.

3DP has been used to process bioresorbable scaffolds for tissue-engineering applications.[18–21] The technology is based on the printing of a binder through a print head nozzle onto a powder bed. The removal of entrapped powder is very difficult.[20] The entire 3DP process is performed under room-temperature conditions, whereas FDM uses a thermoplastic polymer. Hence, 3DP allows the incorporation of biological agents, such as cells, growth factors, and so forth, without inactivation if nontoxic binders such as water can be used.[21] Unfortunately, aliphatic polyesters can be dissolved in highly toxic solvents, such as chloroform and methylene chloride, only. To date,

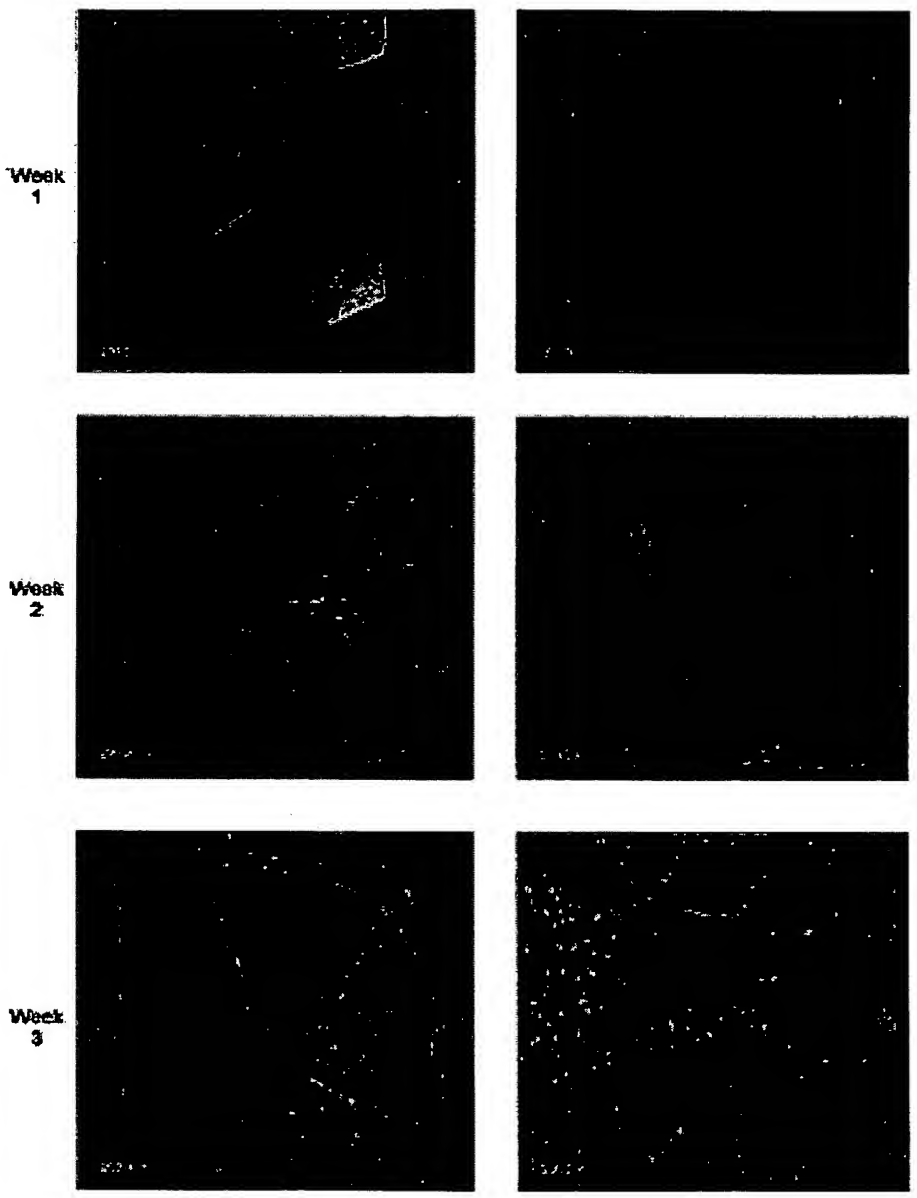

Figure 12. Confocal micrographs revealed a netlike proliferation pattern on the PCL columns and bars. Cell/scaffold constructs were prepared for CLM by the staining of viable cells green with FDA and dead cells red via PI. In the 1st week, a denser cell network was qualitatively observed in the three-angle architecture, whereas at week 3 the five-angle scaffolds showed more cells. Both matrix architectures presented a low rate of apoptosis starting only at week 3 (left row, 0/60/120° lay-down pattern, and right row, 0/72/144/36/108° lay-down pattern). [Color figure can be viewed in the online issue, which is available at www.interscience.wiley.com.]

only bioresorbable scaffolds without biological agents within the polymer matrix and in combination with particle leaching have been processed by 3DP. In addition, the mechanical properties and accuracy of the specimens manufactured by 3DP have to be significantly improved.[20]

To study the performance of bioresorbable 3D scaffolds applying *ex vivo* testing, we must provide conditions that simulate the *in vivo* environment as closely as possible. When we perform the mechanical testing of polymeric materials, such as the ones used in this study, temperature and water appear to be two very important environmental factors. For most synthetic polymers, mechanical properties vary greatly when tested over a range of temperatures. Furthermore, water may have a plasticizing effect on the polymer that

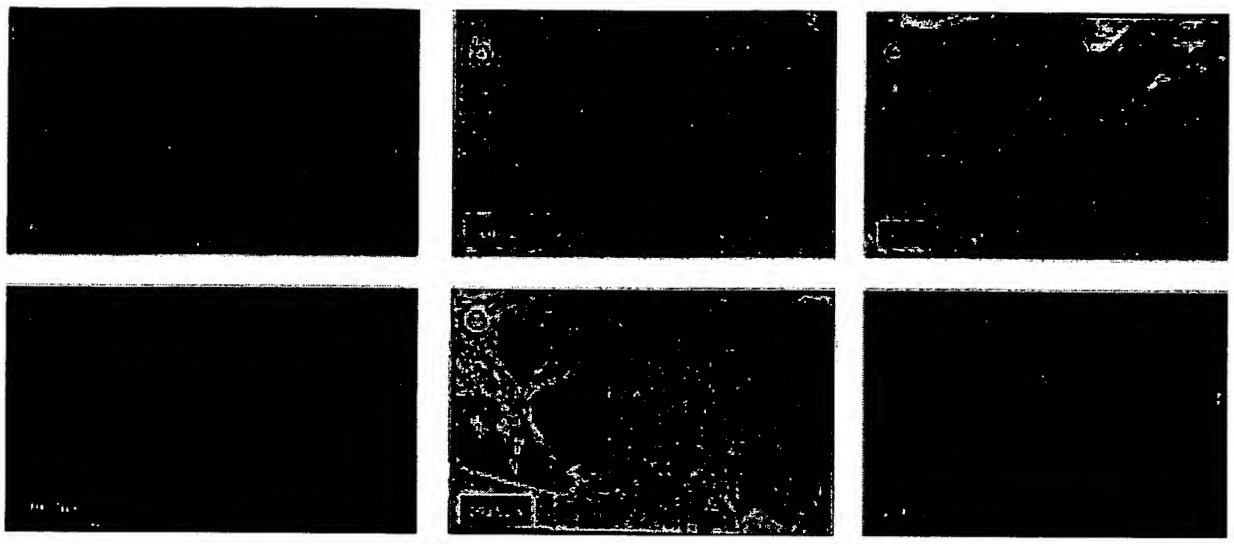

Figure 13. (a,b) Phallodin staining and SEM revealed the proliferation and colonization pattern of the osteoblast-like cells. (c) The cells anchored strongly onto the PCL surface and actin containing stress fibers bonded directly on the polymer surface. In week 2, the cells appeared to span three-dimensionally across the pore structure, preferably with the interjunctions of the columns and rods. Cells continued to proliferate after colonizing the scaffold surface because they were not space-limited and had the possibility of growing in a 3D manner, filling the entire interconnected matrix architecture. (d,e,f) In week 3, a centripetal cell ingrowth within the pores could be observed, with the extracellular matrix acting next to the culture media as support for the cell growth focal adhesion point. [Color figure can be viewed in the online issue, which is available at www.interscience.wiley.com.]

is accentuated with elevated temperature. Unfortunately, a great number of researchers tested their scaffolds only under ambient conditions or in air at 37 °C.[3]

Recently, two groups reported the mechanical testing of preconditioned scaffolds in a simulated physiological environment. Slivika et al.[22] studied the mechanical properties of scaffolds that had a porosity of 60–70% and were composed of a 75/25 poly(D,L-lactide-*co*-glycolide) matrix that was reinforced with polyglycolide (PGA) fibers with a diameter of 15 μm and a length of 2.5 mm. Testing of the fiber-reinforced samples under physiological versus ambient conditions showed a 70-fold decrease in compressive stiffness and a 7-fold decrease in yield strength. The authors concluded that the polymer matrix became softer because of the temperature increase and that the water uptake had an additional plasticizing effect. Two types of scaffolds made of a 75/25 poly(D,L-lactide-*co*-glycolide) matrix and with a porosity of approximately 70% were used by Lohmann et al.[23] The moduli of the nonreinforced scaffold and the 10% PGA fiber-reinforced specimens were reported to be 1.65 ± 0.14 and 31.7 ± 7.4 MPa, respectively, and the yield stresses were 0.16 ± 0.014 and 2.07 ± 0.49 MPa, respectively. Thompson et al.[24] fabricated and tested a foamlike PGA/PLA 75/25 scaffold with a porosity of 54% in air at 37 °C. The yield strength was measured at 1.5 ± 0.1 MPa, whereas a 50/50 PGA/PLA composition would yield at 0.62 ± 0.39 MPa ± 0.1.

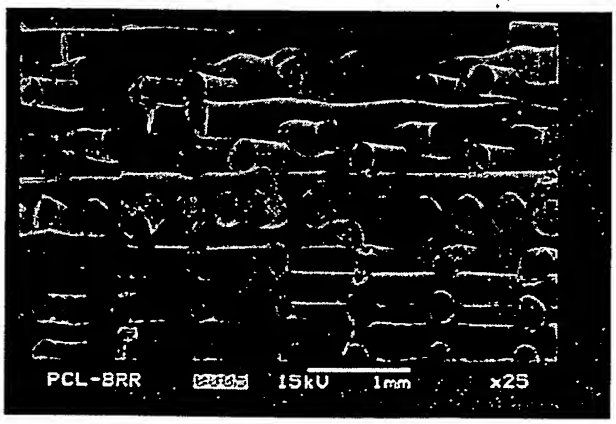

Figure 14. SEM picture of a PCL scaffold with a varying multiple-layer design. A scaffold architecture with (A) a 0/60/120° lay-down pattern of the top part, (B) a nonporous structure for the middle part, and (C) a 0/90 ° lay-down pattern of the bottom part was designed and manufactured via FDM.

Our results show that the compressive modulus of the PCL scaffolds with a porosity of 61% can be benchmarked against the nonreinforced PGA/PLA scaffolds. The testing of PCL scaffolds under simulated physiological conditions versus ambient conditions resulted in a decrease in compressive stiffness and yield strength. However, the decrease was less dominant then in the PGA/PLA scaffolds because of the difference in the glass-transition point of the used 75/

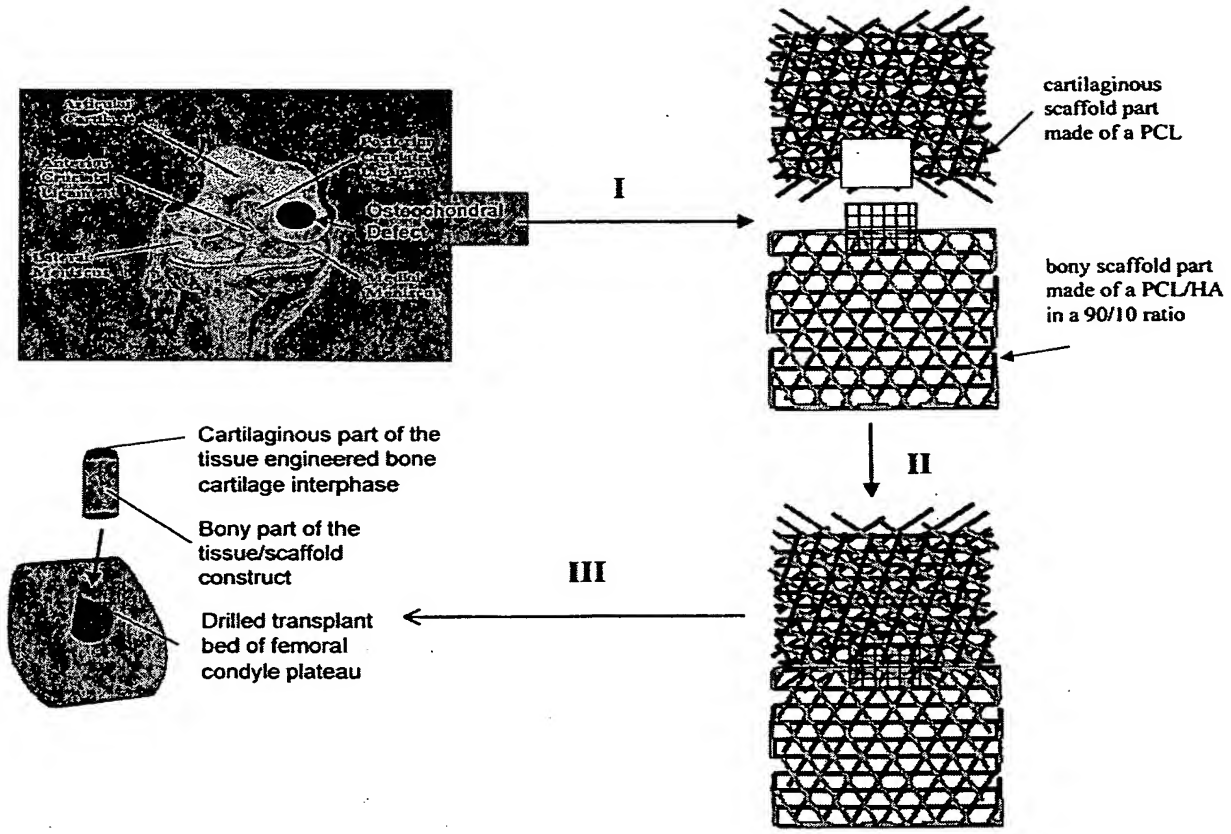

Figure 15. Schematic illustration of the culture concept and the surgical placement of a tissue-engineered osteochondral transplant. (I) After the loading of the bony scaffold part with osteoblasts and the cartilage scaffolds with chondrocytes, the constructs are cultured for 28 days in osteogenic and cartilaginous culture media, respectively. (II) After separate culturing, the bony and cartilage scaffolds are joined together and further cultured for 4 weeks in a 50/50% mixture of the osteogenic and chondrogenic media. (III) The dental cylinder implantlike design of the bony bioresorbable 3D scaffold allows applying a press fit. Hence, a secure and user-friendly transplantation is obtained.

25 PGA/PLA aliphatic polymers. From the mechanical characterization, it can be concluded that the PCL scaffolds have the potential to be applied in tissue-engineering bone and cartilage.

For load-bearing tissues such as cartilage and bone, any bioresorbable 3D scaffold should provide sufficient mechanical strength over a certain period of time to withstand *in vitro* forces, *in vivo* forces, or both. The space for cell proliferation and differentiation, extracellular matrix production, and tissue growth and remodeling has to be maintained until the tissue inside the scaffold architecture is mature enough to support itself. The PCL scaffold presented in this study is designed to retain its mechanical properties for 5–6 months and then gradually lose its physical properties until it is completely metabolized over a period of 2 years. [16]

How cells interact at the scaffold interface is a crucial aspect of studying the biocompatibility of 3D templates for tissue-engineering applications. The many different proliferation and differentiation responses exhibited by cells from different species dictate that human cells should be used for optimal assessment. To this purpose, the evaluation of the FDM-fabricated PCL scaffolds has been performed with a human fibroblast culture. The results of this study show that human fibroblasts colonize on the struts and bars of an FDM-fabricated PCL scaffold and form a cell-to-cell and cell-to-extracellular-matrix interconnective network throughout the entire 3D honeycomb-like architecture.

Several groups[25–27] could show the good biocompatibility of two-dimensional PCL specimens in human osteoblast-like cell cultures. Marra et al.[25,26] concluded from their two-dimensional cell studies that PCL is superior to poly (lactide-*co*-glycolide) (PLGA) for bone cell growth. Cell migration requires a biomolecularly healthy and dynamic interaction among the cell, the scaffold surface, and its cytoskeleton. Numerous studies using immunohistochemical methods have shown the presence of actin in cultured osteoblasts on various scaffold materials.[28] Our qualitative

data of a human osteoblast-like cell culture demonstrate the good biocompatibility of PCL for hard-tissue formation. We could show in the entire PCL 3D scaffold architecture the formation of actin-supported sheetlike protrusions known as lamellipodia up to a period of 3 weeks.

CONCLUSION

A highly reproducible and computer-controlled method for designing and fabricating porous, bioresorbable 3D scaffolds with FDM was developed. The pore volume and structure and the porosity of the scaffolds were mainly defined by the setting of the computer-controlled FDM machine parameters. The honeycomb design resulted in good mechanical properties. PCL scaffolds showed excellent biocompatibility with human fibroblast and periosteal cell culture systems. All in all, the FDM method is a promising new technique for the design and fabrication of tailor-made scaffold architectures for tissue-engineering applications. Future research projects include the tissue engineering of complex hard-tissue and soft-tissue structures *in vitro* and *in vivo*.

The authors would like to thank Dr. Yi Yan Yang and Dr. Chaobin He of the Institute of Materials and Research Engineering (IMRE) for the support in using the GPC equipment and one-shot extruder.

References

1. Thomson RC, Wake MC, Yaszemski MJ, Mikos AG. Biodegradable polymer scaffolds to regenerate organs. Adv Polym Sci 1995;122:245–274.
2. Widmer MS, Mikos AG. Fabrication of biodegradable polymer scaffolds for tissue engineering. In: Patrick Jr. CW, Mikos AG, McIntire LV, editors. Frontiers in tissue engineering. New York: Elsevier Science; 1998. p 107–120.
3. Hutmacher DW. Polymeric scaffolds in tissue engineering bone and cartilage. Biomaterials 2000;21:2529–2543.
4. Crump SS, inventor; Stratasys Incorporated, assignee. Apparatus and method for creating three-dimensional objects. US patent 5,121,329. 1992 June 9.
5. Hutmacher DW, Zein I, Teoh SH, Ng KW, Schantz JT, Leahy JC. Design and fabrication of a 3D scaffold for tissue engineering bone. In: Agrawal CM, Parr JE, Lin ST, editors. Synthetic bioabsorbable polymers for implants. STP 1396. West Conshohocken, PA: American Society for Testing and Materials; 2000. p 152–167.
6. Perrin DE, English JP. Polycaprolactone. In: Domb AJ, Kost J, Wiseman DM, editors. Handbook of biodegradable polymers. Australia: Harwood Academic; 1998. p 63–77.
7. Bezwada RS, Jamiolkowski DD, Lee I, Vishvaroop A, Persivale J, Treka-Benthin S, Erneta M, Suryadevara J, Yang A, Liu S. Monocryl suture, a new ultra-pliable absorbable monofilament suture. Biomaterials 1995;16:1141–1148.
8. Darney PD, Monroe SE, Klaisle CM, Alvarado A. Clinical evaluation of the Capronor contraceptive implant: preliminary report. Am J Obstet Gynecol 1989;160:1292–1295.
9. Pitt CG, Chasalow FI, Hibionada YM, Klimas DM, Schindler A. Aliphatic polyesters I: the degradation of poly(ε-caprolactone) in vivo. J Appl Polym Sci 1981;26:3779–3787.
10. Woodward SC, Brewer PS, Moatamed F. The intracellular degradation of poly(ε-caprolactone). J Biomed Mater Res 1985;19: 437–444.
11. Nam YS, Yoon JJ, Park TG. A novel fabrication method of macroporous biodegradable polymer scaffolds using gas forming salt as a porogen additive. J Biomed Mater Res (Appl Biomater) 2000;53:1–7.
12. Peter SJ, Nolley JA, Widmer MS, Merwin JE, Yaszemski MJ, Yasko AW, Engel PS, Mikos AG. In vitro degradation of a poly(propylene fumarate)/β-tricalcium phosphate composite orthopaedic scaffold. Tissue Eng 1997;3:207–215.
13. Thomson RC, Yaszemski MJ, Powers JM, Mikos AG. Hydroxyapatite fiber reinforced poly(α-hydroxy ester) foams for bone regeneration. Biomaterials 1998;19:1935–1943.
14. Thomson RC, Yaszemski MJ, Powers JM, Mikos AG. Fabrication of biodegradable polymer scaffolds to engineer trabecular bone. J Biomater Sci Polym Ed 1995;7(1):23–38.
15. Gibson LJ, Ashby MF. Cellular solids: structure and properties. 2nd ed. Cambridge, England: Cambridge University Press; 1997.
16. Zein I, Hutmacher DW, Teoh SH, Tan KC. Mechanical properties of polycaprolactone scaffolds fabricated using fused deposition modeling. Forthcoming.
17. Patrick Jr CW, Mikos AG, McIntire LV. Prospectus of tissue engineering. In: Patrick Jr CW, Mikos AG, McIntire LV, editors. Frontiers in tissue engineering. New York: Elsevier Science; 1998. p 3–14.
18. Cima LG, Vacanti JP, Vacanti C, Ingber D, Mooney D, Langer R. Tissue engineering by cell transplantation using degradable polymer substrates. J Biomech Eng 1991;113:143–151.
19. Park A, Wu B, Griffith LG. Integration of surface modification and 3-D fabrication techniques to prepare patterned poly(L-lactide) substrates allowing regionally selective cell adhesion. J Biomater Sci Polym Ed 1998;9:89–110.
20. Giordano RA, Wu BM, Borland SW, Cima LG, Sachs EM, Cima MJ. Mechanical properties of dense polylactic acid structures fabricated by three dimensional printing. J Biomater Sci Polym Ed 1996;8:63–75.
21. Wu BM, Borland SW, Giordano RA, Cima LG, Sachs EM, Cima MJ. Solid free-form fabrication of drug delivery devices. J Controlled Release 1996;40:77–87.
22. Slivka MA, Leatherbury NC, Kieswetter K, Niederauer GG. In vitro compression testing of fiber-reinforced, bioabsorbable, porous implants. In: Agrawal CM, Parr JE, Lin ST, editors. Synthetic bioabsorbable polymers for implants. ASTM STP 1396. West Conshohocken, PA: American Society for Testing and Materials; 2000. p 124–135.
23. Lohmann CH, Schwartz Z, Niederauer GG, Carnes Jr DL, Dean DD, Boyan BD. Pretreatment with platelet derived growth factor-BB modulates the ability of costochondral resting zone chondrocytes incorporated into PLA/PGA scaffolds to form new cartilage in vivo. Biomaterials 2000;21:49–61.
24. Thomson RC, Yaszemski MJ, Powers JM, Mikos AG. Fabrication of biodegradable polymer scaffolds to engineer trabecular bone. J Biomater Sci Polym Ed 1995;7:23–38.
25. Marra KG, Szem JW, Kumta PN, DiMilla PA, Weiss LE. In vitro analysis of biodegradable polymer blend/hydroxyapatite composites for bone tissue engineering. J Biomed Mater Res 1999;47:324–335.
26. Marra KG, Campbell PG, Dimilla PA, Kumta PN, Mooney MP, Szem JW, Weiss LE. Novel three dimensional biodegradable scaffolds for bone tissue engineering. Mater Res Soc Symp Proc 1999;550:155–160.
27. Corden TJ, Jones IA, Rudd CD, Christian P, Downes S, McDougall KE. Physical and biocompatability properties of poly-ε-caprolactone produced using in situ polymerisation: a novel manufacturing technique for long-fibre composite materials. Biomaterials 2000;21:713–724.
28. Anselme K. Osteoblast adhesion on biomaterials. Biomaterials 2000;21:667–668.

TISSUE ENGINEERING
Volume 9, Suppl. 1, 2003

EXHIBIT 3

Scaffold Design and *in Vitro* Study of Osteochondral Coculture in a Three-Dimensional Porous Polycaprolactone Scaffold Fabricated by Fused Deposition Modeling

TONG CAO, Ph.D.,[1] KEE-HAI HO, F.A.M.S.,[1] and SWEE-HIN TEOH, Ph.D.[2]

ABSTRACT

Tissue engineering offers an alternative method that can overcome some of the existing drawbacks of current articular defect repair methods because articular cartilage has a limited capacity to respond to injury. The solution may lie in the design of a three-dimensional load-bearing scaffold. Here we describe the tissue engineering of an osteochondral construct by coculturing osteogenic cells and chondrogenic cells on a three-dimenisonal load-bearing bioresorbable polymer scaffold. Porous polycaprolactone scaffolds were designed and fabricated via fused deposition modeling. Osteogenic cells were seeded and precultured in one-half of the partitioned scaffolds. Chondrogenic cells were later seeded into the other half. The cell-seeded scaffolds were cultured in a coculture medium. Both cell types proliferated, migrated, linked in their scaffold compartments, and integrated at the interface. Osteoblasts and chondrocytes produced different extracellular matrices in each scaffold compartment. Mineralized nodules deposited in the osteogenic cell seeded compartment. High osteocalcin was detected in precultured osteogenic cell supernatant and high alkaline phosphatase was detected in the coculture supernatant of osteochondral constructs. This study suggests that a tissue-engineered osteochondral construct with a three-dimenisonal polycaprolactone scaffold has the potential for osteochondral defect repair.

INTRODUCTION

HUMAN ARTICULAR CARTILAGE LESION REPAIR is a challenging clinical problem. This is because the ability of hyaline cartilage to respond to injury is poor.[1] Once cartilage damage has occurred, an irreversible degenerative process can occur.[2] The resulting defects may lead to osteoarthritis.[2,3] Current attempts to treat articular cartilage lesions include chondral shaving, spongialization,[4] microfracturing of the subchondral plate,[5] mosaicplasty,[6] implantation of artificial matrices and/or growth factors, and drilling through the subchondral bone to allow pluripotent cells from the marrow space to invade and repair the lesion.[7,8] But to date no reliable, reproducible approach has been identified. Even fewer options are available for the repair of joint osteochondral (bone–cartilage) defects.

These requirements could potentially be met by tissue-engineered osteochondral constructs consisting of a load-bearing bioabsorbable porous scaffold combined with autologous osteogenic and chondrogenic cells in different portions of the scaffold. Figure 1 shows this concept schematically, with a scaffold specially designed to allow the proliferation and growth of chondrocytes at the top and osteoblasts at the bottom. The bottom construct addresses the interface issue, that is, where difficulty in attaching cartilage onto the bony defect is often

[1]Faculty of Dentistry and [2]Division of Bioengineering and Mechanical Engineering Department, National University of Singapore, Singapore.

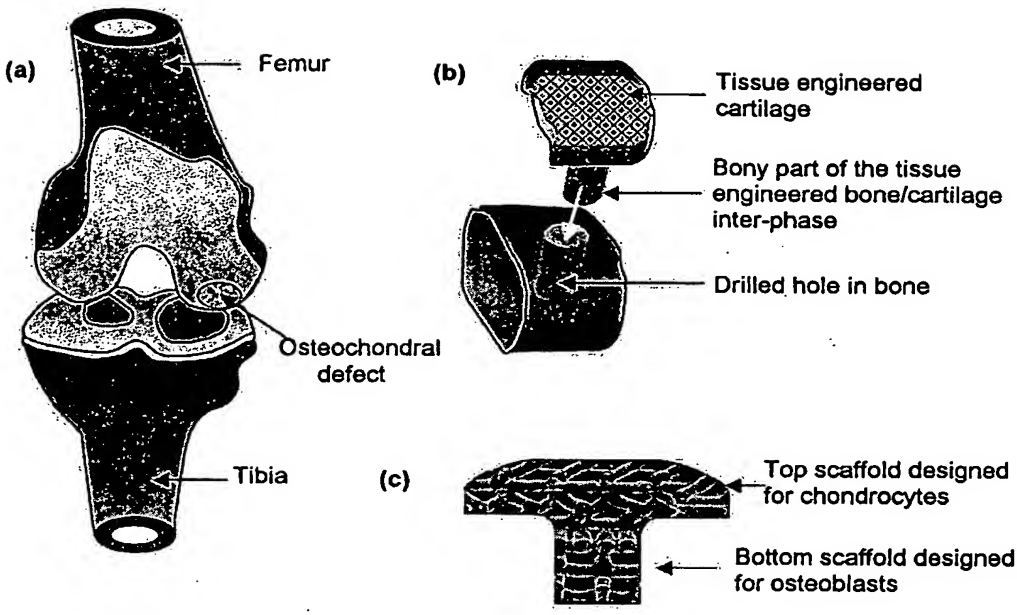

FIG. 1. Schematic illustration of osteochondral defect (a) and new concept of scaffold design (b) in which both chondrocytes and osteoblasts can be integrated so as to produce a construct (c) that will provide anchorage to the native bone, solving the issue of poor mechanical stability encountered in attaching tissue-engineered cartilage onto bone.

encountered. Such restoration would provide mechanical stability, minimize donor site morbidity by using cell culture techniques, and eliminate complications related to allografts and/or mechanical devices. The subchondral bone region of a tissue-engineered osteochondral construct would critically support the overlying neocartilage formation and further help to anchor the graft within the defect, because a bone-to-bone interface integrates better and faster than a cartilage-to-cartilage interface.[9]

Researchers have investigated bioabsorbable scaffolds both for bone and cartilage tissue engineering. Poly(DL-lactic-co-glycolic acid) (PLGA) has frequently been chosen for tissue-engineering applications because its degradation can be tailored; however, in a highly porous configuration its mechanical properties may be limited.[10–12] The ideal biomaterial for osteochondral tissue-engineering reconstruction will have numerous properties. It should be biocompatible, capable of facilitating revascularization, osteoinductive and osteoconductive, chondroinductive and chondroconductive, providing a framework to guide the new osteochondral tissue development. The material needs to be sterile, malleable, storable, and affordable. A high initial stiffness will allow primary union followed by gradual resorption and reduction in stiffness corresponding to the ability of healing osteochondral tissue to serve in a load-bearing capacity. Ideally, the material should be easily processed into complex-shaped components. With the use of computed tomography (CT) patient scan data this creates the possibility of producing accurate tailored implants for elaborate reconstructive surgery. Among various clinical biomaterials, polycaprolactone (PCL) might meet most of these requirements.[13]

A number of different processing techniques have been developed to design and fabricate three-dimensional (3-D) scaffolds for tissue-engineering applications. The imperfection of the current techniques has encouraged the use of a rapid prototyping technology known as *fused deposition modeling* (FDM). A highly reproducible and computer-controlled method for designing and fabricating porous, bioresorbable 3-D scaffolds with FDM was developed.[14] The pore volume and structure and the porosity of the scaffolds were defined mainly by the setting of the computer-controlled FDM machine parameters.

An investigation of the feasibility of tissue engineering an osteochondral construct by using FDM-fabricated PCL porous scaffolds (as shown in Fig. 1) with osteogenic and chondrogenic cells is needed to gain important information about *in vitro* osteochondral constructs before tissue-engineered osteochondral construct transplantation can be attempted *in vivo*. Many studies dictate that human cells should be used for optimal assessment. To this end, an evaluation of FDM-fabricated PCL scaffolds has been performed with human cells. The present *in vitro* study focuses on (1) whether cocultured osteogenic and chondrogenic cells will grow, migrate, and distribute in the honeycomb-like structure of FDM-fabricated porous PCL scaffolds, and (2) whether cocultured cells produce their extracellular matrices in this three-dimensional environment.

MATERIALS AND METHODS

Scaffold fabrication

PCL scaffolds were fabricated by FDM.[14] This technique allows the designing and fabrication of scaffolds of various lay-down patterns, pore sizes, and porosity. In this experiment, rectangularly shaped honeycomb-like scaffolds were fabricated with a three-angle lay-down pattern (0/60/120°). Figure 2 shows the schematic architecture of the scaffolds. The porosity ranges from 60 to 65% and the pore size ranges from 300 to 580 μm. The scaffolds were cut to measure 10 × 10 × 3.2 mm. Each scaffold was partitioned vertically into two halves with a gap between them (Fig. 3). One-half (bone compartment) of the partitioned scaffold was designated for bone marrow stromal cell seeding and the other half (cartilage compartment) was designated for chondrocyte seeding. The scaffolds were surface treated with 5 M sodium hydroxide (J.T. Baker, Phillipsburg, NJ) for 1 h to enhance their hydrophilicity. After being rinsed three times with phosphate-buffered saline (PBS; National University Medical Institutes, Lab Supplies Store, National University of Singapore), the scaffolds were then sterilized in 70% ethanol (Merck, Darmstadt, Germany) for 24 h. This was followed by two more rinses with phosphate-buffered saline and centrifugation at 1000 rpm for 10 min. The scaffolds were dried in a self-sterilizable incubator (WTB Binder, Tuttlingen, Germany) at 37°C in 5% CO_2 for 1 h and soaked with agitation twice for 3 h in Dulbecco's modified Eagle's medium (DMEM; GIBCO-BRL, Rockville, MD) before cell seeding.

Cell isolation and expansion

Human iliac crest and rib cartilage pieces were aseptically obtained from an adult male donor under an institutional review board-approved protocol. The iliac crest and rib cartilage pieces were excised, cleaned of soft tissue, and washed with DMEM containing penicillin (100 U/mL; GIBCO-BRL) and streptomycin (100 μg/mL; GIBCO-BRL). The iliac crest pieces were then cut into small chips and the marrow was flushed from the chips with 25 mL of a primary medium (199 medium [GIBCO-BRL] containing 10% fetal bovine serum [GIBCO-BRL], penicillin [100 U/mL], and streptomycin [100 μg/mL] by vibration/shaking in a sterile Falcon tube. Cell clumps were broken up by repeatedly pipetting the cell suspension. The cells were then centrifuged at 1000 rpm for 10 min. The resulting cell pellets were resuspended in 12 mL of the primary medium, plated in 75-cm^2 flasks, and incubated at 37°C in 5% CO_2, 95% air and 99% relative humidity. After 24 h, hematopoietic cells and other unattached cells were removed from the flasks by repeated washes with phosphate-buffered saline.[15] The culture medium was replaced every third or fourth day. The rib cartilage pieces were minced into small fragments (approximately 2 mm^3) and immersed in collagenase II (2.5 mg/mL; Sigma, St. Louis, MO) for 16 h at 37°C. The solution was centrifuged to pellet the chondrocytes. The chondrocyte pellet was washed repeatedly with phosphate-buffered saline. After the viability was measured by trypan blue dye exclusion, the chondrocytes were diluted in 75-cm^2 flasks and incubated at 5% CO_2, 95% air, 99% relative humidity, and 37°C in F12-Ham medium (GIBCO-BRL) containing 10% fetal

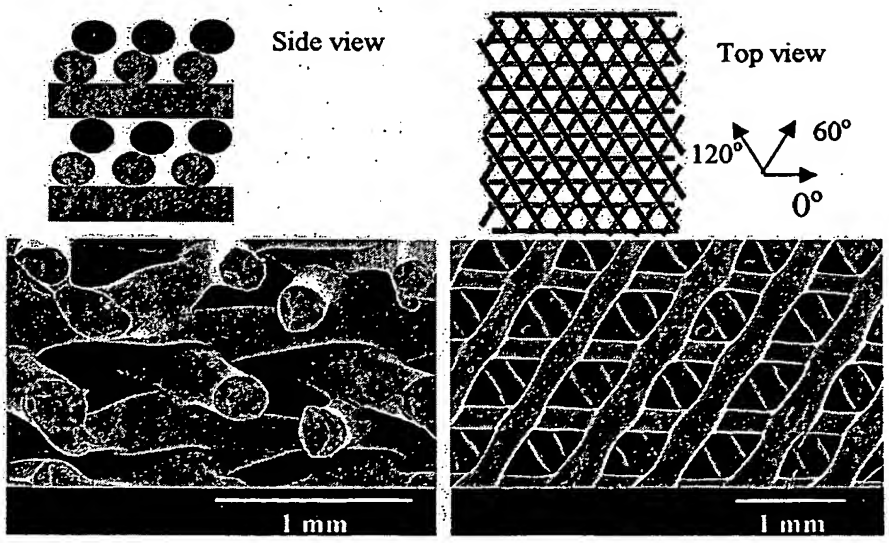

FIG. 2. Schematic views of the scaffold design and corresponding SEM photographs of 3-D PCL scaffold structure produced by FDM and having a 0/60/120° lay-down pattern. Freeze–fractured cross-section reveals the side view (*left*) showing interconnected pore structures; the top view (*right*) shows the typical array of equilateral triangles.

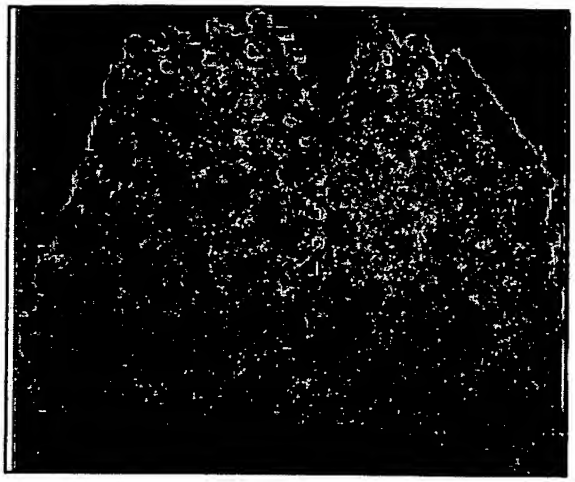

FIG. 3. Photograph showing how the 10 × 10 × 3.2 mm scaffold was partitioned for coculturing experiments.

bovine serum, penicillin (100 U/mL), and streptomycin (100 μg/mL).

Osteochondral composition and coculture

When confluent monolayers were reached at passage 2 (yielding approximately 3×10^6 cells per flask), the adherent stromal cells[16] from iliac crest marrow were enzymatically lifted from the flask with a 625-mg/mL solution of trypsin (Sigma). The cells were centrifuged, pelleted, resuspended, counted with a hemocytometer, and diluted to a concentration of 1×10^7 cells/mL in an osteoblastic medium (199 medium containing 10% fetal bovine serum, penicillin [100 U/mL], streptomycin [100 μg/mL], 10 mM sodium β-glycerol phosphate [Sigma], L-ascorbic acid [50 μg/mL; Sigma] and 5 nM dexamethasone [Sigma]. The cell mortality was less than 5%, as shown by trypan blue staining, and stable cell metabolism was maintained. The marrow stromal cell suspensions were mixed with fibrin glue (Sigma) and pipetted into the scaffold bone compartment, occupying half the treated scaffold, resulting in an even seeding density of 1×10^6 cells per compartment measuring 10 × 5 × 3.2 mm. The marrow stromal cell-seeded scaffolds were then placed in each well of a 24-well plate, left undisturbed in an incubator for 10 min to allow the fibrin glue to coagulate in the scaffolds and incubated at 37°C in 5% CO_2, 95% air and 99% relative humidity in the osteoblastic medium. Osteocalcin expression verified the osteoblastic phenotype. Eighteen days after marrow stromal cell seeding, the chondrocytes from monolayer cultures were then collected, diluted in a coculture medium composed of 45% 199 medium, 45% F12-Ham medium, 10% fetal bovine serum, penicillin (100 U/mL) and streptomycin (100 μg/mL), 10 mM sodium β-glycerol phosphate, L-ascorbic acid (50 μg/mL), and 5 nM dexamethasone. To form the osteochondral construct, the chondrocytes were seeded in combination with fibrin glue into the scaffold cartilage compartment of the previously marrow stromal cell-seeded scaffold, resulting in a seeding density of 2×10^6 cells per compartment measuring 10 × 5 × 3.2 mm. The 24 constructs remained in the well plate for up to 8 weeks and were incubated at 37°C in 5% CO_2, 95% air and 99% relative humidity in the coculture medium, which was changed every 2–3 days. Another 24 scaffolds without cell seeding were incubated under the same conditions as control.

Phase-contrast light microscopy

Adhesion, proliferation, and distribution of the cells were studied by phase-contrast light microscopy (PCLM) (IX70; Olympus, Tokyo, Japan). In addition, the establishment of cell phenotype, intercellular connections, and extracellular matrix production were examined on a daily basis.

Laser confocal microscopy

The constructs were prepared for confocal microscopy by staining the cells with a fluorescent dye. Samples were placed in fluorescein diacetate (FDA, 2 μg/mL; Molecular Probes, Eugene, OR) and incubated for 15 min at 37°C, to stain viable cells green. After being rinsed twice in phosphate-buffered saline, the scaffolds were placed in propidium iodide solution (PI, 1 mg/mL; Molecular Probes) for 2 min, to stain dead cells red. The samples were then rinsed twice in phosphate-buffered saline and observed under a laser confocal microscope (IX70-HLSH100 Fluoview; Olympus). Depth projection micrographs were constructed from 40 to 50 horizontal image sections (3 μm each) through the scaffold–cell constructs.

Scanning electron microscopy

Samples were fixed in 2.5% gluteraldehyde (Merck) at 4°C for 4 h. They were then dehydrated in a graded ethanol series of 30, 50, 90, and 100%, dried, and gold sputtered with a JFC 1200 fine coater for 100 s at 15 mA under high vacuum. The specimens were examined with a JEOL JSM-5800LV scanning electron microscope at 15 kV under high-vacuum mode.

Alkaline phosphatase and osteocalcin assays

Alkaline phosphatase and osteocalcin were examined in supernatant taken from all samples during the medium changes. Substrate solution was prepared by dissolving 2 mg of 0.2% (w/v) *p*-nitrophenol phosphate (pNPP; Sigma) in 1 mL of 1 M diethanolamine-HCl (Sigma). For the alkaline phosphatase standard, 20 μL of *p*-nitrophenol (pNP, 10 μmol/mL; Sigma) was added to 1 mL of 2 M NaOH–0.2 mM ethylenediamine tetraacetic acid to

obtain a diluted solution (0.2 μmol/mL). This solution was further diluted to a range of 0.0 to 0.2 μmol/mL, that is, 0, 0.02, 0.04, 0.08, 0.12, 0.16, and 0.20 μmol/mL. Each 100-μL dilution was aliquoted and dispensed in duplicate to a 96-well plate. For the alkaline phosphatase test proper, 50-μL samples were added to microcentrifuge tubes. Substrate solution (150 μL) was added to each sample. Samples were vortexed and incubated at 37°C for 30 min. To each sample was added 200 μL of 2 M NaOH–0.2 mM ethylenediamine tetraacetic acid. Each mixture was vortexed briefly, and 100-μL samples of the mixtures were dispensed to the wells of a 96-well plate. Sample absorbance was read at 405 nm and product concentration was read off from a standard graph. Osteocalcin was measured with a human osteocalcin ELISA kit (Dako, Glostrup, Denmark). Measurements were expressed as means ± the standard deviation. Analysis of variance (ANOVA) and the Scheffé method were employed to assess the results at significance levels of 95 and 99%.

RESULTS

The FDM designs of the scaffolds were unique. The scaffolds designed by this FDM method were highly similar to coral-like structures. Each had a characteristic three-dimensional interconnected pore structure (Fig. 2). When viewed from the top, the architecture looks like an array of equilateral triangles of length 380 to 500 μm. A side view revealed the intercrossing filaments stacked in horizontal planes, with each filament fused at the cross-junctions. Such architecture should be highly conducive for cell attachment, growth, and communication and should allow an easy path for nutrient and waste product transport to and from the inner core of the scaffold, respectively. As published earlier,[14] this arrangement gave a relative high compressive stiffness of about 40 MPa and a compressive yield strength of 3 MPa.

Laser confocal microscopy revealed that both osteoblasts and chondrocytes attached to the PCL scaffold. They were interconnected and proliferated along the scaffold surfaces. Figure 4a shows the surface of a scaffold containing the osteochondral construct after 11 weeks in culture. The cells had grown over the entire surface of the rods and struts of the PCL scaffold. They filled up the pores in a circular manner. The complete 3-D scaffold architecture was taken up by the cell population. At the interconnected pores, cells appeared to grow along the rods and span across the pore architecture. The osteoblasts and chondrocytes linked and integrated at the interface (the boundary is shown by a white dotted line), at the middle portion of the scaffold via the new extracellular matrix expressed by the cells (Fig. 4b).

Both osteoblasts and chondrocytes produce rich extracellular matrices in their own scaffold compartments (Fig. 5). At the interface (indicated in Fig. 5 by an arrowhead) a mixture of cell types was observed. The surface of the extracellular matrix in the scaffold cartilage compartment (chondrocyte-seeded area) appeared smooth whereas that in the scaffold bone compartment (stromal cell-seeded area) was comparatively rougher (Fig. 6a and b, respectively). Dense and mineralized extracellular matrices (bone nodules) were deposited in the scaffold bone compartment (indicated by an arrowhead in Fig. 7). However, we noted difficulty in using SEM characterization to differentiate osteoblasts from chondrocytes. Nonetheless, the features reported here are consistent with many published SEM pictures of these cell–extracellular matrix structures.

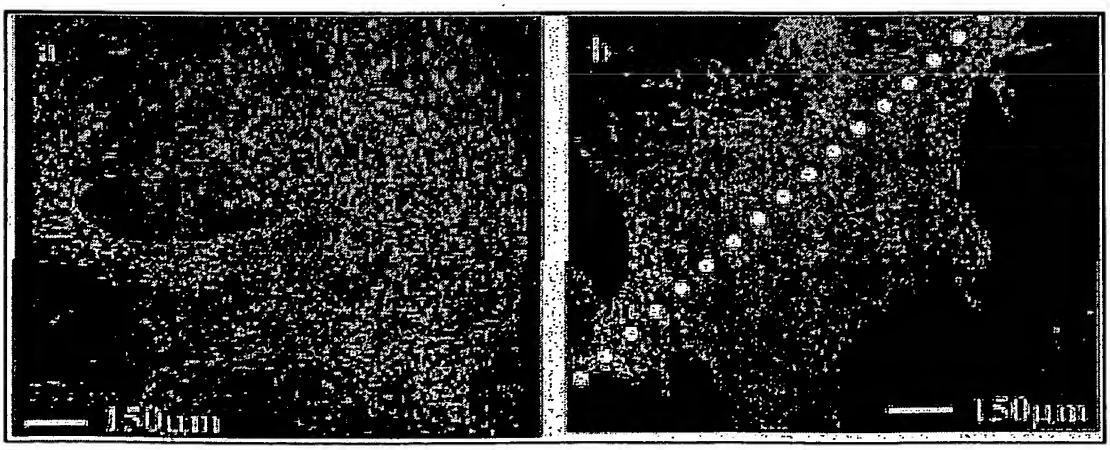

FIG. 4. Laser confocal depth projection micrograph of a cocultured osteochondral construct 11 weeks after bone marrow stromal cell seeding and 8 weeks after chondrocyte seeding. (a) Three-dimensional distribution of osteochondrogenic cells on chondrocyte-seeded side, 150 μm in depth. (b) Single horizontal-section image of integration of osteoblasts and chondrocytes over the gap (dotted line) of the PCL scaffold. (FDA–PI staining, green, living cells; red, metabolic, dead cells).

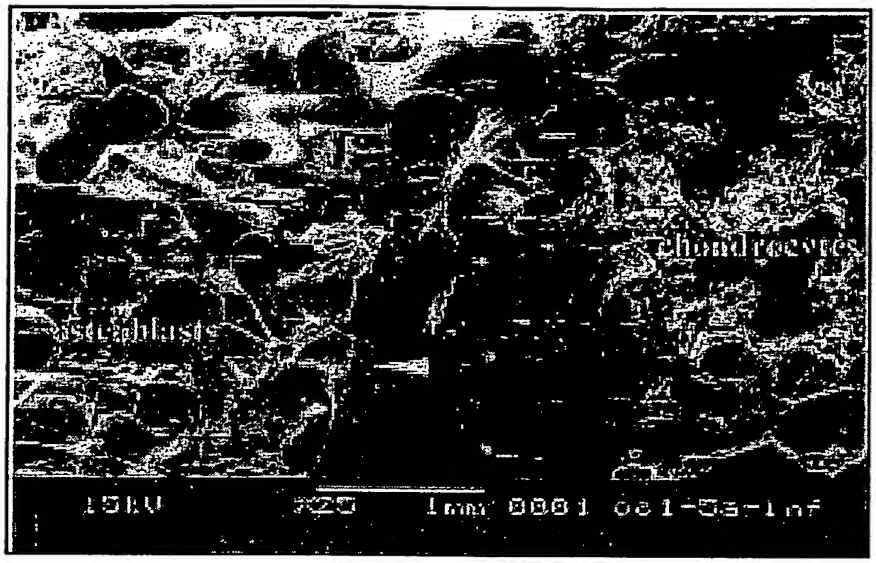

FIG. 5. SEM photograph of osteochondral construct cross-section 51 days after bone marrow stromal cell seeding and 33 days after chondrocyte seeding: stromal cell-seeded area (*right*), chondrocyte-seeded area (*left*), and the middle gap (arrowhead).

Alkaline phosphatase activity and osteocalcin expression were measured for 43 days after marrow stromal cells were seeded. The average alkaline phosphatase concentration was 0.0798 U/mL ± 3.9% in the supernatant of the isolated osteoblast culture before chondrocyte seeding. This was higher than in the control (0.0590 U/mL ± 2.3%; $p < 0.05$). Alkaline phosphatase expression rose to 0.1086 U/mL in the osteochondral coculture. This was significantly higher than in the control, which was only 0.0639 U/mL ± 2.1% ($p < 0.01$) or in the isolated osteoblast culture ($p < 0.05$) (Fig. 8A). The average osteocalcin expression was also higher in the isolated osteoblast culture (11.55 μg/L ± 3.4%) than in the control (7.45 μg/L ± 2.6%%; $p < 0.05$). But in the osteochondral coculture, it was 1.9 μg/L ± 3.1%, which was lower than in the control (6.87 μg/L ± 2.4%; $p < 0.01$) (Fig. 8B).

DISCUSSION

The importance of the 3-D scaffold architecture for tissue engineering has been highlighted by numerous authors. Jakob *et al.*[17] demonstrated that the conditions for expansion of human articular chondrocytes can assist the ability of cells to "re-enter the differentiation program" when they are transferred into an appropriate 3-D environment. This is in agreement with early work by Liu *et*

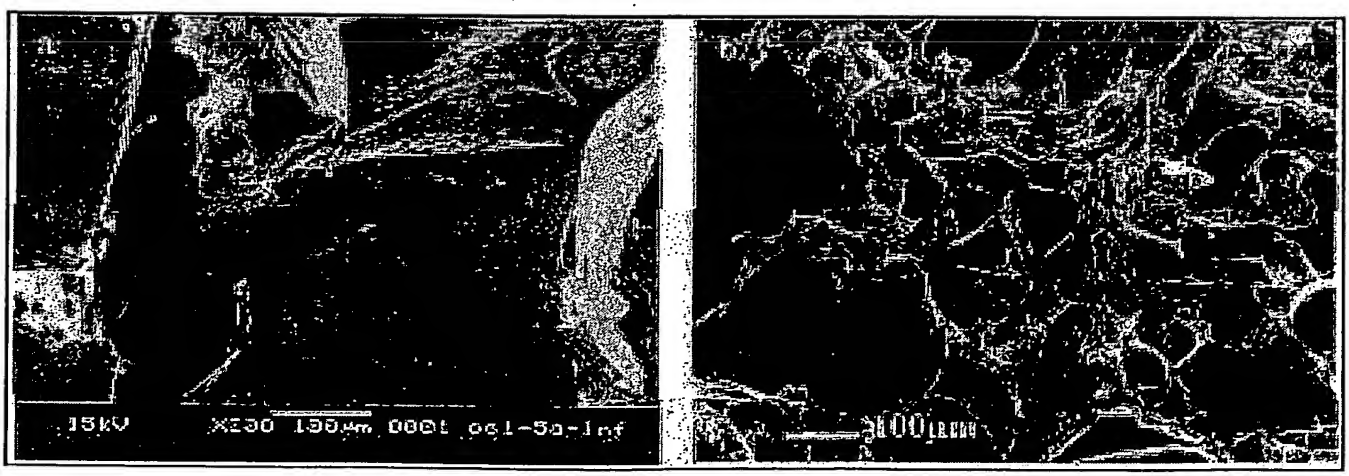

FIG. 6. SEM photographs of the appearance of different extracellular matrices 51 days after bone marrow stromal cell seeding and 33 days after chondrocyte seeding. (a) Extracellular matrix in the stromal cell-seeded compartment. (b) Extracellular matrix in chondrocyte-seeded compartment.

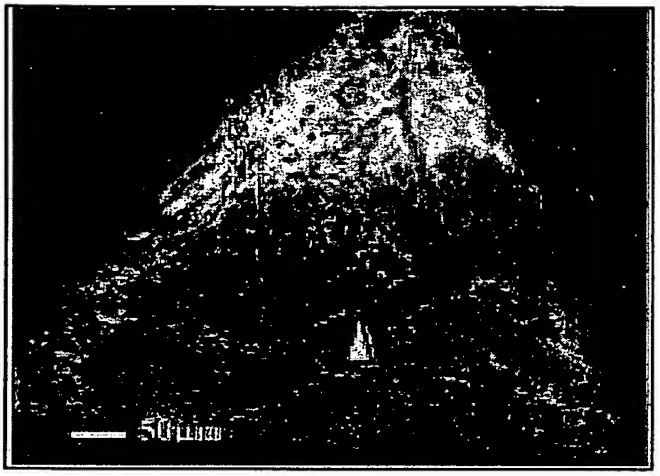

FIG. 7. Phase-contrast light micrograph of mineralized nodules (arrowhead) of extracellular matrix in the stromal cell-seeded compartment, 4 weeks after bone marrow stromal cell seeding.

al.,[18] who showed that chondrocytes became dedifferentiated when subcultured in monolayer and exhibited a fibroblastic morphology. However, when transferred to 3-D beads of alginate, the cells quickly regained their spherical shape. These results provide evidence that apart from growth factors and mechanostimulation, the 3-D environment is an important mediator for cell proliferation and differentiation. To quote Nerem,[19] "whatever the approach, the engineering of an architecture and of functional characteristics that allow one to mimic a specific tissue is critical to achieving any success." It is therefore clear that one of the crucial issues for the success of an osteochondral transplant lies in the design of the scaffolds.

Previously[14] we have shown that the scaffold structure for cell transplantation should be highly porous to provide an environment with a large surface-to-volume ratio into which transplanted cells could be seeded; attached, and allowed to proliferate and express their own extracellular matrix. The presence of fully interconnected channels is essential to enhance the diffusion of nutrients to the center of the scaffold and the transport of waste products away from it. This is particularly true for large constructs. Besides guiding cell organization and growth, and simultaneously allowing cells to be nourished by diffusion, the ideal scaffold should be designed to permit or even actively support vascularization. The transport of nutrients and waste products might be insufficient until angiogenesis takes place. The pore size should, therefore, be large enough to allow ingrowth of vessels. However, the detailed microstructure, such as the degree of porosity or the desired pore size, depends on the type of tissue to be regenerated. Pores give rise to stress concentrations and weaken the mechanical strength of the scaffolds. The ideal scaffold should also be a compromise between the mechanical stability of the scaffold and the interconnectivity of its pore network. Tissue growth depends on many other factors, such as the size and shape of the pores in the scaffold construct and the environment of the cell culture solution. The present results show that FDM-fabricated PCL scaffolds with a three-angle lay-out (0/60/120°) meet the 3-D architectural and biomaterial requirements for coculturing of osteoblasts and chondrocytes. Schaefer *et al.*[20] were the first to report on *in vitro* study intended to tissue engineer an osteochondral transplant by using nonwoven meshes made of polyglycolic acid (PGA), in the form of disks (5 mm in diameter and 2 mm thick). They concluded that it would be best to use mature bonelike constructs (to achieve mineralization) in combination with immature cartilaginous constructs (to promote integration at the tissue interface).

In the present study, the PCL templates supported *in vitro* the adhesion, proliferation, and differentiation of osteoblast-like cells and allowed the formation of mineralized extracellular matrix throughout the entire scaffold architecture. The fully interconnected scaffold architecture was completely filled by cellular tissue. The remarkable cubic distribution of the osteoblasts and chondrocytes as well as the rich formation of extracellular

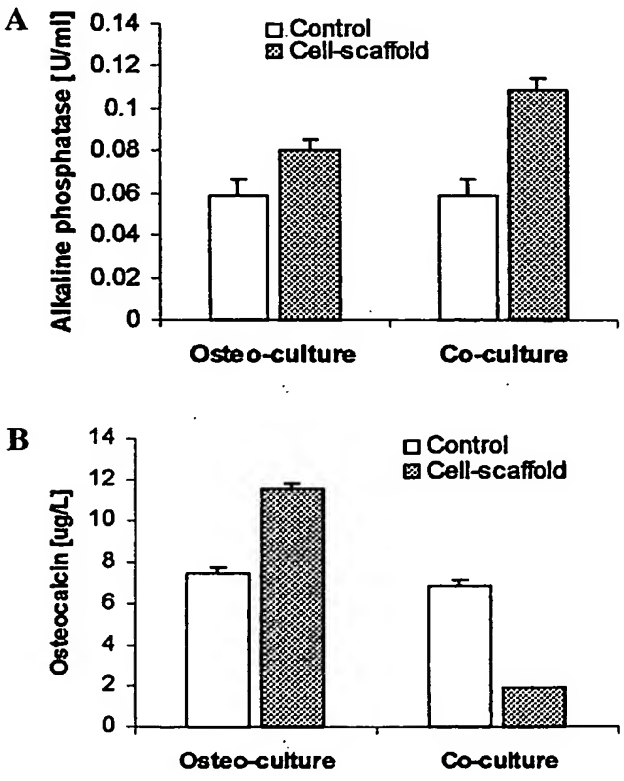

FIG. 8. (A) Average alkaline phosphatase and (B) osteocalcin of osteoculture (isolated osteoblast culture) and coculture (osteochondral coculture) over 43 days.

matrices of both cell types were attributed to the large surface area and the three-dimensional spatial architecture provided by the interconnected porous structure of the PCL scaffold design. This was consistent with previously reported bone tissue engineering using similar PCL scaffold patterns.[21,22] Implantation studies in nude mouse models showed that the PCL scaffold–osteoblast constructs led to bonelike tissue formation.[21]

The results here showed that osteoblasts and chondrocytes produced different extracellular matrices in each scaffold compartment. Both osteoblasts and chondrocytes attach and proliferate in the osteochondral construct coculture middle portion of the PCL scaffold. The microstructure of the extracellular matrix in the scaffold bone compartment was rougher than that in the scaffold cartilage compartment. This was due mainly to denser and more mineralized nodules deposited in the scaffold bone compartment. The *in vitro* tissue-engineered osteochondral construct structurally made of the PCL scaffold with osteochondrogenic cells would functionally maintain the proliferation of these cells and their production of osteochondral extracellular matrix as well. It has been reported that, in addition to forming bone and cartilage matrices, the extracellular matrices of the osteoblasts and chondrocytes are involved in osteogenic and chondrogenic functions of these cells and other cells by interaction with each other through particular proteins and molecules of the matrices.[23–26]

Alkaline phosphatase plays an important role in the formation of bone and cartilage, and is also used as a marker of the formation of these two tissues.[27–30] Before chondrocyte seeding to form the osteoblast–chondrocyte coculture, the alkaline phosphatase level of isolated osteoclast culture was lower. This indicated that alkaline phosphatase activity in the coculture was raised together by the osteoblasts and chondrocytes. Osteocalcin is known to be expressed only by functional osteoblasts.[31] Higher osteocalcin expression verified the osteoblastic phenotype in the isolated osteoblast culture (Fig. 8b, left). However, in our present work osteocalcin expression decreased when chondrocytes were added to the osteochondral coculture. We attribute this to the dilution of osteocalcin during the coculturing process. However, it could also be due to some process that leads to osteoblastic dysfunction in expressing ostoecalcin. Nonetheless, further work needs to be carried out to fully establish the mechanism of osteocalcin expression in the coculture situation. The osteocalcin concentration, the morphology of extracellular matrices, and the formation of mineralized nodules[32] in the extracellular matrices verified not only the osteogenic phenotype of osteoblasts differentiated from stromal cells but also the difference in phenotype between these osteoblasts and the chondrocytes derived from the rib cartilage.

Cartilaginous/bonelike tissue constructs based on autologous cells could have a major impact on joint osteochondral repair, and could overcome many of the existing limitations of osteochondral transplantation. Tissue grafts could potentially be grown *in vitro* starting from a small initial number of cells, obtained by a minimally invasive cell-harvesting procedure. Alternatively, mesenchymal progenitor cells from bone marrow could be induced to differentiate *in vitro* into chondrogenic and osteogenic cells, which would eliminate the need for tissue harvest from the articular joint surfaces. Ideally, tissue-engineered constructs would combine the advantages of a phenotypically stable and mechanically functional cartilage surface that could bear physiological loads, with enhanced integration at the graft–host interface mediated by functional bone tissue.

Rapid prototyping technologies can be used to manufacture scaffolds with more suitable structural and mechanical properties for bone and cartilage regeneration. Various PCL scaffolds were fabricated by novel fused deposition modeling.[13] The slow-degrading matrices produced had a fully interconnected coral-like pore architecture that revealed mechanical properties suitable for bone/cartilage tissue engineering. For load-bearing hard tissues, this FDM-fabricated coral-like scaffold could provide sufficient initial mechanical strength over a certain period of time to endure the *in vitro* and/or *in vivo* forces. The 3-D space for cell proliferation and differentiation, extracellular matrix production, and tissue growth and remodeling must be maintained until the tissue inside the scaffold architecture is mature enough to support the cell populations.

PCL an aliphatic polyester approved by the FDA as a bioabsorbable suture and drug delivery biomaterial.[33,34] *In vitro* biocompatibility of the *in situ*-polymerized PCL material has been assessed with osteoblasts derived from human craniofacial bone cells. The material is highly biocompatible with these cells, which will attach and spread on PCL.[35] PCL retains 60% of the original molecular weight after 15 weeks *in vivo*.[36] This slow biodegradation speed is suitable for new osteochondral tissue growth and reconstruction, as it allows the mechanoinduction of cells to proper phenotype. *In vivo* degradation of PCL begins with random hydrolytic chain scission of the ester linkages, manifested by a reduction in the viscosity and molecular weight of the polymer until the molecular weight has decreased to approximately 5000. The second phase of polymer degradation is characterized by a decrease in the rate of chain scission and the onset of weight loss, implant fragmentation, and intracellular degradation.[37–39] Replacement of the absorbed PCL scaffold by host bone and cartilage subsequently could result in natural bone and cartilage regeneration in the defect site after clinical reconstruction.

Besides its initial stiffness suitable to load bearing, which is critical to bone/cartilage regeneration and articular defect repair, PCL scaffolds can be further tailored

to be bioabsorbable from months to years, depending on clinical needs. It is also considerably less expensive than other biodegradable polyesters such as polylactide, polyglycolide, and their copolymers.[36]

CONCLUSIONS

This study demonstrated for the first time the successful *in vitro* coculturing of osteoblasts and chondrocytes on 3-D FDM PCL scaffolds for more than 50 days. It demonstrated that osteogenic and chondrogenic cells can grow, proliferate, distribute, and produce extracellular matrix in these novel 3-D FDM-fabricated PCL scaffolds under coculture conditions. However, the authors note that the final actual phenotype of the osteoblasts and chondrocytes in the PCL scaffolds can be ascertained only by other, more direct means such as DNA sequencing experiments. The three-dimensional porous PCL scaffold is biocompatible, as evidenced by extensive cell proliferation, and is suitable for *in vitro* osteochondral construct tissue engineering. This scaffold design has potential for use in clinical applications, especially in osteochondral defect repair.

ACKNOWLEDGMENTS

The authors acknowledge the assistance of Mr. K.C. Tan (Temasek Polytechnic) in using FDM to fabricate the PCL scaffolds. Thanks are also due to Dr. M. Harris, Dr. J.T. Schantz, Mr. K.W. Ng, and Ms. A.M. Chou for initial help in cell culture and discussion. Thanks are also due to Prof. C.L. Chew for moral support in this research. This work was supported by the NUS Academic Research Fund (grant R-223-000-002-112 and R-265-000-038-112).

REFERENCES

1. Mankin, H.J. The response of articular cartilage to mechanical injury. J. Bone Joint Surg. **64,** 460, 1982.
2. Newman, A.P. Current concepts: Articular cartilage repair. Am. J. Sports Med. **26,** 309, 1998.
3. Buckwalter, J.A., and Mankin, H.J. Articular cartilage: Degeneration and osteoarthritis, repair, regeneration, and transplantation. In: Cannon, W.D., Jr., ed. American Academy of Orthopaedic Surgery Instructional Course Lectures. Rosemont, IL: American Academy of Orthopaedic Surgeons, 1998, pp. 487–504.
4. Ficat, R.P., Ficat, C., Gedeon, P., and Toussaint, J.B. Spongialization: A new treatment for diseased patellae. Clin. Orthop. **144,** 74, 1979.
5. Chen, F.S., Frenkel, S.R., and DiCesare, P.E. Repair of articular cartilage defects. II. Treatment options. Am. J. Orthop. **28,** 88, 1999.
6. Hangody L., Kish, G., Karpati, Z., Udvarhelyi, I., Szigeti, I., and Bely, M. Mosaicplasty for the treatment of articular cartilage defects: Application in clinical practice. Orthopedics **21,** 751, 1998.
7. Mitchell, N., and Shepard, N. The resurfacing of adult rabbit articular cartilage by multiple perforation through the subchondral bone. J. Bone Joint Surg. **58,** 230, 1976.
8. Levy, A.S., Lohnes, J., Sculley, S., LeCroy, M., and Garrett, W. Chondral delamination of the knee in soccer players. Am. J. Sports Med. **24,** 634, 1996.
9. Goldberg, V.M., and Caplan, A.I. Biologic restoration of articular surfaces. In: Zuckerman, J.D., and Rosemont, J.D., eds. Instructional Course Lectures. Rosemont, IL: American Academy of Orthopaedic Surgeons, 1999, pp. 623–627.
10. Klompmaker, J., Jansen, H.W.B., Veth, R.P.H., deGroot, J.H., Nijenhuis, A.J., and Pennings, A.J. Porous polymer implant for repair of meniscal lesions: A preliminary study in dogs. Biomaterials **12,** 810, 1991.
11. Harris, L.D., Kim, B.-S., and Mooney, D.J. Open pore biodegradable matrices formed with gas foaming. J. Biomed. Mater. Res. **42,** 396, 1998.
12. Slivka, M.A., Leatherbury, N.C., Kieswetter, K., and Niederauer, G.G. In vitro compression testing of fiber-reinforced, bioabsorbable, porous implants. In: Agrawal, C.M., Parr, J.E., and Lin, S.T., eds. Synthetic Bioabsorbable Polymers for Implants, ASTM STP 1396. West Conshohocken, PA: American Society for Testing and Materials, 2000, pp. 124–135.
13. Hutmacher, D.W., Zein, I., Teoh, S.H., Ng, K.W., Schantz, J.T., and Leahy, J.C. Design and fabrication of a 3D scaffold for tissue engineering bone. In: Agrawal, C.M., Parr J.E., and Lin, S.T., eds. Synthetic Bioabsorbable Polymers for Implants, ASTM STP 1396. West Conshohocken, PA: American Society for Testing and Materials, 2000, pp. 152–167.
14. Hutmacher, D.W., Schantz, T., Zein, I., Ng, K.W., Teoh, S.H., and Tan, K.C. Mechanical properties and cell cultural response of polycaprolactone scaffolds designed and fabricated via fused deposition modelling. J. Biomed. Mater. Res. **55,** 203, 2001.
15. Ishaug, S.L., Crane G.M., Miller, M.J., Yasko, A., Yaszemski, M.J., and Mikos, A.G. Bone formation by three-dimensional stromal osteoblast culture in biodegradable polymer scaffolds. J. Biomed. Mater. Res. **36,** 17, 1997.
16. Caplan, A.I. Mesenchymal stem-cells. J. Orthop. Res. **9,** 641, 1991.
17. Jakob, M., Démarteau, O., Schäfer, D., Hintermann, B., Dick, W., Heberer, M., and Martin, I. Specific growth factors during the expansion and redifferentiation of adult human articular chondrocytes enhance chondrogenesis and cartilaginous tissue formation in vitro. J. Cell. Biochem. **81,** 368, 2001.
18. Liu, H., Lee, Y.W., and Dean, M.F. Re-expression of differentiated proteoglycan phenotype by dedifferentiated human chondrocytes during culture in alginate beads. Biochim. Biophys. Acta **1425,** 505, 1998.
19. Nerem, R.M. The challenge of imitating nature. In: Lanza, R.P., Langer, R., and Vacanti, J., eds. Principles of Tissue Engineering, 2nd Ed. New York: Academic Press, Ch. 2, 2000.
20. Schaefer, D., Martin, I., Shastri, P., Padera, R.F., Langer, R.,

Freed, L.E., and Vunjak-Novakovic, G. In vitro generation of osteochondral composites. Biomaterials **21,** 2599, 2000.
21. Cao, T., Hutmacher, D.W., Ho, K.H., Kiefer, T., Chew, C.L., and Teoh, S.H. Bone tissue engineering by using porous poly-ϵ-caprolactone scaffold and human bone marrow stromal cells. Int. J. Oral Maxillofac. Surg. **30,** S64, 2001.
22. Ho, K.H., Cao, T., Hutmacher, D.W., Kiefer, T., Chew, C.L., and Teoh, S.H. Tissue-engineered bone formation in an implant–scaffold construct. Int. J. Oral Maxillofac. Surg. **30,** S66, 2001.
23. Carinci, P., Becchetti, E., and Bodo, M. Role of the extracellular matrix and growth factors in skull morphogenesis and in the pathogenesis of craniosynostosis. Int. J. Dev. Biol. **44,** 715, 2000.
24. Bennett, J.H., Moffatt, S., and Horton, M. Cell adhesion molecules in human osteoblasts: Structure and function. Histol. Histopathol. **16,** 603, 2001.
25. Gronthos, S., Simmons, P.J., Graves, S.E., and Robey, P.G. Integrin-mediated interactions between human bone marrow stromal precursor cells and the extracellular matrix. Bone **28,** 174, 2001.
26. Zhu, J.X., Sasano, Y., Takahashi, I., Mizoguchi, I., and Kagayama, M. Temporal and spatial gene expression of major bone extracellular matrix molecules during embryonic mandibular osteogenesis in rats. Histochem. J. **33,** 25, 2001.
27. Li, X.B., Yang, S.Z., Li, S.G., Jiang P.D., and Lin, Z.H. Effects of simulated microgravity on the alkaline phosphatase activity and intracellular calcium concentration of cultured chondrocytes. Chin. Sci. Bull. **44,** 218, 1999.
28. Namkung-Matthai, H., Diwan, A., Mason, R.S., Murrell, G.A.C., and Diamond, T. Redox. Rep. **5,** 126, 2000.
29. Sasaki, T., Amizuka, N., Irie, K., Ejiri, S., and Ozawa, H. Localization of alkaline phosphatase and osteopontin during matrix mineralization in the developing cartilage of coccygeal vertebrae. Arch. Histol. Cytol. **63,** 271, 2000.
30. Tuckermann, J.P., Pittois, K., Partridge, N.C., Merregaert, J., and Angel, P. Collagenase-3 (MMP-13) and integral membrane protein 2a (Itm2a) are marker genes of chondrogenic/osteoblastic cells in bone formation: Sequential temporal, and spatial expression of Itm2a, alkaline phosphatase, MMP-13, and osteocalcin in the mouse. J. Bone Miner. Res. **15,** 1257, 2000.
31. Nefussi, J.R., Brami, G., Modrowski, D., Oboeuf, M., and Forest, N. Sequential expression of bone matrix proteins during rat calvaria osteoblast differentiation and bone nodule formation in vitro. J. Histochem. Cytochem. **45,** 493, 1997.
32. Buttery, L.D., Bourne, S., Xynos, J.D., Wood, H., Hughes, F.J., Hughes, S.P., Episkopou, V., and Polak, J.M. Differentiation of osteoblasts and in vitro bone formation from murine embryonic stem cells. Tissue Eng. **7,** 89, 2001.
33. Pitt, C.G. Poly(ϵ-caprolactone) and its copolymers. In: Chasin, R., and Langer, R., eds. Biodegradable Polymers as Drug Delivery Systems. New York: Marcel Dekker, 1990, pp. 71–120.
34. Barber, F.A., and Click, J.N. The effect of inflammatory synovial-fluid on the breaking strength of new lasting absorbable sutures. Arthroscopy **8,** 437, 1992.
35. Corden, T.J., Jones, I.A., Rudd, C.D., Christian, P., Downes, S., and McDougal, K.E. Physical and biocompatibility properties of poly-ϵ-caprolactone produced using in situ polymerisation: A novel manufacturing technique for long-fibre composite materials. Biomaterials **21,** 713, 2000.
36. Vandamme, T.F., and Legras, R. Physico-mechanical properties of poly(ε-caprolactone) for the construction of rumino-reticulum devices for grazing animals. Biomaterials **16,** 1395, 1995.
37. Schindler, A., Jeffcoat, R., Kimmel, G.L., Pitt, C.G., Wall, M.E., and Zweidinger, R. Biodegradable polymers for sustained drug delivery. Contemp. Top. Polym. Sci. **2,** 251, 1977.
38. Pitt, C.G., Chasalow F.I., Hibionada, Y.M., Klimas, D.M., and Schindler, A. Aliphatic polyesters. I. The degradation of poly(ϵ-caprolactone) in vivo. J. Appl. Polym. Sci. **26,** 3779, 1981.
39. Vert, M., Li, S.M., Spenlehauer, G., and Guerin, P. Bioresorbability and biocompatibility of aliphatic polyesters. J. Mater. Sci. Mater. Med. **3,** 432, 1992.

Address reprint requests to:
S.H. Teoh, Ph.D.
Division of Bioengineering
National University of Singapore
10 Kent Ridge Crescent
119260 Singapore

E-mail: bietsh@nus.edu.sg

This article has been cited by:

1. Limin Wang , Michael S. Detamore . 2007. Tissue Engineering the Mandibular Condyle. *Tissue Engineering* 13:8, 1955-1971. [Abstract] [PDF] [PDF Plus]
2. L. Moroni , J.A.A. Hendriks , R. Schotel , J.R. de Wijn , C.A. van Blitterswijk . 2007. Design of Biphasic Polymeric 3-Dimensional Fiber Deposited Scaffolds for Cartilage Tissue Engineering Applications. *Tissue Engineering* 13:2, 361-371. [Abstract] [PDF] [PDF Plus]
3. Bina Rai, Megan E. Oest, Ken M. Dupont, Kee H. Ho, Swee H. Teoh, Robert E. Guldberg. 2007. Combination of platelet-rich plasma with polycaprolactone-tricalcium phosphate scaffolds for segmental bone defect repair. *Journal of Biomedical Materials Research Part A* 81a:4, 888. [CrossRef]
4. C. Scotti, M. S. Buragas, L. Mangiavini, C. Sosio, A. Giancamillo, C. Domeneghini, G. Fraschini, G. M. Peretti. 2007. A tissue engineered osteochondral plug: an in vitro morphological evaluation. *Knee Surgery Sports Traumatology Arthroscopy* . [CrossRef]
5. Neethu Mohan, Prabha D. Nair. 2007. Polyvinyl alcohol-poly(caprolactone) Semi IPN scaffold with implication for cartilage tissue engineering. *Journal of Biomedical Materials Research Part B Applied Biomaterials* . [CrossRef]
6. Ching-Chuan Jiang, Hongsen Chiang, Chun-Jen Liao, Yu-Ju Lin, Tzong-Fu Kuo, Chang-Shun Shieh, Yi-You Huang, Rocky S. Tuan. 2007. Repair of porcine articular cartilage defect with a biphasic osteochondral composite. *Journal of Orthopaedic Research* . [CrossRef]
7. J. F. Mano, R. L. Reis. 2007. Osteochondral defects: present situation and tissue engineering approaches. *Journal of Tissue Engineering and Regenerative Medicine* 1:4, 261. [CrossRef]
8. Wei Sun , Yongnian Yan , Feng Lin , Myron Spector . 2006. Biomanufacturing: A US-China National Science Foundation–Sponsored Workshop. *Tissue Engineering* 12:5, 1169-1181. [Abstract] [PDF] [PDF Plus]
9. Massimo Mariani , Frederica Rosatini , Giovanni Vozzi , Antonino Previti , Arti Ahluwalia . 2006. Characterization of Tissue-Engineered Scaffolds Microfabricated with PAM. *Tissue Engineering* 12:3, 547-558. [Abstract] [PDF] [PDF Plus]
10. Suh-Chin Wu, Jung-Chuan Yu, Shan-hui Hsu, David Chanhen Chen. 2006. Artificial extracellular matrix proteins contain heparin-binding and RGD-containing domains to improve osteoblast-like cell attachment and growth. *Journal of Biomedical Materials Research Part A* 79a:3, 557. [CrossRef]
11. Donggang Yao, Aaron Smith, Pratapkumar Nagarajan, Adrian Vasquez, Loan Dang, G. Rasul Chaudhry. 2006. Fabrication of polycaprolactone scaffolds using a sacrificial compression-molding process. *Journal of Biomedical Materials Research Part B Applied Biomaterials* 77b:2, 287. [CrossRef]
12. R. B. Diego, M. P. Olmedilla, Á S. Aroca, J. L. G. Ribelles, M. M. Pradas, G. G. Ferrer, M. S. Sánchez. 2005. Acrylic scaffolds with interconnected spherical pores and controlled hydrophilicity for tissue engineering. *Journal of Materials Science* 40:18, 4881. [CrossRef]
13. R. Brígido Diego, M. Pérez Olmedilla, A. Serrano Aroca, J. L. Gómez Ribelles, M. Monleón Pradas, G. Gallego Ferrer, M. Salmerón Sánchez. 2005. Acrylic scaffolds with interconnected spherical pores and controlled hydrophilicity for tissue engineering. *Journal of Materials Science Materials in Medicine* 16:8, 693. [CrossRef]
14. Chih-Hung Chang, Feng-Huei Lin, Chien-Cheng Lin, Cheng-Hung Chou, Hwa-Chang Liu. 2004. Cartilage tissue engineering on the surface of a novel gelatin-calcium-phosphate biphasic scaffold in a double-chamber bioreactor. *Journal of Biomedical Materials Research* 71b:2, 313. [CrossRef]
15. Tejas S. Karande, Joo L. Ong, C. Mauli Agrawal. 2004. Diffusion in Musculoskeletal Tissue Engineering Scaffolds: Design Issues Related to Porosity, Permeability, Architecture, and Nutrient Mixing. *Annals of Biomedical Engineering* 32:12, 1728. [CrossRef]
16. Boon Chin Heng, Tong Cao, Lawrence Walter Stanton, Paul Robson, Bjorn Olsen. 2004. Strategies for Directing the Differentiation of Stem Cells Into the Osteogenic Lineage In Vitro. *Journal of Bone and Mineral Research* 19:9, 1379. [CrossRef]

EXHIBIT 4

ELSEVIER

Biomaterials 23 (2002) 1169–1185

Biomaterials

www.elsevier.com/locate/biomaterials

Fused deposition modeling of novel scaffold architectures for tissue engineering applications

Iwan Zein[a], Dietmar W. Hutmacher[b,*], Kim Cheng Tan[c], Swee Hin Teoh[a]

[a] *Laboratory for Biomedical Engineering (LBME), E305-16, Department of Mechanical Engineering, National University of Singapore, 10 Kent Ridge Crescent, Singapore 119260, Singapore*

[b] *Department of Orthopaedic Surgery, National University Hospital, 5 Lower Kent Ridge Road, Singapore 119074, Singapore*

[c] *Temasek Engineering School, Temasek Polytechnic, 21 Tampines Avenue 1, Singapore, 529757, Singapore*

Received 13 November 2000; accepted 22 June 2001

Abstract

Fused deposition modeling, a rapid prototyping technology, was used to produce novel scaffolds with honeycomb-like pattern, fully interconnected channel network, and controllable porosity and channel size. A bioresorbable polymer poly(ε-caprolactone) (PCL) was developed as a filament modeling material to produce porous scaffolds, made of layers of directionally aligned microfilaments, using this computer-controlled extrusion and deposition process. The PCL scaffolds were produced with a range of channel size 160–700 μm, filament diameter 260–370 μm and porosity 48–77%, and regular geometrical honeycomb pores, depending on the processing parameters. The scaffolds of different porosity also exhibited a pattern of compressive stress–strain behavior characteristic of porous solids under such loading. The compressive stiffness ranged from 4 to 77 MPa, yield strength from 0.4 to 3.6 MPa and yield strain from 4% to 28%. Analysis of the measured data shows a high correlation between the scaffold porosity and the compressive properties based on a power–law relationship.

Keywords: Tissue engineering; Scaffold; Fused deposition modeling; Bioresorbable polymer; Porosity; Interconnected channel network; Compressive properties

1. Introduction

Different processing techniques have been developed to build scaffolds for tissue engineered constructs [1,2]. These conventional techniques include fiber-bonding, solvent casting and particulate leaching, membrane lamination, melt molding, thermally induced phase separation and gas foaming. None of these conventional techniques has allowed researchers to build scaffolds—with a completely interconnected pore network with large interconnection channels, a highly regular and reproducible scaffold morphology—by using a computer-controlled design and fabrication process [2]. The imperfection of the conventional techniques has encouraged the use of a rapid prototyping (RP) technology, also known as solid freeform fabrication (SFF) technology, in the scaffold design and fabrication stages of tissue engineering. At present, there are a number of RP techniques that have been reported on fabrication of bioresorbable scaffolds. Three-dimensional printing (3DP) led the group with the most publications as a new method of scaffold fabrication using poly(lactic acid) and poly(lactic-co-glycolic acid) [3–5]. The 3DP method requires the use of organic solvents as binder for the powder-based aliphatic polyesters. The other two methods reported recently are known as multi-phase jet solidification [6] and shape deposition manufacturing [7,8]. Our group has applied fused deposition modeling (FDM) [9] to design and fabricate bioresorbable scaffolds with a fully interconnected channel network. In comparison with other SFF techniques, the FDM method does not require any solvent and offers great ease and flexibility in material handling and processing. The use of a filament modeling material also reduces its residence time in the heating compartment and allows continuous production without the need of replacing feedstock.

*Corresponding author.

0142-9612/02/$-see front matter
PII: S0142-9612(01)00232-0

1.1. Fused deposition modeling process

The FDM method forms three-dimensional objects from computer generated solid or surface models like in a typical RP process. Models can also be derived from computer tomography scans, magnetic resonance imaging scans or model data created from 3D object digitizing systems. FDM uses a small temperature-controlled extruder to force out a thermoplastic filament material and deposit the semi-molten polymer onto a platform in a layer by layer process. The monofilament is moved by two rollers and acts as a piston to drive the semi-molten extrudate. At the end of each finished layer, the base platform is lowered and the next layer is deposited. The designed object is fabricated as a three-dimensional part based solely on the precise deposition of thin layers of the extrudate. The deposition path and parameters for every layer are designated depending on the material used, the fabrication conditions, the applications of the designed part and the preferences of the designer. Figs. 1 and 2 illustrate the FDM process.

The processing parameters of filling each layer depend on the earlier inputs into the slicing software. These include the FDM head speed, the roller speed, the slice interval, and the direction of deposition within each layer. Each layer is made of "roads" deposited in the X- and Y-directions, in a raster, a contour or a combination of both. The direction of deposition is known as the "raster angle" for raster filling and this can be specified for each layer between 0° and 180° with respect to the X-axis. The road width (RW) is controlled both by the flow parameters at a set temperature above the melting temperature of the thermoplastic material and also by the fine size of nozzle tip used. As the current standard

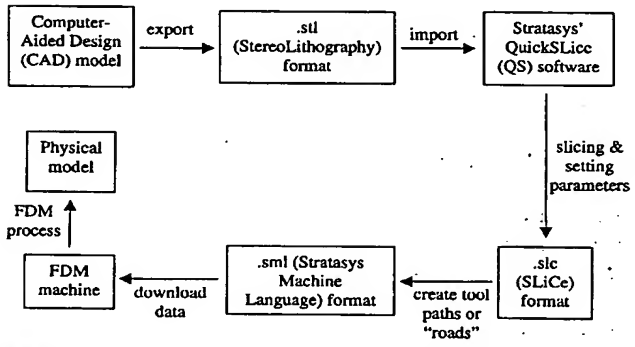

Fig. 1. Summary of a basic FDM process. Step 1: Import of CAD data in. stl (STereoLithography) format into QuickSlice™. Step 2: Slicing of the CAD model into horizontal layers and conversion into a. slc (SLiCe) format. Step 3: Creation of deposition path for each layer and conversion into a. sml (Stratasys Machine Language) format for downloading to FDM machine. Step 4: FDM fabrication process using a filament modeling material to build actual physical part in an additive manner layer-by-layer.

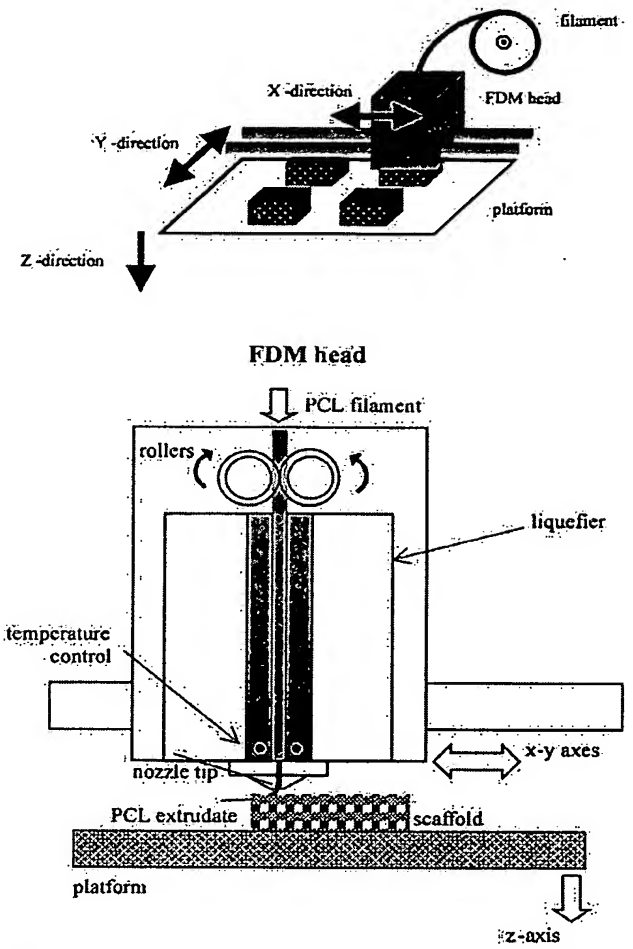

Fig. 2. A schematic diagram of the FDM extrusion and deposition process. The nozzle tip could be changed into different sizes for different RW and thickness. The layers of roads were fused together upon solidification to form a 3D structure.

modeling materials used for RP processes including FDM, are non-bioresorbable, we have first developed our own filament modeling material based on a bioresorbable polyester.

1.2. Poly(ε-caprolactone)

Poly(ε-caprolactone) (PCL) has an unusually low glass transition temperature of −60°C, among the bioresorbable polymers used for biomedical applications. It exists in a rubbery state at room temperature, and also has a low melting temperature of 60°C. Another unusual property of PCL is its high thermal stability. Whereas other tested aliphatic polyesters had decomposition temperatures (T_d) between 235°C and 255°C, PCL has a T_d of 350°C [10]. The mechanical properties of solid PCL ($M_w = 44,000$) have been

reported [11], with a tensile strength of 16 MPa, tensile modulus of 400 MPa, flexural modulus of 500 MPa, elongation at yield of 7.0% and elongation at break at 80%.

In comparison with the other commercially available bioresorbable polymers, PCL is one of the most flexible and easy to process materials. The structural stability and less sensitive manner to environmental conditions, such as temperature, moisture, etc. make PCL an ideal material for the FDM fabrication process. Among the many biodegradable and bioresorbable polymers studied for medical and drug delivery devices as well as scaffold materials, we have selected a high molecular weight PCL as our modeling material. Extensive in vitro and in vivo biocompatibility and efficacy studies have been performed, resulting in FDA approval of a number of medical and drug delivery devices composed of PCL [11–15].

The in vitro and in vivo performance of PCL scaffolds, build by FDM, in tissue engineering bone and cartilage has been reported elsewhere [16–18]. This paper reports on the physical properties of PCL scaffolds designed and fabricated via FDM.

2. Materials and methods

2.1. Filament fabrication

A one-shot extruder (Alex James & Associates Inc., Greensville, SC) was first used to fabricate PCL monofilaments of diameter 1.70 + 0.08 mm from PCL pellets purchased from Aldrich Chemical Company, Inc. (Milwaukee, Winconsin). The filament diameter was required for use with an unmodified FDM machine. The average M_n was quoted as ca. 80,000 (GPC) and the pellets were used as received.

2.2. Gel permeation chromatography

The polymer molecular weight distribution was determined by gel permeation chromatography equipped with a differential refractor (Waters, Model 410, Milford, MA) and an absorbance detector refractor (Waters, Model 2690, Milford, MA). The samples were dissolved in tetrahydrofuran and eluted in a series of configurations through a Styragel columns refractor (Waters, Milford, MA) at a flow rate of 1 ml/min. Polystyrene standards (Polysciences, Warrington, PA) were used to obtain a calibration curve.

2.3. DSC analysis

A thermal analysis differential scanning calorimeter (TA Instruments DSC 2910, New Castle, DE) was used to determine the thermal response of raw PCL for filament fabrication and subsequent FDM processing. The instrument was calibrated with an indium standard. The sample weight used was 7–10 mg. All samples were placed in aluminum pans and scanned from 25°C to 100°C at a ramp rate of 5°C/min, using argon as purge gas. A total of three samples were analyzed.

2.4. Optimization of FDM processing parameters

An optimized FDM process involves complex interactions among the hardware, software and material properties [19]. Preliminary trials revealed that the liquefier temperature and the filament feed rate had the most direct influence on the material flow for the fabrication of porous models. Hence, the optimization of the processing parameters for PCL was primarily focused on both the liquefier temperature and the roller speed (groove radius 5 mm). Using a low FDM head speed of 6.35 mm/s for steady material deposition in a minimum fabrication time, we first determined the minimum roller speed to obtain a specific extrudate diameter for a constant volumetric flow [20]. After which we obtained optimum values of liquefier temperature and filament feed rate through an iterative modification to achieve a target raster RW.

The RW was targeted slightly above the inner diameter of the smallest nozzle tip in-use, for stable flow during extrusion. With the smallest nozzle tip T10 (inner diameter 0.010 in), the target RW was set as approximately 0.254 mm. Thin layers of trial specimens with a slice thickness (ST) of 0.254 mm were fabricated in succession until the target RW was achieved. The workable range of FDM liquefier temperature and roller speed were determined as 125 ± 5°C and 0.080 ± 0.005 rps, respectively, for processing our PCL filaments. The next larger tip size T16 (0.016 in) was also used without changing the build or flow parameters. Only these two tip sizes were experimented, as we wanted to keep RW as small as possible to produce a fine microstructure for our scaffolds.

2.5. Scaffold design and fabrication

PCL scaffolds were fabricated for two experiments. The first experiment was to investigate the anisotropy of scaffolds with different internal architecture. The second experiment was to study the effect of different porosity and channel size on the scaffold mechanical properties.

For experiment I, two rectangular prisms, each measuring 32.0 mm (length) by 25.5 mm (breadth) by 13.5 mm (height), were first created in the Unigraphics CAD software (EDS, Plano, TX). The geometric models were exported into the QuickSlice™ software (Stratasys, Eden Prairie, MN) in.stl file format. Each scaffold model was cut into 54 horizontal layers with a ST of 0.254 mm. For all the layers, a single contour and raster-

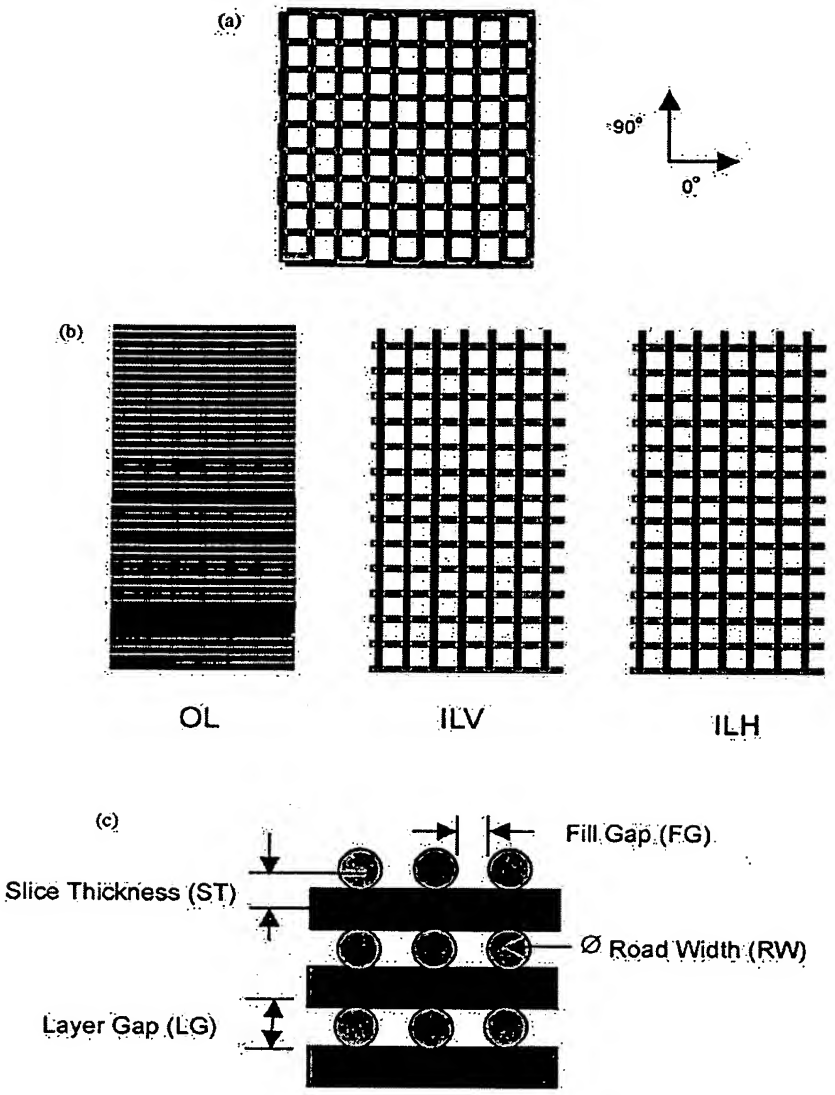

Fig. 3. (a) Lay-down pattern of 0/90° forming square honeycomb pores viewed in the $-Z$ direction of the FDM build process. (b) Alignment of filaments in scaffold specimens with a 0/90° lay-down pattern. In the OL orientation, the filaments are aligned in the XY-plane. In both ILV and ILH orientations, the filaments are aligned in the XZ-plane and YZ-plane, respectively. (c) Cross-section viewed in the XZ plane of the FDM build process. Symbols are denoted as RW: road width, FG: fill gap, ST: slice thickness, LG: layer gap.

fill pattern was adopted. Two lay-down patterns 0/90° (Figs. 3a–c) and 0/60/120° (Figs. 4a–c) were used to form the honeycomb patterns of square (Fig. 3a) and triangular (Fig. 4a) pores, respectively. A single fill gap (FG) of 0.610 mm was selected to impart similar porosity to both scaffold models. Based on two lay-down patterns and one FG, two blocks of scaffolds were fabricated using the FDM 3D Modeler system, with the T16 nozzle tip. The liquefier temperature was set at 125°C and the ambient temperature was maintained at 25±2°C during the fabrication process. After fabrication, the two PCL scaffold blocks were removed from the base and stored in a dessicator. The scaffold with a 0/90° lay-down pattern was labeled as C2-16-24 and the other with a 0/60/120° pattern as C3-16-24.

For experiment II, four rectangular prisms of the same size were created and sliced at the same thickness ST 0.254 mm. The two lay-down patterns of 0/90° and 0/60/120° were used with two different FG 0.508 and 0.711 mm. Based on the two lay-down patterns and two FGs, four blocks of scaffolds were fabricated first with the T16 nozzle tip. The entire process was repeated with

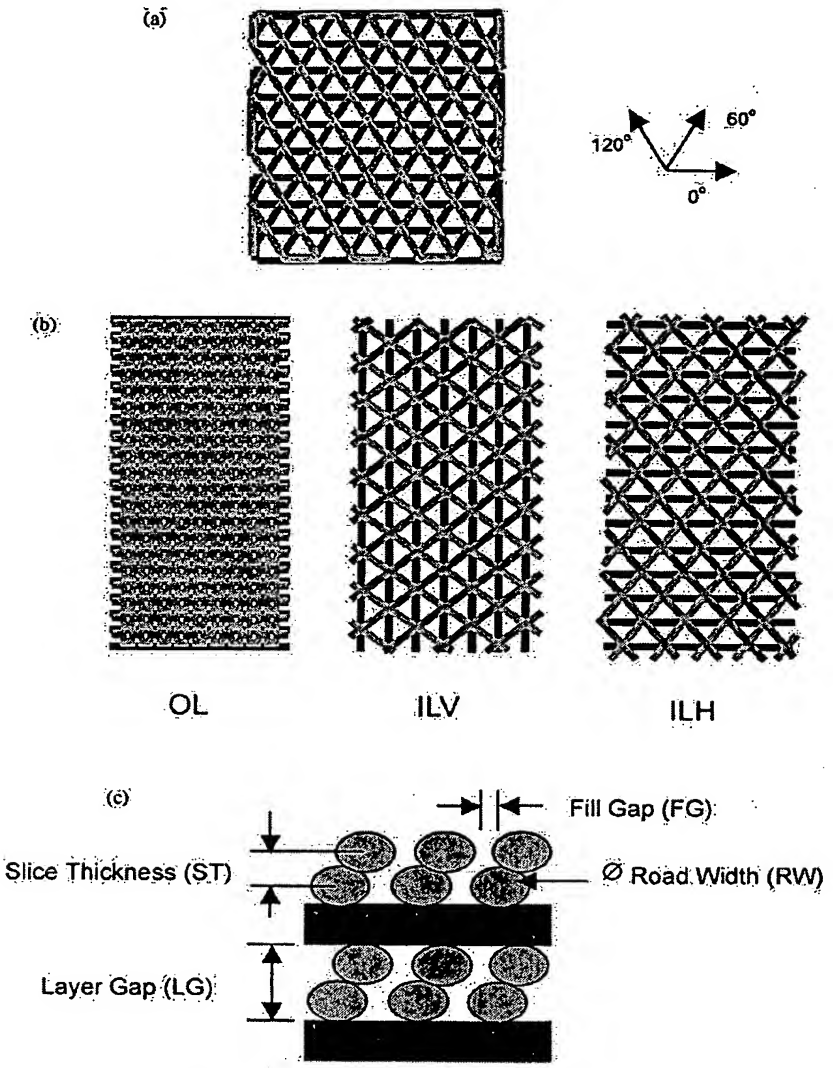

Fig. 4. (a) Lay-down pattern of 0/60/120° forming triangular honeycomb pores viewed in the $-Z$ direction of the FDM build process. (b) Alignment of filaments in scaffold specimens with a 0/60/120° lay-down pattern. In the OL orientation, the filaments are aligned in the XY-plane. In both ILV and ILH orientations, the filaments are aligned in the XZ-plane and YZ-plane, respectively. (c) Cross-section viewed in the XZ plane of the FDM build process. Symbols are denoted as RW: road width, FG: fill gap, ST: slice thickness, LG: layer gap.

the finer T10 nozzle tip to produce another four scaffold blocks. The fabrication conditions were the same as for the first experiment. Ten blocks of PCL scaffolds were fabricated for both experiments. They are labeled in Table 1 according to their lay-down pattern, tip size used, set values of ST and FG, and approximate RW values. All scaffold specimens were stored in a dessicator prior to usage.

2.6. Preparation of test specimens

The fabricated blocks were first measured for its true volume using a gas pycnometer as described in the following section. For experiment I, after calculating the porosity based on true volume measurement, each block was cut using a sharp blade in three orthogonal planes to produce 12 small rectangular specimens each measuring 7.0 mm (length) by 7.0 mm (breadth) by 13.5 mm (height). A fresh blade was replaced after every ten cuts. The specimens were labeled for three orientations out-of-layer (OL), in-layer-vertical (ILV) and in-layer-horizontal (ILH), according to the alignment of filaments in the longitudinal direction of the final specimen. For scaffolds with a 0/90° lay-down pattern, the alignment of the filaments for each group is shown in Fig. 3b. For

Table 1
Scaffold specimen groups for experiments I and II[a]

Specimen group	Tip size used	Lay-down pattern (°)	ST (mm)	RW (mm)[b]	FG (mm)
C2-16-24	T16	0/90	0.254	0.406	0.610
C3-16-24	T16	0/60/120	0.254	0.406	0.610
C2-10-20	T10	0/90	0.254	0.254	0.508
C2-10-28	T10	0/90	0.254	0.254	0.711
C3-10-20	T10	0/60/120	0.254	0.254	0.508
C3-10-28	T10	0/60/120	0.254	0.254	0.711
C2-16-20	T16	0/90	0.254	0.406	0.508
C2-16-28	T16	0/90	0.254	0.406	0.711
C3-16-20	T16	0/60/120	0.254	0.406	0.508
C3-16-28	T16	0/60/120	0.254	0.406	0.711

[a]The first two rows are for specimens in experiment I. Rows 3–10 are for specimens in experiment II.
[b]Estimated based on inner diameter of tip size in-use.

scaffolds with a 0/60/120° lay-down pattern, the alignment of filaments for each group is shown in Fig. 4b. From an initial two large blocks, six sets of test specimens were prepared in three orientations of filament alignment, with each set consisting of four individual specimens. Three specimens from each set were used for compressive testing.

For experiment II, after calculation of porosity, the scaffold block was cut into two different planes to also produce 12 small rectangular prisms of 7.0 mm (length) by 7.0 mm (breadth) by 13.5 mm (height). From an initial eight large blocks, 16 sets of test specimens were prepared in two orientations OL and ILV of filament alignment, with each set consisting of six individual specimens. One specimen from each of the 16 sets was put aside for scanning electron microscopy (SEM) study and the remaining five specimens were used in compression testing.

2.7. Characterization of scaffolds

2.7.1. Porosity

The true volume of each scaffold specimen was measured using a gas pycnometer (Quantachrome Ultrapycnometer 1000, Quantachrome Corporation, Boynton Beach, FL) at 25°C in pure argon to determine the scaffold bulk porosity P_1(%). The theoretical porosity P_2(%) was estimated based on the amount of PCL deposited in raster roads of diameter RW according to the tip size used. Each porosity value was generally determined as

$$P = (V_a - V_t)/V_a \times 100\%, \quad (1)$$

where V_a (mm^3) is the apparent volume calculated based on the geometry of each "skinned" scaffold block, and V_t (mm^3) the scaffold true volume. For each FDM scaffold block, assuming that the roads (laid filaments) had a circular cross-section of uniform diameter RW, the amount of material deposited (V_t) was estimated by

$$V_t = L \times N \times V_{RW}, \quad (2)$$

where L is the number of roads per layer (determined from QS as the average number of roads created in the 0° raster direction), N(= 54) the number of layers per block, and V_{RW} the volume of each road with the geometry of a cylindrical tube.

2.7.2. Morphology

For experiment II, each piece of scaffold specimen 7.0 mm (length) by 7.0 mm (breadth) by 13.5 mm (height) from the T16 set was freeze-fractured after dipping in liquid nitrogen for 30 min. The T10 specimens could not be freeze-fractured due to their microstructure. Therefore, they were cut with a fresh blade to prepare for gold sputtering. The scaffold morphology was studied under a scanning electron microscope JSM-5800LV (JEOL USA, Peabody, MA) operating at 15 kV with the scaffold surfaces gold sputtered using a JEOL fine coater JFC-1200.

The SEM micrographs were used to measure the RW (mm) values besides studying the scaffold morphology. Other parameters like FG (mm) and ST (mm) were measured and compared with the set values. Measurement of a fourth dimension, a layer gap (LG), was also included. LG was defined as the edge-to-edge distance between layers of filaments of the same alignment. This served to indicate the amount of vertical space as compared with FG for the horizontal space between adjacent filaments. ST and LG values were measured from the cross-section views of scaffold specimens, which showed the stacked layers. RW and FG values were measured from the layer views, which showed the lay-down pattern. The dimensions RW, FG, ST and LG are illustrated schematically in Figs. 3c and 4c. All dimensions were measured with respect to the scale bar on each SEM micrograph (magnification 30 ×) using a

ruler. The average and standard deviation from 10 measurements were reported for each sample group.

2.7.3. Compression testing

For both experiments I and II, the mechanical properties of the scaffold specimens were measured using an Instron 4502 Uniaxial Testing System and a 1 kN load-cell (Canton, MA, USA) adopting the guidelines for compression testing of bone cement set in ASTM F451-99a. This is the latest edition of the same standard used in reports of characterization of mechanical properties of bioresorbable scaffolds of a similar geometry [21–24].

In experiment I, three specimens were tested, each of square cross-section 7.0×7.0 and 13.5 mm in height. The specimens were compressed at a cross head speed of 1 mm/min between two steel platens until a strain level of approximately 70%, with the load F (kN) versus deformation d (mm) values recorded throughout. A stress–strain curve was plotted based on the apparent stress σ (MPa) and strain ε (%) values determined by dividing the load value with the initial cross-sectional area A_o (mm^2) of each test specimen and the deformation values with the initial specimen height h_o (mm), respectively. In experiment II, five specimens were tested under the same conditions to record the load-displacement data.

For all specimens tested, the apparent modulus of elasticity E (MPa) was calculated as the slope of the initial linear portion of the stress–strain curve. Compression strength at yield σ_y (MPa) was defined as the intersection of the stress–strain curve with the modulus slope at an offset of 1% strain. Compression yield strain ε_y (%) was defined as the strain at which the yield occurred, neglecting the toe-region during initial specimen alignment.

For experiment I, the compression tests were conducted with the specimen filaments aligned in three orientations, OL, ILV and ILH as shown in Figs. 3b and 4b for both lay-down patterns. In OL loading, layers of deposited filaments were compressed together. For a 0/90° lay-down pattern (Fig. 3b) in both ILV and ILH loading, one out of every two layers of filaments was aligned in the direction of loading. For a 0/60/120° lay-down pattern (Fig. 4b) in ILV loading, one out of every three layers of filaments was aligned in the direction of loading. In ILH loading, one out of every three layers of filaments was aligned normal to the direction of loading. For experiment II, the compression tests were conducted with the filaments aligned in only two orientations OL and ILV for both lay-down patterns.

2.7.4. Statistics

For the mechanical properties measured in experiment I, a one-way ANOVA test was used to compare the means from the three independent sample groups OL, ILV and ILH. For experiment II, a student's t-test was performed in comparing means from two independent sample groups OL and ILV. A significance level of 0.05 was used in all the statistical tests performed. A MiniTab statistics software version 12.2 (MiniTab Inc., State College, PA, USA) was used for the statistical analysis.

3. Results and discussion

3.1. Differential scanning calorimetry and gel permeation chromatography

Table 2 shows the results of DSC and GPC analysis. The crystallinity fraction of PCL was not observed to rise significantly when the polymer was processed into filaments via the melt-extrusion process and subsequently through the FDM process. The values ranged between 56% and 58%. The shear forces on the polymer melt during the filament extrusion as well as FDM processes did not cause the percentage of crystallites to change significantly. PCL being a semi-crystalline polymer shows a well-defined melting profile. All samples were completely melted above 60°C. Potential degradation of PCL by the melt processing methods, filament extrusion and FDM, was characterized by measuring the molecular weight. The filament extrusion and FDM processing did not result in a significant change of the molecular weight.

3.2. Morphology

The structure of the 3D scaffolds designed and fabricated using the FDM method was highly similar to the honeycomb of a bee [25], with its regular array of identical pores, when viewed in the Z-direction of the

Table 2
Molecular weight distribution and DSC results of the different PCL specimens

PCL sample	M_n	M_w	Polydispersity M_w/M_n	Crystallinity fraction (%)
Raw pellet	78,500	140,000	1.78	56
Raw filament	82,000	141,500	1.72	58
PCL scaffold	87,000	147,700	1.68	57

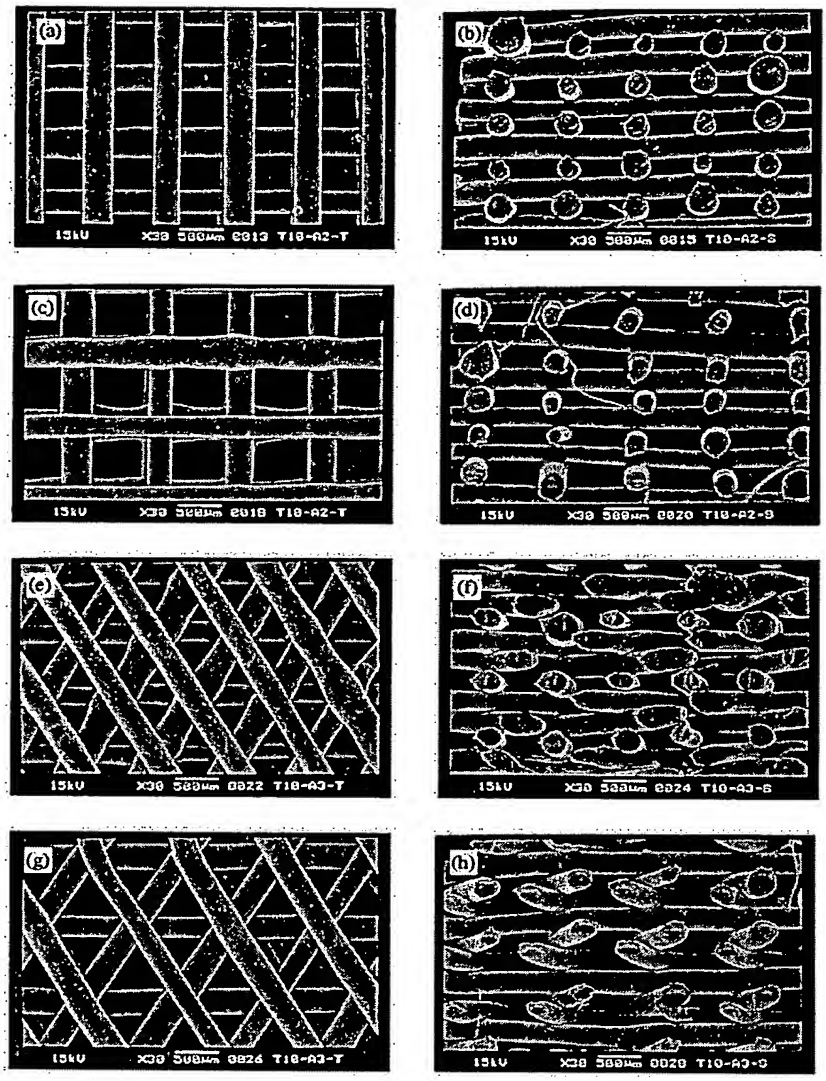

Fig. 5. Cut surface of PCL scaffold fabricated using T10 tip, sample group: (a) C2-10-20 plan-view; (b) C2-10-20 side-view; (c) C2-10-28 plan view; (d) C2-10-28 side-view; (e) C3-10-20 plan-view; (f) C3-10-20 side-view; (g) C3-10-28 plan-view; (h) C3-10-28 side-view;observed under SEM.

fabrication process (Fig. 1). The main difference lies in the shape of the pores: the bee's honeycomb comprises of hexagonal pores surrounded by solid faces which nest together to fill a plane, but the FDM scaffold structure was built from neatly aligned filaments stacked in horizontal layers and comprised of pores surrounded by solid struts.

The present scaffolds were of two distinctive honeycomb-like patterns. One group with square pores as a result of a 0/90° lay-down pattern (Figs. 5a–d and Figs. 6a–d), and the other with triangular pores as a result of a 0/60/120° lay-down pattern (Figs. 5e–h and Figs. 6e–h). Both lay-down patterns were directly designed in the QS scaffold models where the deposition paths were first created on computer. More complex lay-down patterns could be designed using the QS software to produce less regular pore shapes [4].

When the scaffolds were viewed in the X- or Y-direction of the fabrication process, the pores seen from the cross-sections revealed a network of interconnected channels of high regularity. Hence, the FDM scaffolds not only had honeycomb-like patterns but in a 3D sense, the structure was that of an open-pore cellular solid with the pores interconnecting through adjacent faces [25]. Scaffolds with a 0/90° lay-down pattern comprised of large square pores in the Z-direction but the structure had smaller channel size in the X- and Y-directions, especially those fabricated using the T16

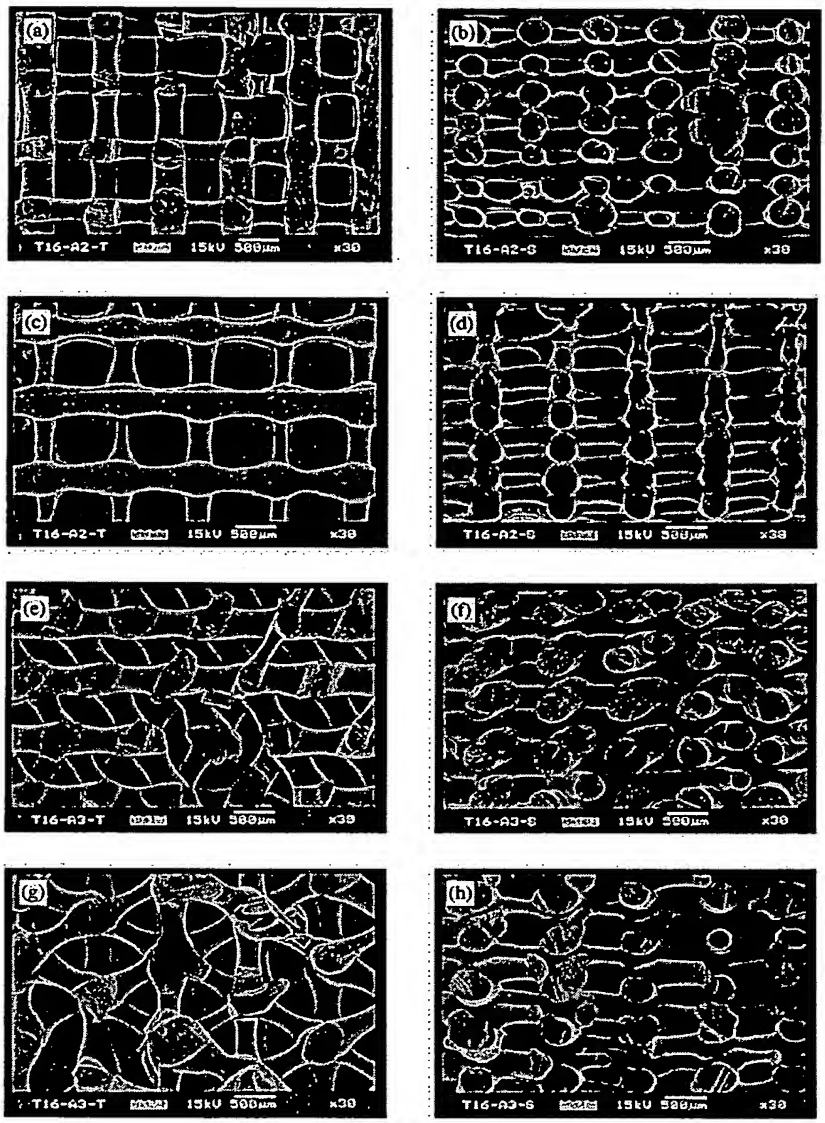

Fig. 6. Freeze-fractured surface of PCL scaffold fabricated using T16 tip, sample group: (a) C2-16-20 plan-view; (b) C2-16-20 side-view; (c) C2-16-28 plan view; (d) C2-16-28 side-view; (e) C3-16-20 plan-view; (f) C3-16-20 side-view; (g) C3-16-28 plan-view; (h) C3-16-28 side-view, observed under SEM.

tip (Figs. 6a–d). On the other hand, a 0/60/120° lay-down pattern provided channels of bigger magnitude in the X- and Y-directions with relatively smaller triangular pores in the Z-direction, for both nozzle tips used (Figs. 5g and h and Figs. 6g and h). Hence, by increasing the number of layers with different raster angles and arranging the sequence of raster directions in a multi-layered scaffold, it was possible to create a porous 3D scaffold with various degrees of channel dimensions. The use of a finer nozzle tip allowed the fabrication of scaffolds with bigger channel size than using the T16 tip, under similar settings of FG and ST.

Scaffolds fabricated using the fine T10 tip had smaller filaments of circular cross-section and a higher surface area to volume ratio (Figs. 5a–h) than those fabricated using a wider T16 tip (Figs. 6a–h). The continuity of thin filaments throughout the scaffold internal structure was similar to that fabricated using the fiber-bonding technique. Due to insufficient adhesion between adjacent layers, delamination of layers was observed in some T10 scaffold specimens (Figs. 5c and d). This might have arisen during specimen cutting that caused the weak filament joints to tear. The ST could be reduced for the T10 scaffolds to improve layer-to-layer adhesion but this

Table 3
Measurement of structural features of PCL scaffolds from SEM micrographs. Average of 10 measurements with ±SD[a]

Specimen group	RW (μm)	ST (μm)	FG (μm)	LG (μm)
C2-10-20	277±41	256±22	521±41	227±42
C2-10-28	256±34	246±20	704±76	237±46
C3-10-20	298±35	250±19	477±43	425±49
C3-10-28	285±22	253±15	646±51	433±53
C2-16-20	342±39	213±20	468±53	158±35
C2-16-28	308±57	216±21	648±44	160±56
C3-16-20	372±38	210±22	408±36	294±27
C3-16-28	328±50	215±18	644±40	374±71

[a] RW: road width, ST: slice thickness, FG: fill gap, LG: layer gap.

would also reduce the scaffold porosity. Further reduction in the nozzle tip size would allow fabrication of finer structures.

The FG value played an important role in imparting the porosity for each scaffold model. To maximize porosity, the FG could be widened between adjacent raster roads. However, this value could not be increased indefinitely as slacking would occur when there was insufficient strength for an extruded filament to bridge a wide gap. It was essential that every layer be well deposited as the preceding layer served as the only foundation for the next layer of deposition. The values of FG selected for the present scaffold models at 500 and 700 μm were adequately large for tissue engineering bone and cartilage [4]. Based on the SEM micrographs, measurements of the scaffold structural features were compared with the original QS settings (Table 3). For the T10 scaffolds, the actual features were close to the set dimensions, indicating that the optimized FDM flow parameters for the thinner trial specimens had also worked for thicker structures and allowed reproducibility of scaffold micro-architecture. On the other hand, the T16 scaffolds had smaller RW than targeted, meaning that a higher roller speed would be required to increase flow rate. The smaller than expected RW might be acceptable for the purpose of creating a more porous structure. Measurements of FG and LG showed that the scaffold channel size ranged between 160 (vertical) and 700 μm (horizontal). Bigger channel sizes could be achieved by slightly increasing FG or repeating the raster angle for consecutive layers, 0/0/90/90° and 0/0/60/60/120/120°. The FDM method allowed both precise control and variation of channel size. Depending on the cell-culture environment, static or dynamic, the channel size could be tailor-made to ensure unobstructed flow of nutrients and wastes through the scaffold structure.

3.3. Porosity

Values of scaffold bulk porosity P_1 (Table 4) based on true volume measurement using a gas pycnometer showed little variations due to the high accuracy in volume measurement by the fluid displacement technique. The technique was suitable for the porous scaffolds due to their highly interconnected channels as observed from the SEM micrographs. Furthermore, the non-destructive nature of the measurement method allowed subsequent use of the scaffolds for SEM and compression tests.

Table 4
Measured (P_1) and theoretical (P_2) porosity of PCL scaffolds

Specimen group	P_1 (%)	N	L	P_2 (%)[a]
C2-16-24	55	54	20	44
C3-16-24	56	54	20	44
C2-10-20	71	54	22	76
C2-10-28	77	54	18	80
C3-10-20	73	54	22	76
C3-10-28	76	54	18	80
C2-16-20	53	54	22	38
C2-16-28	61	54	18	49
C3-16-20	48	54	22	38
C3-16-28	61	54	18	49

[a] Based on target RW in Table 1.

In general, scaffolds of two groups of porosity range were produced. Using a T10 tip, scaffolds of high porosity were produced in the range of 71–77%. Using a T16 tip, the scaffold porosity ranged between 48% and 61%. The more porous scaffolds would allow a higher cell seeding capacity due to the larger available pore space. To produce scaffolds of higher porosity in the range of 80–90% or even higher, the FDM head speed setting could be increased to stretch the extruded filaments during deposition. However, this might compromise the stability of the extrudate flow and therefore effect the reproducibility. The measured scaffold porosity P_1 for each sample group was compared with the theoretical porosity P_2 (Table 4). The latter was calculated based on the target RW for each nozzle tip. For the T10 scaffold specimens, P_1 was lower than P_2 due to the larger RW than the targeted value of 254 μm (Table 3). For the T16 specimens, P_1 was higher than P_2 because the measured RW values

were smaller than targeted. This indicated that the wider tip had delivered less than the expected volume under the T16 flow settings.

3.4. Mechanical properties

3.4.1. Experiment I

Two $\sigma-\varepsilon$ curves representing PCL scaffolds undergoing compression loading are shown in Fig. 7. One curve represents a 55% porosity scaffold with a 0/90° lay-down pattern (C2-16-24-ILV) and the other represents a similarly porous 56% porosity scaffold with a 0/60/120° lay-down pattern (C3-16-24-ILV). Both specimens demonstrated a typical behavior of a porous material undergoing deformation as described in the literature [25]. The curves each comprised of three distinct regimes: a linear-elastic regime followed by a plateau of roughly constant stress, leading into a final regime of steeply rising stress. The $\sigma-\varepsilon$ curves of both 0/90° and 0/60/120° scaffolds loaded OL and ILH also had a common trend. At the porosity of 55–56%, scaffolds with a 0/90° lay-down pattern showed a steeper initial linear regime and a higher plateau than scaffolds with a 0/60/120° lay-down pattern when compressed in-layer (both ILV and ILH). When compressed OL, the $\sigma-\varepsilon$ curves of scaffolds with both lay-down patterns showed little difference. Also, the curves of the 0/90° scaffolds showed marked increases in the initial linear gradient and plateau height when compressed in-layer (IL) than OL, whereas no such increase in both initial linear gradient and plateau height was visible from the 0/60/120° scaffolds. Statistical analysis was performed to check the difference in the averages among the OL, ILV and ILH measurements.

When compressed IL (as shown earlier in Figs. 3b and 4b), it was the axially aligned filaments that bear the loading stress, behaving as columns. The PCL filaments bent, demonstrating linear elasticity at the beginning. When a critical stress level was reached the channels began to collapse with elastic buckling of the column-like filaments. The alignment of filaments of the 0/90° scaffolds in the loading direction provided a high resistance against the compressive load before buckling began, regardless of either ILH or ILV orientations. In the 0/60/120° scaffolds, the larger number of filaments aligned in the loading direction under the ILV orientation provided a larger resistance than under the ILH orientation. Hence, the scaffolds were expected to be stronger when compressed in the direction with a higher degree of filament alignment. In both lay-down patterns, at high level of strains above 50%, the channels collapsed sufficiently that adjacent filaments touched and further deformation compressed the scaffold material itself. This manifested itself as the final, steeply rising portion of each $\sigma-\varepsilon$ curve.

When compressed OL, it was the filament junctions of adjacent layers that bear the applied load at the beginning. The initial linear-elastic deformation in this case involved significant shear deformation of the filament joints. On further compression, the linear-elastic regime was truncated by sliding of filament layers, which also manifested as a plateau of constant stress on the $\sigma-\varepsilon$ curve. Final failure occurred when the filaments of adjacent layers were crushed. A larger number of filament joints would be expected to strengthen the scaffold structure when compressed OL. The strengthening effect also depended on the bond strength between filaments at their joints, which was in turn dependent on the build and flow parameters during the FDM fabrication process.

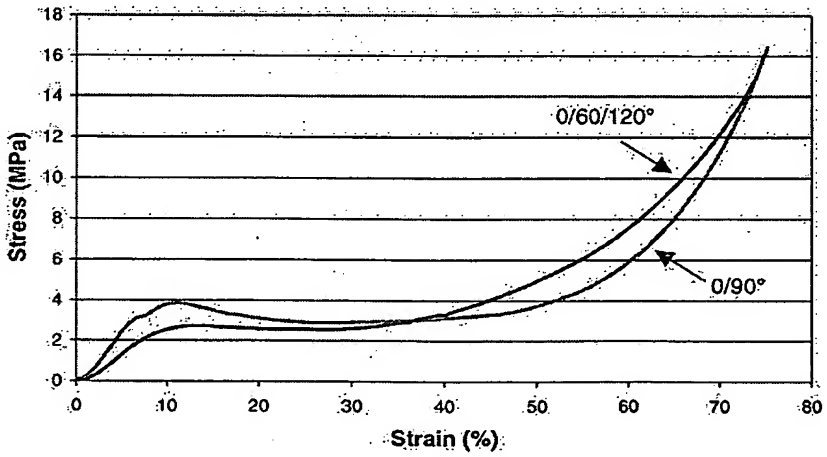

Fig. 7. Stress–strain curves of 0/90° and 0/60/120° lay-down patterns PCL scaffolds compressed in the ILV orientation. The scaffold porosity was 55% and 56%, respectively.

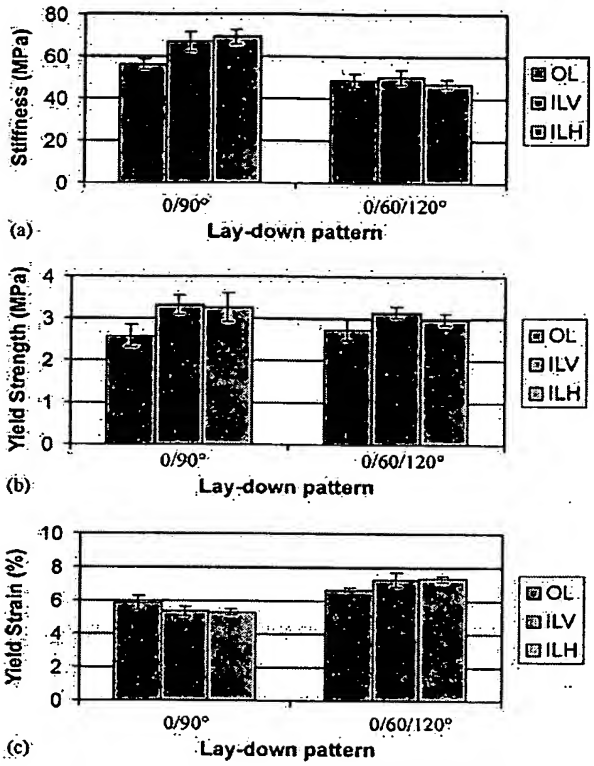

Fig. 8. Results of experiment I: (a) compression stiffness; (b) compression yield strength; (c) compression yield strain, of both 0/90° and 0/60/120° lay-down pattern PCL scaffolds tested in three orthogonal directions (average±s.d., sample size $n = 3$).

3.4.1.1. Stiffness. Scaffolds fabricated with a 0/90° lay-down pattern, 55% porosity (C2-16-24-ILH) had the highest measured compression stiffness E, at 69.2± 3.6 MPa, when loaded IL. Scaffolds fabricated with a 0/60/120° lay-down pattern, 56% porosity (C3-16-24-ILH) had the lowest measured stiffness at 47.1± 1.9 MPa, also loaded IL. The average values of E and their standard deviations for both lay-down patterns are shown in Fig. 8a. Statistical analysis using a one-way ANOVA test did not show any significant difference ($p > 0.05$) among the compression stiffness of the 0/60/120° scaffolds tested in three orientations (OL, ILV and ILH). However, there is statistical evidence that the compression stiffness of the 0/90° scaffolds depended on the loading direction ($p \leqslant 0.05$), with E being lowest in the OL orientation.

3.4.1.2. Yield strength. Scaffolds fabricated with a 0/90° lay-down pattern, 55% porosity (C2-16-24-ILV) had the highest measured compression yield strength σ_y, at 3.32±0.24 MPa, when loaded IL, and the lowest measured yield strength at 2.58±0.27 MPa, when loaded OL. Scaffolds fabricated with a 0/60/120° lay-down pattern, 56% porosity (C3-16-24-ILV) also had the highest measured compression yield strength, at 3.15±0.14 MPa, when loaded IL, and the lowest measured yield strength at 2.74±0.25 MPa, when loaded OL. The average values of σ_y and their standard deviations for both lay-down patterns are shown in Fig. 8b. Statistical analysis using a one-way ANOVA test shows evidence ($p \leqslant 0.05$) that there is significant difference among the compression yield strength of the 0/90° scaffolds tested in three orientations (OL, ILV and ILH) but there is insufficient evidence with the 0/60/120° scaffolds ($p > 0.05$). In the 0/90° lay-down pattern, the scaffolds were stronger when loaded with their filaments aligned in the direction of compression (IL orientation) than with the filaments aligned in the stacked layers. Insufficient bond strength between filaments could have given way to shear deformation at the joints during scaffold compression. However, it is also possible that the higher degree of filament alignment in the IL orientations strengthened the scaffold in those loading directions.

3.4.1.3. Yield strain. Scaffolds fabricated with a 0/90° lay-down pattern, 55% porosity (C2-16-24) had generally lower measured compression yield strain ε_y, between 5.29±0.18% and 5.86±0.45% than scaffolds with a 0/60/120° lay-down pattern, 56% porosity (C3-16-24), between 6.67±0.12% and 7.34±0.17%. The average values of ε_y and their standard deviations for both lay-down patterns are shown in Fig. 8c. Statistical analysis using a one-way ANOVA test shows evidence ($p \leqslant 0.05$) that there is significant difference among the compression yield strain of the 0/60/120° scaffolds tested in three orientations (OL, ILV and ILH) but no such evidence was seen with the 0/90° scaffolds ($p > 0.05$). In the 0/90° lay-down pattern, the scaffolds yielded at a higher strain level when loaded with their filaments aligned normally in the stacked layers (OL orientation) than when the filaments were aligned in the direction of compression (IL orientations). The reverse took place with the 0/60/120° lay-down pattern. The scaffolds yielded at a lower strain level when loaded in the OL orientation than the IL orientations. The spatial arrangement of filaments in the 0/60/120° scaffolds might have allowed the internal structure to maintain its form up to a higher strain level before permanent deformation set in.

3.4.2. Experiment II

Two $\sigma-\varepsilon$ curves representing PCL scaffolds undergoing compression loading are shown in Fig. 9. One curve represents a low 48% porosity scaffold (C3-16-20-IL) and the other represents a high 76% porosity scaffold (C3-10-28-OL). Both curves again illustrate the typical behavior of a porous material undergoing deformation [25]. The $\sigma-\varepsilon$ curves of both 0/90° and 0/

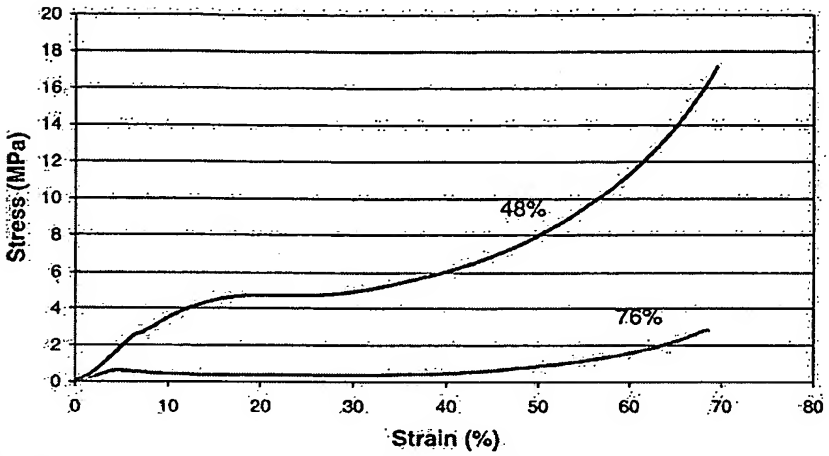

Fig. 9. Stress–strain curves of 48% and 76% porous PCL scaffolds compressed in the ILV orientation. The scaffold lay-down pattern was 0/60/120°.

60/120° scaffolds loaded OL and ILH of other porosity also exhibited a similar pattern. At low porosity of 48–61%, scaffolds of both lay-down patterns showed a much steeper initial linear regime and a higher plateau than scaffolds with higher porosity 71–77% when compressed IL. When compressed OL, the $\sigma-\varepsilon$ curves of high porosity scaffolds of both lay-down patterns showed a long initial linear regime with a shorter plateau. Statistical analysis was performed to check the difference in the averages among the sample groups of different scaffold porosity. The flattening of the $\sigma-\varepsilon$ curves (longer and lower plateau regime) was apparent as the porosity increased from a low of 48% to a high of 76%. This is characteristic of honeycombs undergoing compression loading [25].

3.4.2.1. Stiffness. Scaffolds fabricated using the T16 tip with a 0/90° lay-down pattern and porosity of 53% (C2-16-20-IL) had the highest compression stiffness at 77.0 ± 7.6 MPa, when loaded IL. On the other hand, scaffolds fabricated using the T10 tip with a 0/60/120° lay-down pattern and porosity of 76% (C3-10-28-OL) had the lowest stiffness at 3.96 ± 0.48 MPa. The measured stiffness values were shown in Figs. 10a and b for scaffolds with 0/90° and 0/60/120° lay-down pattern, respectively. Both T10 (high porosity) and T16 (low porosity) scaffolds with a 0/90° lay-down pattern were stiffer when compressed IL than OL (student's t-test, $p \leqslant 0.05$). However, T16 scaffolds with a 0/60/120° lay-down pattern did not show any statistical difference in stiffness when tested in different directions (student's t-test, $p > 0.05$), as was observed also from results of experiment I. Student's t-test confirmed that there is statistical evidence ($p \leqslant 0.05$) that for each nozzle tip size used, for each lay-down pattern, and for each loading direction, the measured stiffness was lower when the porosity was higher. On the whole, the range of data measured for compression stiffness (4–77 MPa) of the PCL scaffolds fabricated using the FDM method is of the same order as that of human trabecular bone (50 MPa) [26].

3.4.2.2. Yield strength. Scaffolds fabricated using the T16 tip with a 0/90° lay-down pattern and porosity of 53% (C2-16-20-IL) had the highest compression yield strength at 3.62 ± 1.22 MPa, when loaded IL. On the other hand, scaffolds fabricated using a T10 tip with a 0/90° lay-down pattern and porosity of 77% (C2-10-28-OL) had the lowest yield strength at 0.42 ± 0.06 MPa, loaded OL. The measured yield strength values were shown in Figs. 10c and d for scaffolds with 0/90° and 0/60/120° lay-down pattern, respectively.

The T16 (low porosity) scaffolds of both lay-down patterns were stronger when compressed IL than OL (student's t-test, $p \leqslant 0.05$), as was observed from the results of experiment I. However, the higher porosity T10 scaffolds of both lay-down patterns were stronger when compressed OL than IL (student's t-test, $p \leqslant 0.05$). The reverse trend could be attributed to the lower bond strength between filaments in scaffolds fabricated using the finer T10 tip. Delamination of the filament layers was also observed during the compression testing of these high porosity scaffold specimens. However, student's t-test still confirmed that there is statistical evidence ($p \leqslant 0.05$) that for each nozzle tip size used, for each lay-down pattern, and for each loading direction, the measured yield strength was lower when the porosity was higher, similar to the decrease of stiffness with increasing scaffold porosity. The PCL scaffolds fabricated using the FDM method had yield strength (ranging from 0.4 to 3.6 MPa) lower than the minimum required value of 5 MPa for replacement of human trabecular bone [26]. The incorporation of short fibers in a PCL matrix could be beneficial to improve the

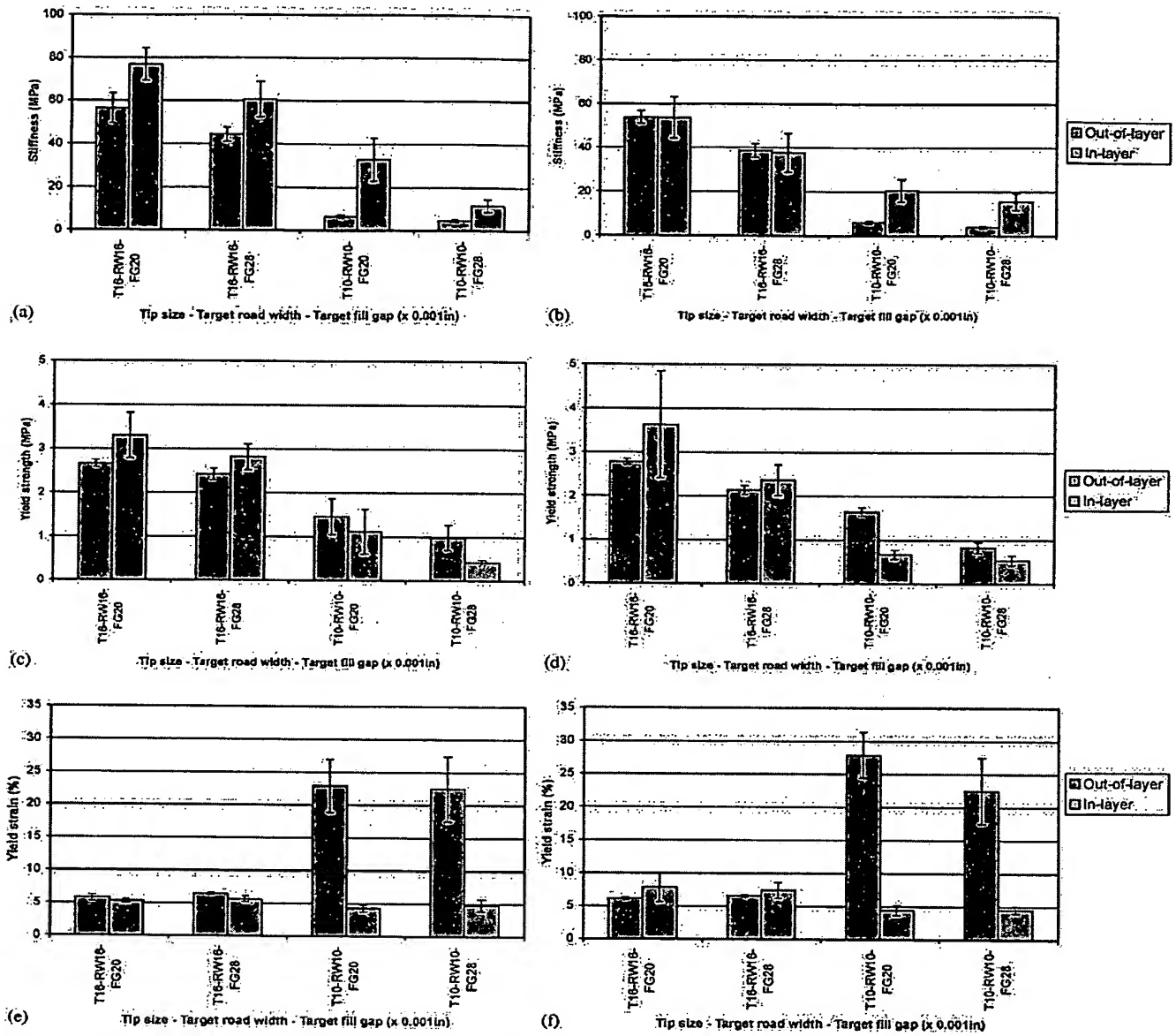

Fig. 10. Results of experiment II: (a) compression stiffness of 0/90°; (b) compression stiffness of 0/60/120°; (c) compression yield strength of 0/90°; (d) compression yield strength of 0/60/120°; (e) compression yield strain of 0/90°; (f) compression yield strain of 0/60/120° of PCL scaffolds as a function of the nozzle tip used, target RW and FG with increasing porosity (average ± s.d., sample size $n = 5$).

mechanical properties for the design of scaffolds for bone tissue engineering [23].

3.4.2.3. Yield strain. The highest yield strain was measured from 73% porous scaffolds fabricated using the T10 tip at 27.9 ± 3.5% (C3-10-20-OL). However, most of the sample groups showed yield strain values within a narrow range of 4.29 ± 0.56% (C2-10-20-IL, 71% porosity) to 7.83 ± 2.22% (C3-16-20-IL, 48% porosity). The measured yield strain values were shown in Figs. 10e and f for scaffolds with 0/90° and 0/60/120° lay-down pattern, respectively. The abnormally high yield strain of the high porosity (71–77%) T10 scaffolds, loaded OL, suggested that the fine round filaments might have rolled sideways right from the onset of loading due to insufficient bond strength between filaments, observable from the SEM micrographs of T10 scaffold specimens (Figs. 5a–h). The insufficient filament-to-filament adhesion was probably further reduced during the cutting of the large scaffold block.

When compressed IL, the sheer high number of filaments aligned in the loading direction compensated for the low filament-to-filament bond strength and the specimens proceeded to yield in the range of 4–5% strain before delamination set in.

3.5. Dependence of compressive properties on porosity

Models of porous structures constructed of beams with square cross-section [25], had predicted that the compressive stiffness E and yield strength σ in compression are each related to the porosity of the scaffold by a power–law relationship of the form:

$$E = C_1(100 - P)^n, \quad (3)$$

$$\sigma = C_2(100 - P)^n, \quad (4)$$

where C_1, C_2 and n are constants and $100 - P$ the relative density.

For foams with open pores, made from materials which have a plastic yield point, such as high molecular weight PCL homopolymers, the theoretical values of n are 2 and 1.5 for predicting E and σ, respectively. Similarly for honeycombs with polygonal pores, the theoretical values of n are 3 and 1 for predicting E under transverse and axial loading, respectively, and 2 and 1 for predicting σ under transverse and axial loading, respectively. Comparing all the sample groups of the FDM-PCL scaffolds, the compressive stiffness, yield strength and yield strain were found to decrease with increasing porosity regardless of the lay-down pattern, channel size, RW or loading direction.

The experimental data obtained are presented in Figs. 11a–c, which illustrate the variation of mechanical properties with porosity. Scaffold compressive stiffness and yield strength decreased rapidly as the porosity increased, and these declines were described using a power law function of the form given by Eqs. (3) and (4), respectively. The best fit line to the experimental data gave an exponent value of 2.88 and 2.07 for predicting E (Fig. 11a) and σ (Fig. 11b), respectively. The exponent values are comparable to the theoretical results of $n = 3$ and $n = 2$ for honeycombs and open-pore foams, respectively. In comparing the theoretical values of n for compression of honeycombs, it was found that the FDM scaffolds' mechanical properties also depended on porosity in the same manner like

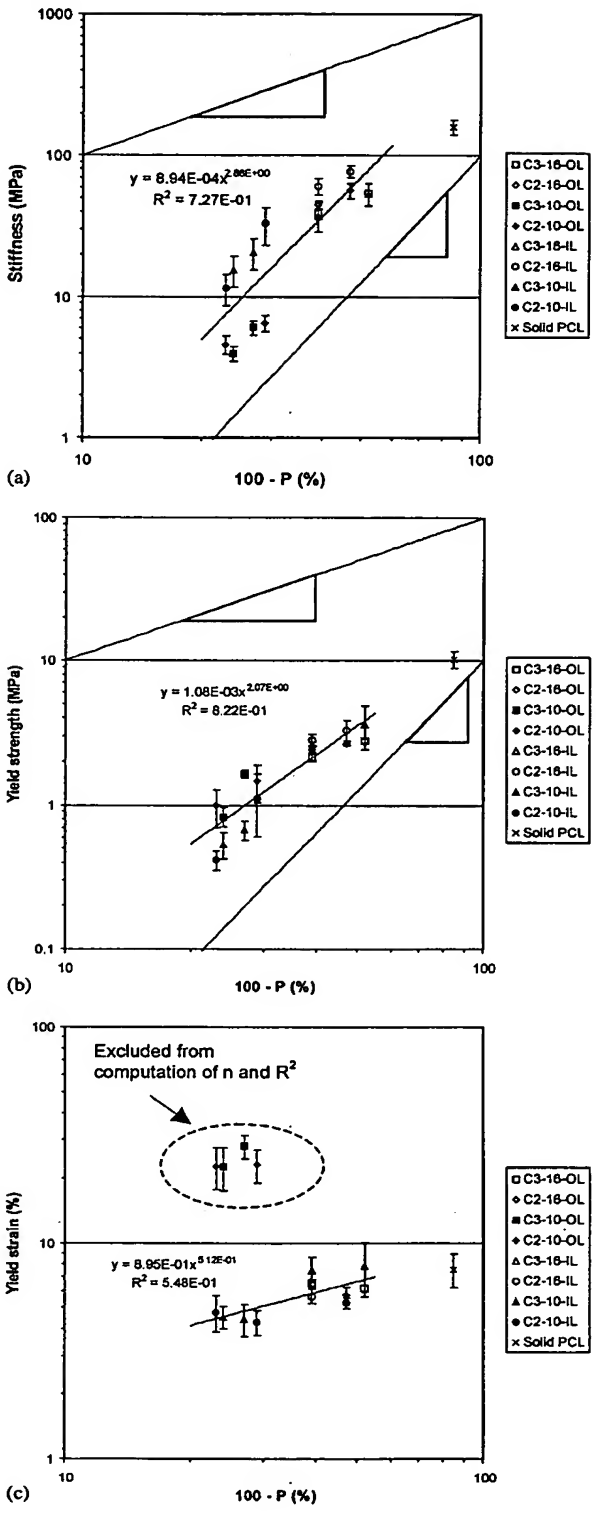

Fig. 11. (a) Compression stiffness; (b) compression yield strength; (c) compression yield strain as a function of porosity of PCL scaffolds. The symbols in the legend represent the scaffolds designed and fabricated with the lay-down pattern, target RW and loading direction indicated (five specimens of each group were tested under the same conditions). The high yield strain values of the specimens C2 and C3 (T10 scaffolds, out-of-layer) were not included to compute the exponent value as the yield strain values could have remained in the range of 4–8% if delamination occurred after yielding.

honeycomb structures. For predicting yield strain ε, an exponent value of 0.588 (Fig. 11c) was similarly found based on a power–law relationship:

$$\varepsilon = C_3(1-p)^n, \quad (5)$$

where C_3 and n are also constants. The high yield strain values of 22.48±5.00% to 27.92±3.47% (T10 scaffolds, OL) were not included to compute this exponent value as the yield strain values could have remained in the range of 4–8% if delamination occurred after yielding.

The measured data indicated a qualitative relationship between the scaffold porosity and each of the mechanical properties. In Fig. 11b, the best fit line of slope 2.07 adequately describes the decline in yield strength with porosity and is valid over the porosity range of the data (48–77%) with a R-squared value of 0.822. Based on the experimental data and an extrapolation, a 100% solid PCL scaffold (zero porosity) has a yield strength of 14.9 MPa, which is of the same order of magnitude as the tensile strength of 16 MPa reported by Engelberg and Kohn [11]. Similarly in Fig. 11c, the best fit line also describes the decline of yield strain over the same porosity range ($R^2 = 0.548$). On extrapolation, a yield strain of 9.5% was obtained, again of the same order of magnitude as the elongation at yield 7% reported. In both figures, the best fit line fits all of the data independent of the lay-down pattern, channel size, RW or loading direction. This suggests that yield strength and yield strain are independent of pore size, the former which is in agreement with theoretical results described in the literature. The strong dependence of mechanical properties on scaffold porosity had also been reported by Thomson et al. [24] for foam-like architectures. In Fig. 11a, on extrapolating the data a stiffness of 510 MPa was obtained, which is again of the same order of magnitude as the tensile and flexural moduli reported of solid PCL [11].

4. Conclusion

Fused deposition modeling (FDM), a rapid prototyping technology, was investigated and successfully applied in this research to produce novel 3D scaffolds with fully interconnected channel networks, and highly controllable porosity and channel size. A bioresorbable polymer poly(ε-caprolactone) was developed as a filament to produce scaffolds by this computer-controlled extrusion and deposition method. Porous FDM scaffolds were made of layers of directionally aligned microfilaments within a geometrical 3D structure. Honeycomb scaffold architectures were made of layers of directionally aligned PCL microfilaments within a geometrical 3D structure. Analysis of the mechanical properties contributed to a better understanding of the anisotropic nature of different designs. Examination of the mechanical deformation indicated that the porous PCL scaffolds demonstrated stress–strain behavior highly similar to that of a typical porous material undergoing compression. The mechanical properties were found to be generally dependent on its porosity, regardless of the lay-down pattern and channel size, this being in agreement with theoretical concepts on the structure–properties relationships of porous solids. In summary, the efficacy of the FDM technique for scaffold design and fabrication had been proven in this research. The results of the in vitro and in vivo studies based on the novel PCL scaffolds are presented elsewhere [16–18,27,28].

References

[1] Widmer MS, Mikos AG. Fabrication of biodegradable polymer scaffolds for tissue engineering. In: Patrick Jr CW, Mikos AG, McIntire LV, editors. Frontiers in tissue engineering. New York: Elsevier, 1998. p. 107–20.

[2] Hutmacher DW. Polymeric scaffolds in tissue engineering bone and cartilage. Biomaterials 2000;21:2529–43.

[3] Giordano RA, Wu BM, Borland SW, Cima LG, Sachs EM, Cima MJ. Mechanical properties of dense polylactic acid structures fabricated by three dimensional printing. J Biomater Sci Polym Edn 1996;8(1):63–75.

[4] Kim SS, Utsunomiya H, Koski JA, Wu BM, Cima MJ, Sohn J, Mukai K, Griffith LG, Vacanti JP. Survival and function of hepatocytes on a novel three-dimensional synthetic biodegradable polymer scaffold with an intrinsic network of channels. Ann Surg 1998;228(1):8–13.

[5] Park A, Wu B, Griffith LG. Integration of surface modification and 3D fabrication techniques to prepare patterned poly(L-lactide) substrates allowing regionally selective cell adhesion. J Biomed Sci Polym Edn 1998;9:89–110.

[6] Koch KU, Biesinger B, Arnholz C, Jansson V. Creating of bio-compatible, high stress resistant and resorbable implants using multiphase jet solidification technology. In: Park R, editor. Time-compression technologies. Interactive Computing Europe, CATIA-CADAM Solutions, formation, International Business Machines Corporation–IBM: Time-compression Technologies '98 Conference London, GB: Rapid News Publications, 1998. p. 209–14.

[7] Marra KG, Szem JW, Kumta PN, DiMilla PA, Weiss LE. In vitro analysis of biodegradable polymer blend/hydroxyapatite composites for bone tissue engineering. J Biomed Mater Res 1999; 47(3):324–35.

[8] Marra KG, Campbell PG, Dimilla PA, Kumta PN, Mooney MP, Szem JW, Weiss LE. Novel three dimensional biodegradable scaffolds for bone tissue engineering. Mater Res Soc Symp Proc 1999;550:155–60.

[9] US Patents. US5121329: Apparatus and method for creating three-dimensional objects. Crump S.S. (inventor), Stratasys Inc., Minneapolis, MN (applicant), issued/filed dates: June 9, 1992/ Oct. 30, 1989.

[10] Suggs LJ, Mikos AG. Synthetic biodegradable polymers for medical applications. In: Mark JE, editor. Physical properties of polymers handbook. New York: American Institute of Physics, 1996. p. 615–24.

[11] Engelberg I, Kohn J. Physicomechanical properties of degradable polymers used in medical applications—a comparative study. Biomaterials 1991;12(3):292–304.

[12] Deshpande AA, Heller J, Gurny R. Bioerodible polymers for ocular drug delivery. Crit Rev Therapeutic Drug Carrier Systems 1998;15(4):381–420.
[13] Bezwada RS, Jamiolkowski DD, Lee I, Vishvaroop A, Persivale J, Treka-Benthin S, Erneta M, Suryadevara J, Yang A, Liu S. Monocryl suture, a new ultra-pliable absorbable monofilament suture. Biomaterials 1995;16:1141–8.
[14] Darney PD, Monroe SE, Klaisle CM, Alvarado A. Clinical evaluation of the Capronor contraceptive implant: preliminary report. Am J Obstet Gynecol 1989;160:1292–5.
[15] Pitt CG, Schindler A. Biodegradation of polymers. In: Bruck SD, editor. Controlled drug delivery. Boca Raton, FL: CRC Press, 1983. p. 55–80.
[16] Hutmacher DW, Zein I, Teoh SH, Ng KW, Schantz JT, Leahy JC. Design and fabrication of a 3D scaffold for tissue engineering bone. In: Agrawal CM, Parr JE, Lin ST, editors. Synthetic bioabsorbable polymers for implants, STP 1396. West Conshohocken, PA: American Society for Testing and Materials, 2000. p. 152–67.
[17] Hutmacher DW, Schantz JT, Zein I, Ng KW, Tan KC, Teoh SH. Mechanical properties and cell cultural response of polycaprolactone scaffolds designed and fabricated via fused deposition modeling. J Biomed Mat Res 2001;55:203–16.
[18] Hutmacher DW, Fu X, Tan BK, Schantz JT. Solid-free form fabrication and characterization of polymeric scaffolds for cartilage regeneration, submitted for publication.
[19] Comb JW, Priedeman WR, Turley PW. Layered manufacturing control parameters and material selection criteria. Manufacturing Science and Engineering Vol. 2, PED-vol. 68-2, ASME, 1994.
[20] Agarwala MK, Jamalabad VR, Langrana NA, Safari A, Whalen PJ, Danforth SC. Structural quality of parts processed by fused deposition. Rapid Prototyping J 1996;2(4):4–19.
[21] Peter SJ, Miller ST, Zhu G, Yasko AW, Mikos AG. In vivo degradation of a poly(propylene fumarate)/β-tricalcium phosphate injectable composite scaffold. J Biomed Mater Res 1998; 41:1–7.
[22] Peter SJ, Nolley JA, Widmer MS, Merwin JE, Yaszemski MJ, Yasko AW, Engel PS, Mikos AG. In vitro degradation of a poly(propylene fumarate)/β-tricalcium phosphate composite orthopaedic scaffold. Tissue Eng 1997;3(2):207–15.
[23] Thomson RC, Yaszemski MJ, Powers JM, Mikos AG. Hydroxyapatite fiber reinforced poly(α-hydroxy ester) foams for bone regeneration. Biomaterials 1998;19:1935–43.
[24] Thomson RC, Yaszemski MJ, Powers JM, Mikos AG. Fabrication of biodegradable polymer scaffolds to engineer trabecular bone. J Biomater Sci Polym Edn 1995;7(1):23–38.
[25] Gibson LJ, Ashby MF. Cellular solids: structure and properties. Cambridge: Cambridge University Press, 1997.
[26] Goldstein SA. The mechanical properties of trabecular bone: dependence on anatomic location and function. J Biomech 1987;20:1055–61.
[27] Hutmacher DW, Goh JCH, Teoh SH. Biodegradable materials for tissue engineering application. Ann Acad Med Singapore 2001;30:183–91.
[28] Hutmacher DW. Scaffold design, fabrication technologies for engineering tissues—state of the art and future perspectives. J Biomater Sci Polym Edn 11:107–24.

EXHIBIT 5

Cell Transplantation, Vol. 11, pp. 125–138, 2002
Printed in the USA.

0963-6897/02 $20.00 + .00

Induction of Ectopic Bone Formation by Using Human Periosteal Cells in Combination With a Novel Scaffold Technology

Jan-Thorsten Schantz,*# Dietmar Werner Hutmacher,†‡ Harvey Chim,§ Kee Woei Ng,*¶ Thiam Chye Lim,# and Swee Hin Teoh*¶

*Laboratory for Biomedical Engineering, †Department of Bioengineering, ‡Department of Orthopaedic Surgery, §Faculty of Medicine, ¶Department of Mechanical Engineering, National University of Singapore, 10 Kent Ridge Crescent, Singapore 119260
#Department of Plastic Surgery, National University Hospital, 5 Lower Kent Ridge Road, Singapore 119074

Due to their osteogenic germination potential, periosteum-derived osteoprogenitor cells are a potential source for tissue engineering a bone graft that could be used to regenerate skeletal defects. In this study we evaluated if ectopic bone formation could be induced by a construct made of human periosteal cells and a novel scaffold architecture whose mechanical properties are in the range of cancellous bone. Biopsies from human calvarial periosteum were harvested and cells were isolated from the inner cambial layer. Fifty thousand periosteal cells were seeded into the scaffolds measuring $6 \times 6 \times 2$ mm. The cell–scaffold constructs were cultured for a period of 3 weeks prior to implantation into balb C nude mice. Mice were sacrificed and implants were analyzed 6 and 17 weeks postoperatively. Immunohistochemical analysis confirmed the osteoblastic phenotype of the seeded cells. Formation of focal adhesions and stress fibers could be observed in both scaffold architectures. Three-dimensional cell proliferation was observed after 2 weeks of culturing with centripetal growth pattern inside the pore network. The deposition of calcified extracellular matrix was observed after 3 weeks of culturing. In vivo, endochondral bone formation with osteoid production was detectable via von Kossa and Osteocalcin staining after 6 and 17 weeks. Histology and SEM revealed that the entire scaffold/bone grafts were penetrated by a vascular network. This study showed the potential of bone tissue engineering by using human periosteal cells in combination with a novel scaffold technology.

Key words: Bone tissue engineering; Periosteal cells; Scaffolds; Polycaprolactone; Rapid prototyping

INTRODUCTION

Hard tissue generation via tissue engineering strategies is one of the most promising techniques in the area of bone grafting because it would eliminate problems of donor site scarcity, immune rejection, and pathogen transfer (44). Almost all tissue engineering concepts require the use of some form of porous scaffold, which serves as a template for cell attachment as well as proliferation and ultimately tissue formation. Osteoblasts, periosteal cells, and bone marrow-derived stem cells (BMSCs) in combination with different scaffold types have been applied in bone tissue engineering. The cell source and type is an important aspect in bone tissue engineering, and the state of the art, especially in the area of BMSCs, has been surveyed by a number of excellent review articles (2,5,25,30,37).

In his "Sur le development et la crue des os des animaux" published in 1742, Duhamel studied the osteogenic potential of periosteum (8). Ollier (26) later on discovered, while working with bone grafts, that transplanted periosteum could induce new bone formation. Tonna and Cronkite (36) demonstrated in 1961 the capability of osteoblast-like cells derived from the periosteum to revert to the osteoprogenitor stage and continue to divide. In the 1990s periosteal cells have been extensively used in bone tissue engineering (4,17,24,28,32,33,38). These concepts aim at mimicking the clinical success of bone autografts by isolating osteoprogenitor cells from the patient's periosteum and seeding a sufficient quantity of cells into bioresorbable scaffolds. The highly porous matrices support the induction of bone regeneration by providing a three-dimensional template that facilitates progenitor cell migration, proliferation, and differentiation as well as graft vascularization (35). In this way, a host tissue/scaffold/cell environment might be created that allows reproducing the intrinsic properties of autogenous bone, which include the ability to be incorporated into the surrounding host bone and to part of the normal bone remodeling processes.

Accepted January 16, 2002.
Address correspondence to Assistant Professor Dietmar W. Hutmacher M.S., Ph.D., M.B.A., Department of Bioengineering, National University of Singapore, 10 Kent Ridge Crescent, Singapore 119260. Tel: 65 874 5101; Fax: 65 777 3537.

Ideally, a scaffold for bone tissue engineering applications should have the following characteristics: (i) highly porous with interconnected pore network for cell growth and flow transport of nutrients and metabolic waste, (ii) biocompatible and bioresorbable with controllable degradation and resorption rate to match tissue replacement, (iii) suitable surface chemistry for cell attachment, proliferation, and differentiation, (iv) mechanical properties to match those of the tissues at the site of implantation for a sufficient period of time, (v) be reproducible processed into a variety of shapes and sizes, (vi) should allow to design and fabricate defect-specific matrices by using computer tomography, computational modeling, and solid free form fabrication (10,13).

Many different processing techniques have been developed to design and fabricate three-dimensional (3D) scaffolds for hard tissue generation (1,35). These conventional techniques include fiber bonding, solvent casting, particulate leaching, membrane lamination, melt molding, temperature-induced phase separation (TIPS), and gas foaming. However, each of these techniques has drawbacks. For example, several research groups have observed a limit to osseous tissue ingrowth and mineralization if foam-like and textile matrices are used (15,16, 28,32). Hutmacher (13) reviewed the current bone tissue engineering literature from a scaffold point of view and concluded that new concepts and technologies are required to design and fabricate scaffolds with complex microarchitectures and macroscopic shapes, which might be able to more adequately mimic the physical properties of bone. Such matrices would allow generating highly vascularized and mineralized hard tissue structures of larger quantity and better quality.

Recently, rapid prototyping technologies have emerged to manufacture scaffolds that might be highly suitable for bone tissue engineering (10,12,22,27,31). Researchers in our laboratory showed that novel PCL scaffolds can be designed and fabricated by fused deposition modeling. The matrices have a fully interconnected honeycomb-like pore architecture that revealed mechanical properties that were in the range of cancellous bone. A number of cell culture studies showed that such PCL templates support the adhesion, proliferation, and differentiation of osteoblast-like cells and allowed the formation of mineralized extracellular matrix throughout the entire scaffold architecture (12,14). The objective of this study was to evaluate bone formation and vascularization of an in vitro tissue-engineered PCL scaffold–cell construct in a nude mice model.

MATERIALS AND METHODS

Scaffold Design and Fabrication

Polycaprolactone scaffolds were fabricated by FDM as described by Hutmacher et al. (14). PCL scaffolds each with lay-down patterns of 0/60/120° and 0/72/144/36/108° and a porosity of 65% measuring $6 \times 6 \times 2$ mm were fabricated. One day prior to cell seeding, the 3D scaffolds were sterilized in 70% ethanol overnight. The ethanol was removed by centrifuging three times in changes of phosphate-buffered saline (PBS) for 15 min at 1000 rpm. Then the scaffolds were transferred for 24 h into an incubator at 37°C for drying.

Cell Culture and Seeding

Primary human osteoprogenitor cells were isolated from a periosteal sheet (3×3 cm), which was stripped off under sterile conditions from the underlying parietal calvarium of a patient undergoing routine craniofacial surgery. Extreme care was taken when separating the cambial layer from the overlying fibrous tissue. The tissue sample was then transferred into sterile Ringer solution and manually minced into 1×1-mm sections. Monolayer cell culture flasks were filled with 3–5 small pieces and Dulbecco's modified Eagle medium (Gibco, Grand Island, NY, USA) with 10% fetal bovine serum, 1% penicillin, and 1% streptomycin and 1% amphoterecin (Gibco) was used. The flasks were then placed in a self-sterilizable incubator (WTB Binder, Tuttlingen, Germany) at 37°C in 5% CO_2, 95% air, and 99% relative humidity. Explants were monitored for outgrowth once a day and fresh medium was added every third day.

After confluent monolayers were achieved by the fourth passage, the cells were enzymatically lifted from the flask using 0.25% trypsin/EDTA (Hyclone, UT, USA) and counted using a hemocytometer. The cells had mortality less than 5% as shown by trypan blue staining and maintained a stable metabolism. Twenty PCL scaffolds with lay-down patterns of 0/60/120° and 0/72/144/36/108° and a porosity of 65% were seeded with 50,000 cells/15 µl culture medium. Subsequently, the seeded scaffolds were placed into 24-well plates and maintained in an incubator to allow the cells to build adhesion plaques on the polymer surface. After 2 h, 1 ml of osteoblastic medium (containing 50 mycr/ml ascorbic acid 2 phosphate and 10 nM dexamethasone) was added into each well. Cell–scaffold constructs were then cultured for a period of 3 weeks.

Phase Contrast Light, Scanning Electron, and Confocal Laser Microscopy

Adhesion, proliferation, and distribution of the cells were studied by phase-contrast light microscopy (IX70 Olympus, Japan). In addition, the establishment of the cell phenotype, intercellular connections, and extracellular matrix production were examined on a routine base. Cell morphology and the surface conditions of the bioresorbable scaffolds were studied via scanning electron microscopy (SEM). Specimens were fixed in 2.5% glut-

eraldehyde (Merck, Germany) for 2 h at 4°C. They were then dehydrated in a graded ethanol series of 30%, 50%, 90%, and 100% for 5 min at each grade, dried, and examined with a Jeol JSM-5800LV SEM at 15 kV.

Cell–scaffold constructs were prepared for confocal laser microscopy (CLM) by staining viable cells green with the fluorescent dye Fluorescein Diacetate (FDA, Molecular Probes Inc., Oregon). The 3D cultures were incubated at 37°C with 2 μg/ml FDA in PBS for 15 min. After rinsing twice in PBS, each sample was then placed in 0.1 mg/ml propidium iodide solution (PI, Molecular Probes) for 2 min at room temperature to stain dead cells red. The samples were then rinsed twice in PBS and viewed under a Confocal Laser Microscope (Olympus IX70-HLSH100 Fluoview). Depth projection images of approximately 125 μm were constructed from up to 25 horizontal image sections through the scaffold–cell constructs.

Cell Morphology and Adhesion

Samples were first fixed in 3.7% formaldehyde at room temperature for 30 min. After rinsing two times with PBS at 5 min each time, 200 μg/ml RNAse A was added and left for 30 min at room temperature. Phalloidin (A12379 Alexa Fluo 488 phalloidin, Molecular Probes Inc.) was then added in a 1:200 dilution for 45 min at room temperature and in darkness. Samples were subsequently counterstained with 5 μg/ml PI solution, dried, and mounted for viewing under fluorescence microscope (IX70 Olympus, Japan).

Metabolic Activity Assay

Cell metabolization and proliferation were studied using an MTS assay (CellTiter 96TM Aqueous One Solution Cell Proliferation Assay, Promega Corp., USA). The MTS tetrazolium compound (Owen's reagent) is bio-reduced by cells into a colored formazan product that is soluble in tissue culture medium. This conversion is presumably accomplished by the NADPH or NADH produced by dehydrogenase enzymes in metabolically active cells. After different time points, PCL scaffolds and 2D tissue culture polystyrene (TCPS) control cultures were assayed. The medium was removed from the wells and 500 μl of FBS-free culture medium added. The MTS reagent (0.1 ml) was then added (100 μl/well), and the plates were incubated for 3 h (37°C, 5% CO_2). The samples were then vortexed with a pipette to ensure a homogenous mixture, and five 100-μl aliquots of each sample were pipetted into a 96-well culture plate. Cell metabolization and growth were determined by measuring the absorbance at 490 nm in a plate reader (Microplate reader, Anthos, USA), and the mean of the five readings was calculated for each time point. Background absorbance was corrected by assaying control wells containing medium and scaffold for the 3-angled and 5-angled scaffolds, and medium only for the TCPS control cultures. Corrected absorbance was obtained by subtracting the average 490 nm absorbance from the "no cell" control wells.

Alkaline Phosphatase Assay

Alkaline phosphatase activity of osteoblast-like cell culture study was measured by using a standard assay method. Supernatant was drawn after different time points. Aliquots of 50 μl were incubated with 450 μl of a 1 M diethanolamine-hydrochloric acid and 0.2% *p*-nitrophenyl phosphate (Product No. 104-0, Sigma) solution for 30 min at 37°C. The reaction was stopped by adding 500 μl of a 2 M NaOH and 0.2 M EDTA solution. The production of *p*-nitrophenol was measured by monitoring absorbance at 405 nm using a plate reader (Microplate reader, Anthos). The mean of six readings was taken for each time point, and cells grown on TCPS were used as a positive control.

Osteocalcin Assay

The supernatant from scaffold–cell constructs of both groups was collected at weeks 1 to 3 and immediately frozen at −80°C. Prior to analysis, 10 μl of each sample was brought to room temperature and dissolved in 1 ml assay buffer. The quantity of human osteocalcin was determined using an ELISA assay (DSL-10-7600 Active Human Osteocalcin ELISA Kit). All tests were performed in quadruplicate.

Surgical Procedure

The animals were housed in the Animal Holding Facility, Department of Experimental Surgery, National University Hospital, for the entire duration of the experiment. Housing and feeding were done according to standard animal care protocols. The studies had been approved by the Animal Welfare Committee of the National University of Singapore and had been licensed by the National Institute of Health's Guide for Care and Use of Laboratory Animals.

Implantation of experimental (six cultured scaffold constructs of each group of the in vitro experiment) and control (four noncultured scaffolds of each group) specimen was performed under sterile conditions in a laminar flow hood. Twenty male 6–8-week-old athymic Balb C nude mice, weighing 20–22 g each, were used for the in vivo study. The mice were anesthetized with 0.15 ml of an anesthetizing cocktail (Dormicum in combination with Hypnorm, 1:1) IP before the operation.

The backs of the mice were prepared with iodine and 70% alcohol and the animals were placed in a prone position on the table. An approximately 10-mm-long incision, slightly to the left of the spine, was made and

widened with a pair of iris scissors. A subcutaneous pocket was created into which the implants were inserted (left and right side). Animals were sacrificed 6 and 17 weeks postimplantation.

Histology and Immunohistochemistry

One half of each of the explanted specimens was fixed in Schaffers solution and embedded in PMMA (Technovit 9100 Heraeus-Kulzer Wehrheim, Germany). Sections (5 μm thick) were cut using a microtome (Leica RM 2165, Germany) and mounted on poly-L-lysine (Sigma, NJ)-coated slides. Sections were deplastified using 2-methoxyethyl-acetate (Merck, Germany) and a decreasing ethanol series. Additional cryosections from fresh tissue samples were also performed. Both types of slides were stained with von Kossa silver nitrate, Trichrome Goldner, and toluidine blue.

Immunohistochemistry with antibodies raised against the human HLA I epitope was carried out on calcified sections. Slides were incubated in humidified chambers for 1 h at 37°C with the primary antibodies. For identifying and separation between mouse and human tissue, slides were incubated with monoclonal antibodies raised against the human HLA 1 ABC epitope (Clone W 5/32 Mouse Anti-Human, Dako, Denmark). Nonspecific sites of the antibody were shut off with a peroxidase block. Primary antibodies were detected with a 3,3-diaminobenzidine substrate and a chromogen peroxidase system (Dako EnVision+ System Peroxidase DAB). Counterstaining was performed with Gills hematoxylin (Sigma Diagnostics, NY). Positive and negative controls were carried out on murine osteoblasts (negative) and human osteoblasts (positive) fixed cultures.

Osteocalcin immunostaining was carried out to further evaluate the tissue mineralization and calcification process. Monoclonal mouse anti-human/bovine osteocalcin antibody (Biodesign, Saco, ME, USA) was used in a dilution of 1:100. Slides were then incubated with a peroxidase-labeled polymer, which is connected with secondary antibodies (Dako En Vision Peroxidase DAB, Hamburg, Germany). Then counterstaining with Gills hematoxylin was performed as described above.

Gas Permeation Chromatography

Triplicates from each PCL specimen were taken to measure the molecular weight to study in vivo degradation. The polymer molecular weight distribution was determined by gel permeation chromatography equipped with a differential refractor (Waters, Model 410, Milford, MA) and an absorbance detector refractor (Waters, Model 2690). The samples were dissolved in tetrahydrofuran (THF) and eluted in a series of configurations through a Styragel columns refractor (Waters) at a flow rate of 1 ml min^{-1}. Polystyrene standards (Polysciences, Warrington, PA) were used to obtain a calibration curve.

Statistical Analysis

The data from the MTS cell proliferation assay, ALP, and osteocalcin test are presented as means ± SD. The statistical significance between the two groups was evaluated by the Student's paired *t*-test.

RESULTS

In Vitro Study

Microscopically, it was observed that the cells had proliferated and spread on the PCL bars and cross sections, presenting a star-shaped morphology from days 1 to 5. Cells filled pores of the PCL specimens of both groups by two different ways. Centripetal cellular ingrowth was observed, with cells growing inward from a circular rim of cells bridging adjacent PCL struts/bars, observed as early as day 6. Cells first formed a crescent monolayer at the PCL bars interconnections (Fig. 1a). Multiple cell layers in combination with ECM formation could be observed from days 7 to 15. Direct bridging across the midline of scaffold pores was also seen. However, this phenomenon was only revealed from day 15 onwards and occurred less frequently than the first mechanism. By day 18, there was evidence of ECM formation within the PCL scaffold architecture of each group. Mineralized extracellular matrix formation and cell-to-cell contact via filopodia could be microscopically detected throughout the entire scaffold architecture (Fig. 1b).

SEM was applied to study the cell and tissue morphology as well as the cell–tissue PCL interface. Figure 2a and b demonstrates osteoblast attachment on PCL struts of both groups after 6 days in culture. Osteoblasts have formed a confluent monolayer with cell–cell connections, showing stellate osteoblast morphology and filopodia. PCL scaffolds were covered with multiple cell layers and also demonstrated extracellular matrix formation 6–15 days postseeding. The formation and mineralization of nodules could be seen throughout the entire scaffold architecture at days 15–18. Evidence of nodule formation was also seen in the SEM images on tissue layers bridging scaffold pores (data not shown).

Comparing the micrographs obtained by phallodine staining (Fig. 3a) and SEM (Fig. 3b) further revealed the proliferation and colonization pattern of the osteoblast-like cells. The cells anchored strongly onto the PCL surface via focal adhesion points. Actin-containing stress fibers bonded directly onto the polymer surface. In week 2, the cells appeared to span three-dimensionally across the pore structure preferably using the interjunctions of the columns and rods of the honeycomb scaffold architecture.

A cell viability assay using a combination of FDA

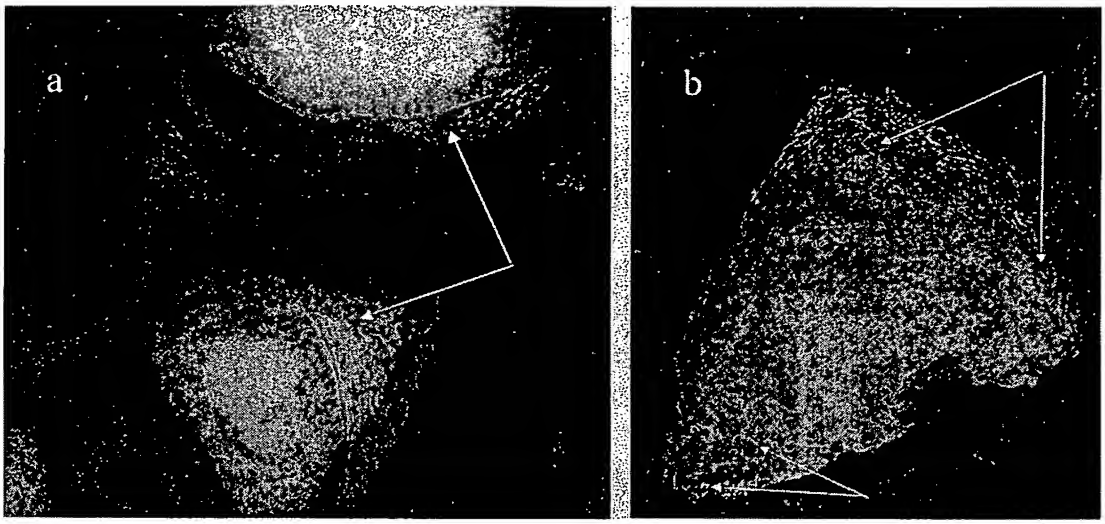

Figure 1. Phase light contrast microscopy images (original magnification ×100) of PCL scaffolds with a 0/60/120° lay-down pattern 7 days postseeding (a). Centripetal cellular ingrowth was observed, with cells growing inward from a circular rim of cells bridging adjacent PCL struts (arrows). Individual cells had a long, thin, spindle-shaped morphology typical for the cells originating from mesencymal tissues. Micrographs of periosteal cells cultured within a PCL specimen with a 0/72/144/36/108° lay-down 18 days postseeding. The formation and mineralization of nodules (b, arrows) could be seen throughout the entire scaffold architecture.

and PI labeling has been used in this study (Fig. 4a, b). Upon addition of FDA, functional esterase enzymes in the cytoplasm of viable cells hydrolyze the nonpolar FDA, resulting in an accumulation of fluorescent, polar fuorescein in the cytoplasm. Due to its polarity, fluorescein is trapped within viable cells, and the entire cytoplasm thus emits green fluorescence under the confocal laser microscope. PI, on the other hand, is excluded by the plasma membranes of viable cells due to its cationic nature. A characteristic feature during the initial phase of apoptosis is the preservation of the structural integrity and most of the plasma membrane functions. PI thus

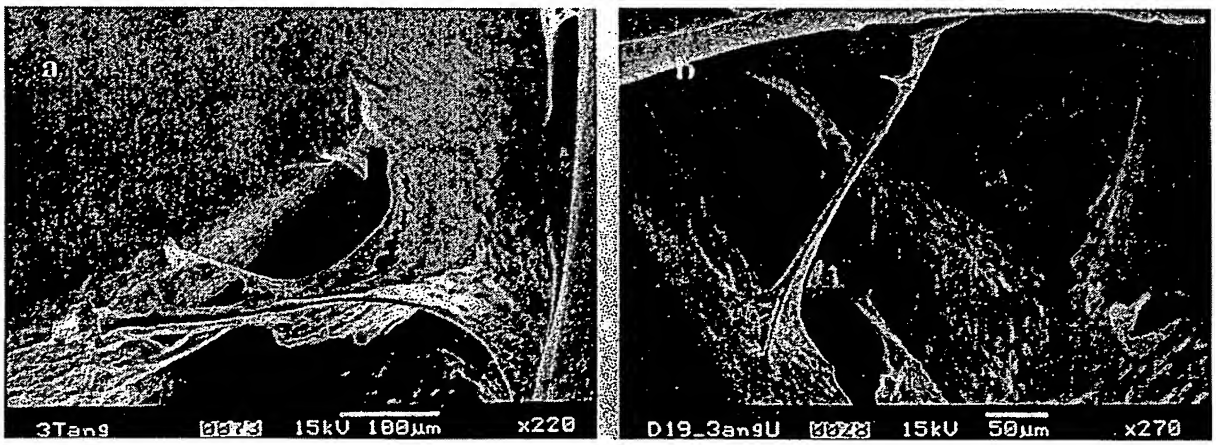

Figure 2. Representative SEM images of periosteal cells bridging specimens of 3-angled (a) and 5-angled (b) PCL scaffolds. Cells had formed a monolayer with cell–cell connections 3–6 days postseeding. Higher magnification showed a stellate osteoblast morphology and filopodia. The cells colonized on PCL bars/struts like roots of a tree and have a stable anchorage to fill the entire pore volume.

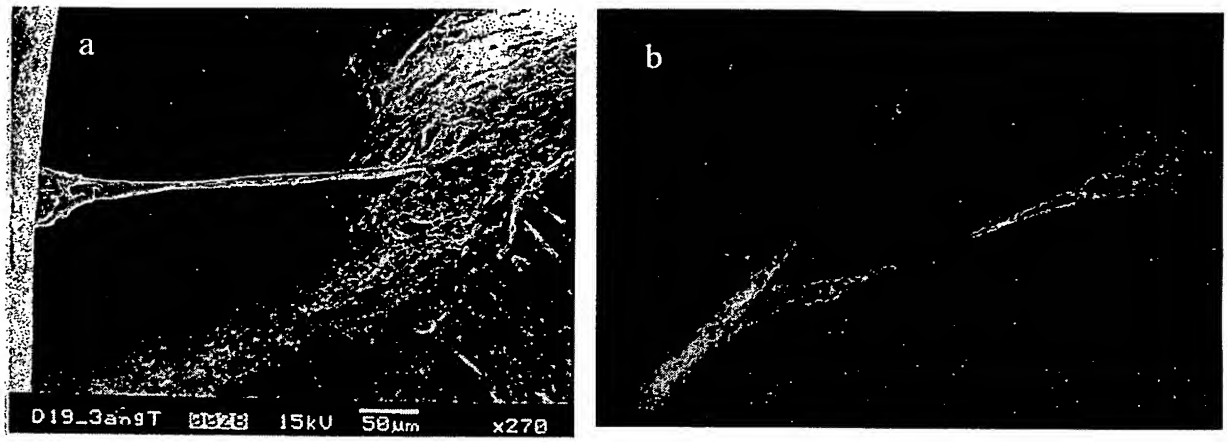

Figure 3. Representative fluorescence microscopy image (original magnification ×200) and corresponding SEM micrograph (original magnification ×270) of a 5-angled PCL scaffold cultured for 9 days. In the phalloidin-propidiumiodide-stained specimen, the adhesion and proliferation of the osteoblast-like cells on the PCL surface and the cell-to-cell contact was shown by studying the actin fiber (which stained green) and cell nucleus (which stained red) arrangement. Intracellular bundles of f-actin filament (stress fibers) indicated the formation of focal adhesions. The cells were forming focal contact patches on the bars of the scaffold whereas most prominent intracellular f-actin filaments could be detected when cells were bridging pores. There was no visible difference in the fibril pattern of cells on 3- or 5-angle scaffolds. The cells first colonized the PCL bars/struts and then branched out to fill the pore volume with cells and ECM.

penetrates only cells with damaged membranes (necrotic and late apoptotic cells) and forms a red complex with nuclear DNA. Confocal micrographs revealed a net-like proliferation pattern on the PCL columns and bars.

In the first week a denser cell network was qualitatively observed in the 3-angle architecture (Fig. 4a) whereas at week 3 the 5-angle scaffolds (Fig. 4b) showed more cells and ECM. Both matrix architectures presented a

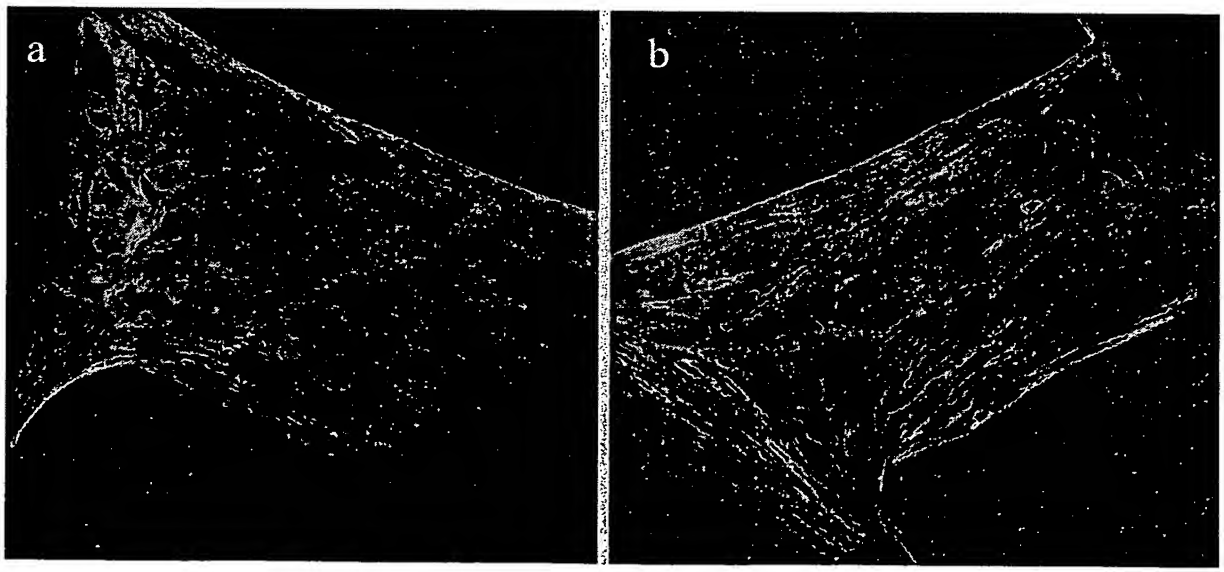

Figure 4. Confocal micrographs revealed a net-like proliferation pattern on the PCL columns and bars. In the first week a denser cell network was qualitatively observed in the 3-angle architecture (a) whereas at week 3 the 5-angle scaffolds (b) showed more cells. Both matrix architectures presented a low rate of apoptosis starting only at week 3.

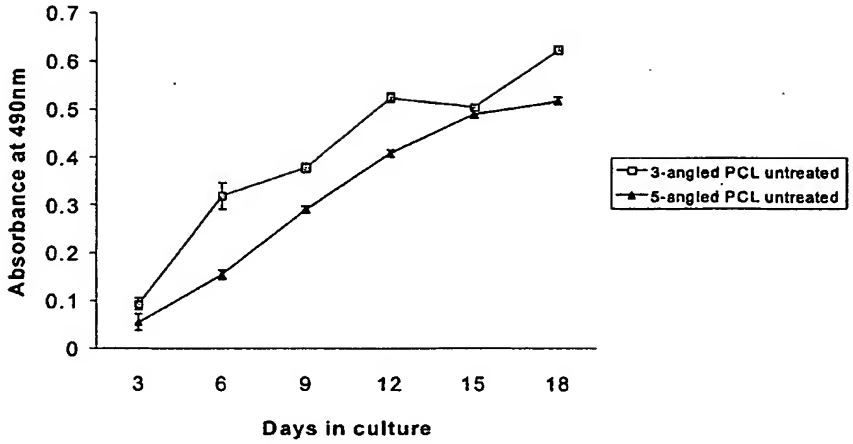

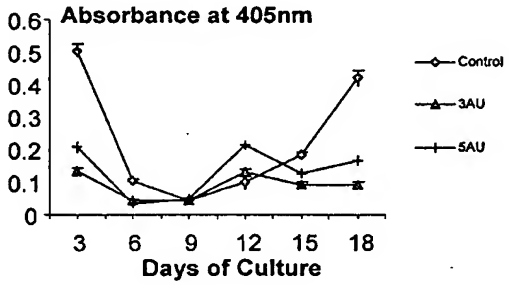

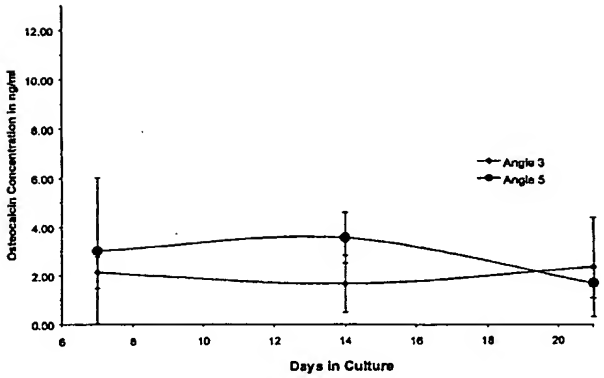

Figure 5. Osteoblast-like cell metabolization and proliferation on 3- and 5-angled PCL scaffolds as measured by the MTS assay. Values represent the mean ± SD of five readings. Alkaline phosphatase (ALP) activity and osteocalcin concentrations measured in the supernatant of the different scaffold specimens. Values represent the mean ± SD of eight samples. The up and down regulation of the ALPase activity in all groups is related to the fact that primary human cell cultures compared to cell lines contain a very inhomogeneous cell population. Osteocalcin levels peaked at week 1, followed by a steady decrease in weeks 2 and 3.

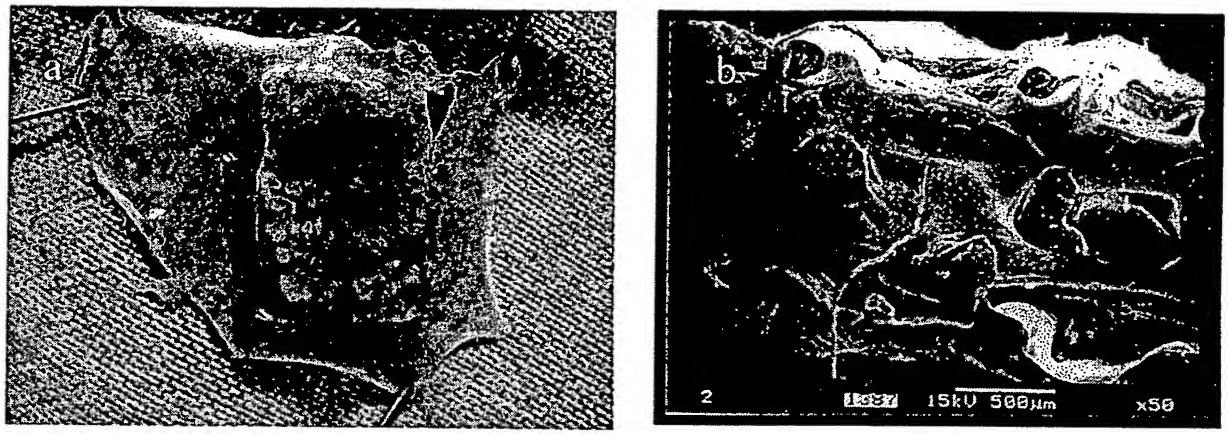

Figure 6. At the time of harvesting (6 weeks after implantation), homogenous tissue blocks could be found, which upon gross examination appeared well integrated into the surrounding host tissue. Macroscopically, angiogenesis could be observed with many vessels infiltrating the entire scaffold–tissue macrostructure (a). A corresponding SEM micrograph is showing a vascular structure infiltrating the scaffold–tissue contruct (b, original magnification ×50).

low rate of apoptosis starting only at week 3. Similar proliferation and growth pattern could be observed for the 3- and 5-angle scaffold morphology. Cells continued to proliferate after colonizing the scaffold surface in a three-dimensional manner because they were not space limited and had the possibility of filling the entire interconnected matrix architecture. ECM formation was observed in the confocal laser microscopy, with thick confluent interconnecting multilayers of osteoblasts observed on PCL struts by day 18 within both scaffold groups.

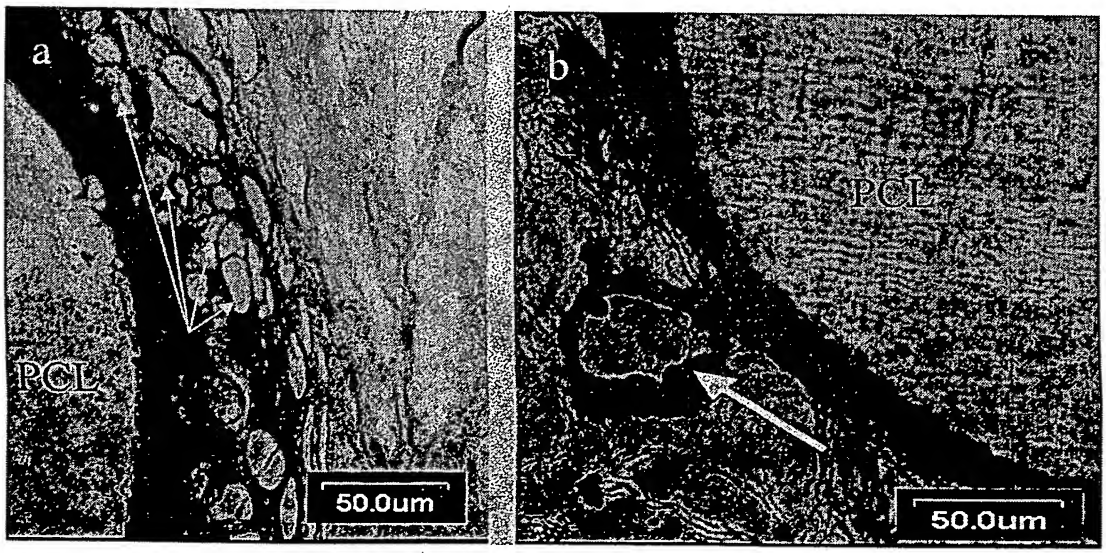

Figure 7. Histological assessment via cryosections showed a mineralization of the matrix and a regular osteoid formation around the osteoblastic cells (a, arrows). Vascular sinusoids (b, arrow) could be detected throughout the entire scaffold architecture. An ingrowth from surrounding fibrous tissue could be observed, although there was no granular encapsulating tissue, usually indicating a foreign body reaction. Precalcified tissue with osteoblast lining on the scaffold surface resulted in three-dimensional woven bone formation. Mineralized matrix was found around cuboideal-shaped osteoblasts that formed clusters of 3–5 cells (a). The was no significant difference of tissue formation detectable between 3-angle and 5-angle scaffolds.

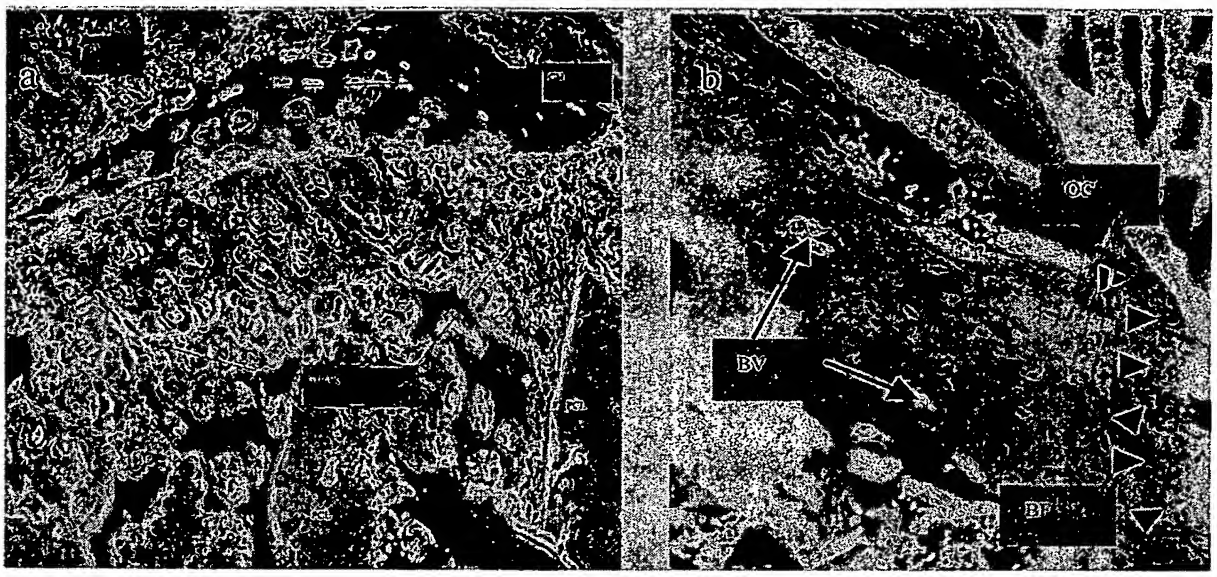

Figure 8. Histological micrograph of an explanted PCL scaffold–tissue construct of the osteoblast-like cell seeded group. Callus-like tissue (CT) was formed around PCL matrix. Isogenous groups (IG) can be detected, which are indicative of interstitial growth. The black stained area is indicating calcified extracellular matrix (CM) (a, Von Kossa staining, original magnification ×15). Histological micrograph of an explanted PCL scaffold–tissue construct of the osteoblast-like cell seeded group. Osteocytes (OC) trapped within mineralized bone matrix and blood vessel (BV) are shown. Osteocytes aligned in a row can be seen directly at the interface were bone is formed (BF) (b, toludine blue staining, original magnification ×20).

Based on the confocal laser microscopy, a significant difference of the proliferation patterns of the two different scaffold architectures could not be observed.

In summary, qualitative image analysis revealed no significant difference between the two different scaffold architectures. In both scaffold morphologies periosteal cells attached and proliferated in monolayers in the initial phase. Sequentially multiple cell layers were formed and ECM formation began at junctions of PCL struts and bars, and proceeded by filling up the honeycomb pores by centripetal growth patterns within a period of 21 days.

Quantitative analysis was performed by a MTS assay and measuring the ALP activity of the supernatant. MTS assay (Fig. 5) revealed that metabolic activity of the attached and proliferated cells increased approximately ninefold between days 3 and 21. Osteoblasts seeded on 3-angled PCL scaffolds had higher MTS values in the first 2 weeks, leveling off after day 18. There was a significant difference between 3-angled and 5-angled PCL scaffolds ($p < 0.05$) in the first 18 days of culture. Cells seeded on 5-angled PCL scaffolds demonstrated an initial slower metabolization rate; however, by day 21 comparable cell activity was achieved.

Alkaline phosphatase activity was measured in the supernatant of all specimen constructs every third day. PCL samples demonstrated high levels of ALP activity (Fig. 5), which was comparable to cells cultured on 24-well tissue culture plates (TCPS). There was no significant difference ($p < 0.05$) in enzyme activity between cells cultured on 3-angled and 5-angled scaffolds (Fig. 7). Osteocalcin production (Fig. 5) in the supernatant showed no significant difference ($p < 0.05$) for both groups. The basal osteocalcin synthesis on the periosteal–cell seeded constructs ranged from 1.5 to 3.8 ng/ml.

In Vivo Study: Macroscopic Appearance

All the mice tolerated the surgical procedures and implantation without any postoperative inflammation, foreign body reaction, or impaired wound healing. At 6 and 17 weeks after implantation, homogenous PCL scaffold–tissue blocks could be seen on the back of the nude mice. Two areas of increased firmness could be touched on the mice skin. Tissue-engineered constructs of both lay-down patterns (0/60/120° and 0/72/144/36/108°) could be excised at the time of harvesting.

Upon gross examination the implants appeared well integrated into the surrounding host tissue. There was no change in size of all implants to the original dimension of the PCL scaffold. The subjective consistency of the fresh explanted specimen was evaluated by probing with a pair of forceps. The samples of the osteoblast

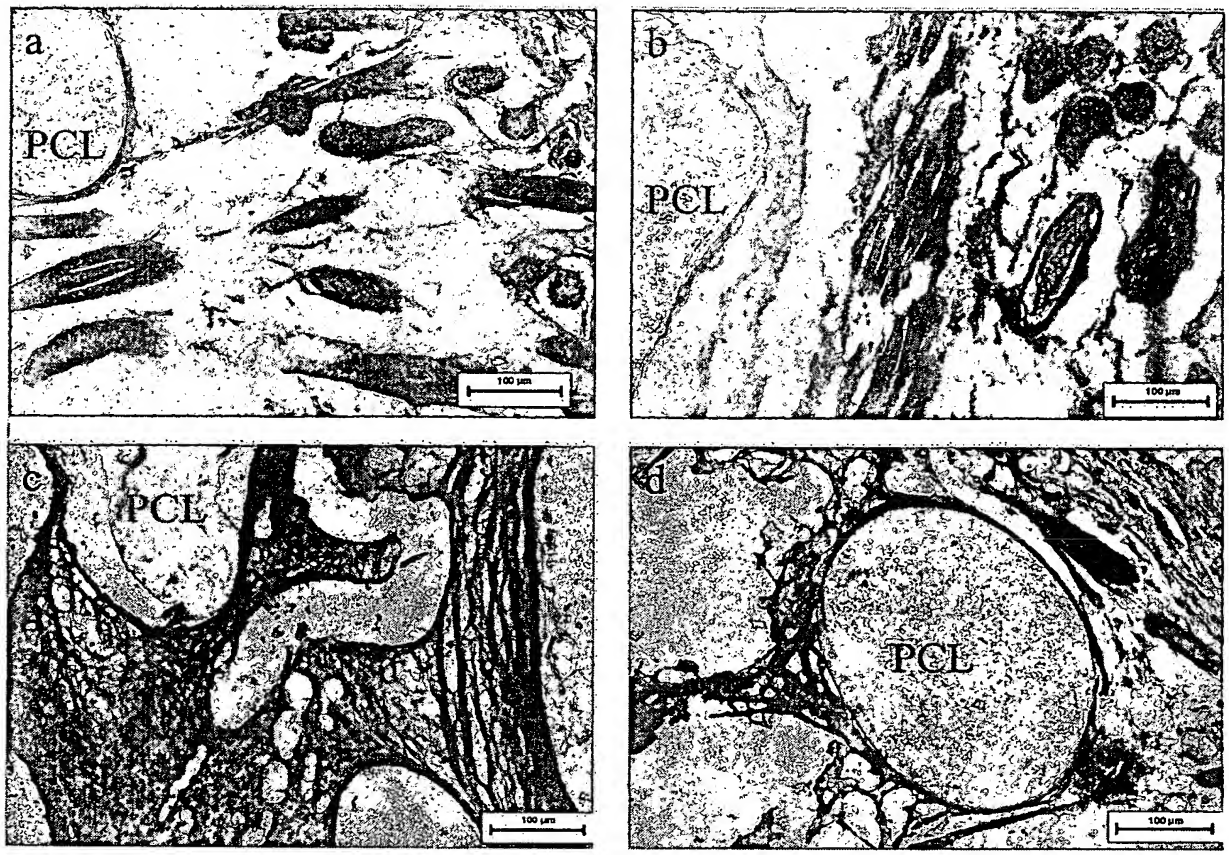

Figure 9. Representative histological sections and immunohistochemical staining, using a monoclonal antibody against human osteocalcin of the implants 17 weeks postimplantation (all pictures original magnification ×100). In vertical cross sections the von Kossa silver nitrate staining shows in dark brown/black areas of calcium phosphate deposits in the conical caps of the bone forming loci (a). In between loose nonmineralized fibrous tissue, light brown color is present. Note in a horizontal section the murine muscular paniculus carnosus is shown (b). Immunohistochemical sections from 3-angle (c) and 5-angle (d) constructs show a positive reaction with the osteocalcin antibody in mineralized areas. Intensive staining for osteocalcin (brown) is seen around the bars and struts of the polymer material. Tissue in the periphery towards the skin of the nude mice shows only sparsely stained brown areas (osteocalcin positive) or are negative for osteocalcin (blue hematoxylin counterstain).

seeded groups demonstrated a certain hardness and rigidity whereas control specimens (nonseeded and cultured) exhibited softer indentation under compression after 6 and 17 weeks of implantation.

Macroscopically, angiogenesis (Fig. 6a) could be observed with many vessels infiltrating the osteoblast seeded and nonseeded specimens with both lay-down patterns. This was also confirmed by SEM analysis (Fig. 6b). From a macroscopic point of view a fibrous tissue capsule or fibrotic reaction could not be detected for any of the specimens. A highly vascularized connective tissue layer of the nude mice skin was always firmly attached to the top of the scaffold (Fig. 6a). The PCL bars/struts at the bottom side of the scaffold–tissue construct were clearly visible for the nonseeded specimens whereas the seeded samples were covered with a firm tissue structure.

Histological assessment showed mineralization of the matrix and a regular osteoid formation around the osteoblastic cells. Mineralized matrix was found around cuboideal-shaped osteoblasts, which formed clusters of 3–5 cells (Fig. 7a). Vascular sinusoids could be detected at numerous locations (Fig. 7b) throughout the entire scaffold architecture of both groups. An ingrowth from surrounding fibrous tissue could be observed, although there was no granular encapsulating tissue, usually indi-

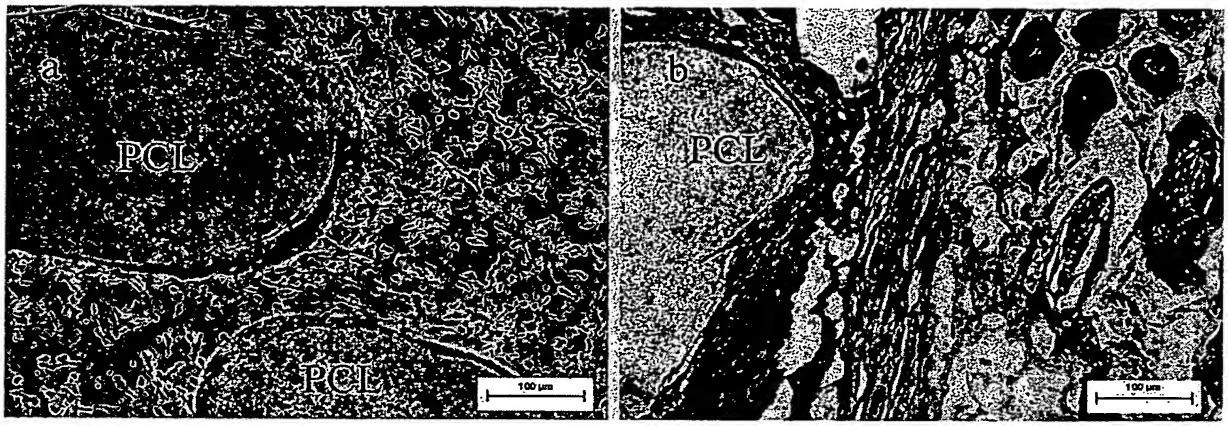

Figure 10. Immunohistochemistry using monoclonal antibodies against the human HLA I epitope. (a) The unseeded negative control. Reticular fibrous tissue is present with no human cells (original magnification ×100). Brown stained areas indicate the HLA-positive tissue formed by human periosteal cells. Counterstaining with Gill's hemotoxylin (blue) for mouse tissue (b, original magnification ×100).

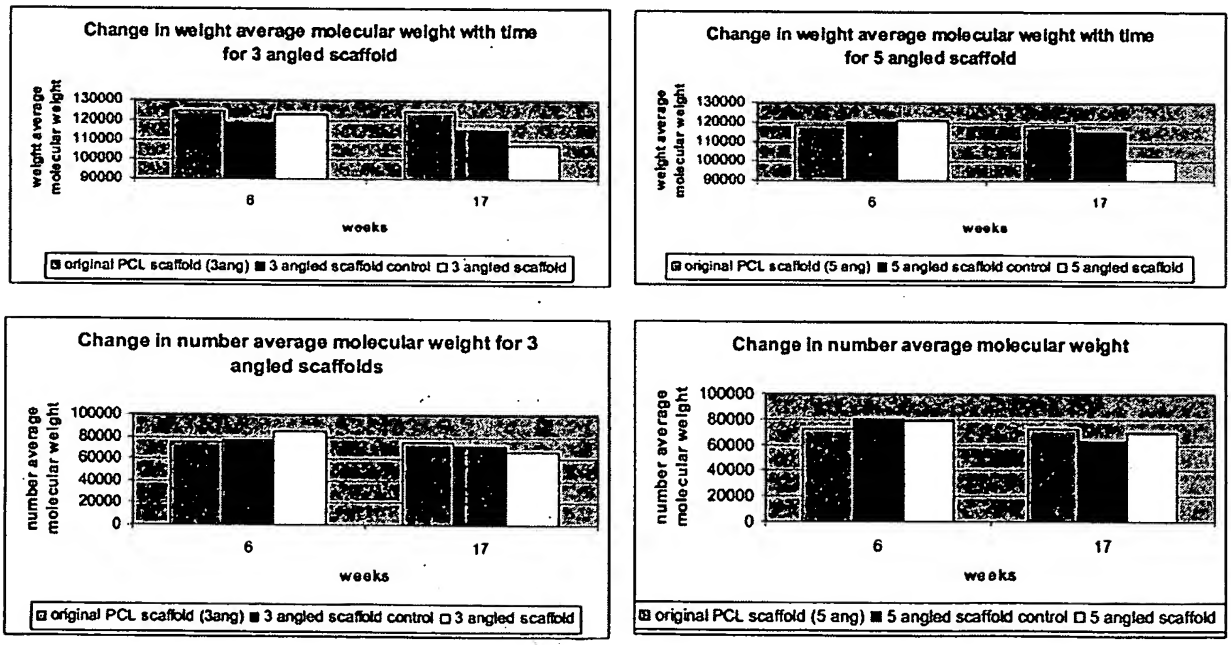

Figure 11. The first stage of the degradation process of PCL involves nonenzymatic, random, hydrolytic ester cleavage and its duration is determined by the initial molecular weight of the polymer as well as its chemical structure. The second phase is characterized by the onset of weight loss. GPC was employed to assess the molecular weight distribution as function of the degradation kinetics. Perhaps the best representation of the change in molecular weight is visible in the polydispersity index (PI). The PCL scaffold with both lay-down patterns did not show significant changes after 3 weeks of culturing and 6 weeks of implantation. In contrast, the molecular weight of the 17-week specimen revealed a decrease of about 20% and the polydispersity showed a change of 40%. High PI corresponds to a conglomerate of chains spanning a wide range of molecular weights. The PCL scaffolds initially had a low PI value and during implantation of 17 weeks the longer molecular chains were cut by hydrolysis into small fragments of wide ranges, which resulted in an increased PI.

cating a strong foreign body reaction. There was no significant difference of tissue formation detectable between 3-angle and 5-angle scaffolds. In the control groups where unseeded scaffolds were implanted only fibrous tissue infiltration could be observed (histology not shown, immunohistochemistry see Fig. 10).

Cryosections showed that there was homogenous bone formation within the entire scaffold architecture with no abundant bone in the surrounding soft tissue areas. Histological characterization showed that organized lamellae areas were found besides immature woven sites. This suggests that mature lamella bone slowly replaced the immature woven areas via a remodeling process (Fig. 8a, b). After 17 weeks, upon gross examination, constructs appeared well integrated in the surrounding soft tissue and invasion of capillaries was present throughout the entire honeycomb scaffold architecture. A thin tissue encapsulation with a nonprominent foreign body reaction was detectable.

Examination of the histological results showed lamellae bone formation with scattered islands of cuboideal-shaped osteoblasts within the 3- and 5-angle scaffold architecture. The von Kossa staining revealed that portions of these clusters had been mineralized with mineral deposits characteristically located at the conical cap (Fig. 9a, b). The appearance of these cellular condensation units is similar to those seen in enchondral ossification or secondary bone healing via callus formation. The HLA immunostaining (Fig. 10a, b) revealed a great amount of HLA I-positive human cells, which played a major role in the bone formation process. However, it has to be stressed that in the nude mice model the vascularization is coming from murine cells, which migrate from the surrounding tissue into the scaffold–cell constructs. The entire scaffold architecture was intact 17 weeks postimplantation and, therefore, the new tissue did fill out the entire pore volume of 65%. Comparing the 6-week results to the 17-week findings indicates that there was no increase of bone formation regardless of implantation time. The two different scaffold architectures gave similar results at both time points. Analysis of the unseeded control specimens showed homogeneous fibrous tissue formation of mouse origin in the implants with 3-angle and 5-angle lay-down patterns (Fig. 10a).

The results of the GPC analysis are shown in Figure 11. The PCL scaffold with both lay-down patterns did not show a significant change in the molecular weight distribution after 3 weeks of culturing and 6 weeks of implantation. In contrast, the molecular weight of the 17-week specimen revealed a decrease of about 20% and the polydispersity showed a change of 40%.

DISCUSSION

Several groups have tissue engineered bone in different animal models by using periosteal cells in combination with textiles (4,23,29,34,36,39) as well as foams (15,17) made of PGA and PGA/PLA. The tissue engineers could show that transplantation of osteoprogenitor cells in combination with a bioresorbable scaffold is an encouraging approach to further enhance the process of bone regeneration. Primary human periosteal cells seeded and cultured on PCL scaffolds, which have been shown by immunohistochemistry to maintain their osteogenic potential in cell culture for up to 21 days, have been used in the study presented in this article. From the MTS assay it was evident that the cells continually proliferated in both scaffold groups over a period of 3 weeks. The qualitative results from the light, confocal laser, and scanning electron microscopy seemed to further support these observations.

By implanting the tissue-engineered grafts in extra-osseous sites it was shown by immunostaining that osteogenesis was induced by the transplanted scaffold–tissue construct, in combination with the vascular network of the nude mice. Tissue-engineered constructs have to match the intrinsic properties of autogenous bone grafts to demonstrate clinical feasibility. Hence, in vivo mineralization of tissue grown in vitro is a condition sine qua non. Mineralized matrix deposition and calcification of tissue as well as osteoid formation could be observed in the explanted constructs. There was bone formation within the whole PCL scaffold with no superfluous bone in the surrounding soft tissue areas, indicating that de novo tissue formation takes part only in the provided matrix structures and that no uncontrolled tumor-like growth occurred.

Histologically, there was no detectable immunoresponse, which was concordant with the macroscopic findings where good tissue integration was observed without any thick fibrous capsule formation and/or inflammation. The anti-human HLA class I antibody was used first in the area of bone tissue engineering by Prabhakar et al. (32) to analyze the bone formation of human bone marrow-derived cells that were injected into the back of nude mice. We followed their protocol and it was shown that mineralized tissue was formed by the transplanted periosteal cell inside the PCL scaffold. Histological characterization of the newly formed bone revealed that organized lamination areas were found adjacent to immature woven sites, which might suggest that lamella bone slowly replaces the immature woven areas during the remodeling process inside the PCL scaffold. This is in accordance with Yoshikawa et al. (43), who demonstrated in a long-term in vivo study that bone showed consistent lamella bone remodeling 50 weeks after ectopical implantation.

The volume, density, and size of the pores and interconnections are important factors for bone ingrowth into porous matrix systems. The effects of pore size on bone ingrowth have been widely studied on ceramic

scaffolds with a porosity ranging from 50% to 70% (7,9,18–20,42,43). The studies of the groups discussed here conclude that mineralized bone formation in vivo was highest in matrix systems with a pore size of 300–600 μm.

These results led tissue engineers to study the effects of pore size and porosity on cell proliferation and in vitro as well as in vivo tissue formation on seeded scaffolds (41). Based on the results of the studies on two-dimensional matrices, three-dimensional scaffolds for tissue engineering have been fabricated by using poly(lactide-*co*-glycolide) copolymers and solvent casting in combination with particulate leaching (15,21,22). Rat bone marrow cells grown on these structures produced only a superficial mineralized layer on the outer scaffold surface (11,15,16). Although these scaffolds demonstrated the promise of bone tissue engineering, the morphology (pore size and geometry, size and geometry of pore interconnections, interconnectivity) of the first generation of foams did not allow 3D bone-like tissue formation inside the scaffold.

The pore interconnections inside a scaffold act as pathways for nutrients, cells, and ultimately for vascularization in vivo. A number of in vivo studies (9,18,20, 43) on ceramic matrix systems noted that the size of pore interconnections must be over 100 μm to favor mineralized bone tissue formation. The FDM-designed and fabricated PCL scaffolds have a fully interconnected scaffold architecture that is designed by a large and highly regular channel network (13). Such a honeycomb-like structure allows in vitro cell proliferation and mineralized ECM production throughout the entire matrix due to sufficient transport of nutrients and waste (12). The mineralized bone tissue formation appears throughout the entire scaffold.

For tissue engineering a bone transplant, the creation of a vascularized bed ensures the survival and function of transplanted cells, which have access to the vascular system for nutrition, gas exchange, and elimination of by-products (38). The vascularization of a scaffold architecture with large pores (300–600 μm) but small pore interconnections (10–50 μm) may be compromised because it relies primarily on capillary ingrowth from the host tissue. In situ, the distance between blood vessels and mesenchymal cells is not larger than 100–200 μm (39). The detection of blood vessels within the newly formed bone inside the PCL scaffolds demonstrated the vascularization and viability of the generated tissue. The FDM design and fabrication of a honeycomb-like pore structure combined with large channel interconnections provided a morphology that allowed the host tissue of the nude mice to develop a capillary network inside the entire scaffold architecture.

The molecular weight of the PCL scaffold did not change significantly after being exposed 3 weeks in cell culture media followed by 17 weeks of in vivo exposure. Hence, the PCL scaffold was able to maintain its structural properties for a sufficient period of time for tissue engineering bone in a nude mice model. It is reported in the literature that medical and drug delivery devices made of PCL start degrading after 4–6 months and are completely metabolized by the body after 18–24 months (3,6,30,40). Therefore, as a next step towards a clinical application, the tissue response of the host as well as the properties of the tissue-engineered bone inside the novel PCL scaffold has to be studied in an immunocompetent animal model over a period of up to 2 years. Such studies are currently performed in our laboratory.

REFERENCES

1. Agrawal, C. M.; Bay, R. R. Biodegradable polymeric scaffolds for musculoskeletal tissue engineering. J. Biomed. Mater. Res. 55:141–150; 2001.
2. Anselme K. Osteoblast adhesion on biomaterials. Biomaterials 21:667–681; 2000.
3. Bezwada, R. S.; Jamiolkowski, D. D.; Lee, I.; Vishvaroop, A.; Persivale, J.; Treka-Benthin, S.; Erneta, M.; Suryadevara, J.; Yang, A.; Liu, S. Monocryl™ suture, a new ultrapliable absorbable monofilament suture. Biomaterials 16: 1141–1148; 1995.
4. Breitbart, A. S.; Grande, D. A.; Kessler, R.; Ryaby, J. T.; Fitzsimmons, R. J.; Grant, R. T. Tissue engineered bone repair of calvarial defects using cultured periosteal cells. Plast. Reconstr. Surg. 101(3):567–576; 1998.
5. Caplan, A. I.; Bruder, S. P. Mesenchymal stem cells: Building blocks for molecular medicine in the 21st century. Trends Mol. Med. 7(6):259–264; 2001.
6. Darney, P. D.; Monroe, S. E.; Klaisle, C. M.; Alvarado, A. Clinical evaluation of the Capronor contraceptive implant: Preliminary report. Am. J. Obstet. Gynecol. 160:1292–1295; 1989.
7. Dennis, J. E.; Haynesworth, S. E.; Young, R. G.; Caplan, A. I. Osteogenesis in marrow-derived mesenchymal cell porous ceramic composites transplanted subcutaneously: Effect of fibronectin and laminin on cell retention and rate of osteogenic expression. Cell Transplant. 1:23–32; 1992.
8. Duhamel, H. L. Sur le developpement et la crue des os des animaux. Mem. Acad. R Sci. 55:354–370; 1792.
9. Eggli, P. S.; Muller, W.; Schenk, P. K. Porous hydroxyapatite and tricalcium phosphate cylinders with two different pore size ranges implanted in the cancellous bone of rabbits. A comparative histomorphometric and histologic study of bony ingrowth and implant substitution. Clin. Orthop. 232:127–138; 1988.
10. Feinberg, S. E.; Hollister, S. J.; Halloran, J. W.; Chu, T. M.; Krebsbach, P. H. Image-based biomimetic approach to reconstruction of the temporomandibular joint. Cells Tissues Organs 169(3):309–321; 2001.
11. Goldstein, S. A.; Zhu, G.; Morris, G. E.; Meszleniyi, R. K.; Mikos, A. G. Effect of osteoblastic culture conditions on the structure of poly (DL-lactic-coglycolic acid) foam scaffolds. Tissue Eng. 5:421–433; 1999.
12. Hutmacher, D. W.; Zein, I.; Teoh, S. H.; Ng, K. W.; Schantz, J. T.; Leahy, J. C. Design and fabrication of a 3D scaffold for tissue engineering bone. In: Agrawal, C. M.; Parr, J. E.; Lin, S. T., eds. Synthetic bioabsorbable polymers for implants, STP 1396. West Conshohocken,

PA: American Society for Testing and Materials; 2000: 152–167.
13. Hutmacher, D. W. Polymeric scaffolds in tissue engineering bone and cartilage. Biomaterials 21:2529–2543; 2000.
14. Hutmacher, D. W.; Schantz, J. T.; Zein, I.; Ng, K. W.; Tan, K. C.; Teoh, S. H. Mechanical properties and cell cultural response of polycaprolactone scaffolds designed and fabricated via fused deposition modeling. J. Biomed. Mater. Res. 55:1–15; 2001.
15. Ishaug, S. L.; Crane-Krueger, G. M.; Miller, M. J.; Yasko, A. W.; Yaszemski, M. J.; Mikos, A. G. Bone formation by three-dimensional stromal osteoblast culture in biodegradable polymer scaffolds. J. Biomed. Mater. Res. 36: 17–28; 1997.
16. Ishaug-Riley, S. L.; Crane, G. M.; Gurlek, A.; Miller, M. J.; Yasko, A. W.; Yaszemski, M. J.; Mikos, A. G. Ectopic bone formation by marrow stromal osteoblast transplantation using poly(DL-lactic-co-glycolic acid) foams implanted into the rat mesentery. J. Biomed. Mater. Res. 36:1–8; 1997.
17. Isogai, N.; Landis, W. J.; Mori, R.; Gotoh, Y.; Gerstenfeld, L. C.; Upton, J.; Vacanti, J. P. Experimental use of fibrin glue to induce site-directed osteogenesis from cultured periosteal cells. Plast. Reconstr. Surg. 105:953–963; 2000.
18. Kuhne, J.; Bartl, R.; Frisch, B.; Hammer, C. V.; Zimmer, M. Bone formation in coralline hydroxyapatite. Effects of pore size studied in rabbits. Acta Orthop. Scand. 65:246; 1994.
19. Lu, J. X.; Flautre, B.; Anselme, K. Study of porous interconnections of bioceramic on cellular rehabilitation in vitro and in vivo. In: Sedel, L.; Rey, C., eds. Bioceramics 10. Paris: Pergamon, Elsevier Science; 1997:583–586.
20. Lu, L.; Petera, S. J.; Lymanb, M. D.; Laib, H. L.; Leiteb, S. M.; Tamadab, J. A.; Uyamac, S.; Vacanti, J.; Langer, R.; Mikos, A. G. In vitro and in vivo degradation of porous poly(lactic-co-glycolic acid) foams. Biomaterials 21: 1837–1845; 2000.
21. Maquet, V.; Jerome, R. Design of macroporous biodegradable polymer scaffolds for cell transplantation. Mater. Sci. Forum 250:15–42; 1997.
22. Marra, K. G.; Campbell, P. G.; Dimilla, P. A.; Kumta, P. N.; Mooney, M. P.; Szem, J. W.; Weiss, L. E. Novel three dimensional biodegradable scaffolds for bone tissue engineering. Mater. Res. Soc. Symp. Proc. 550:155–160: 1999.
23. Mikos, A. G.; Bao, Y.; Cima, L. G.; Ingber, D. E.; Vacanti, J. P.; Langer, R. Preparation of poly(glycolic acid) bonded fiber structures for cell attachment and transplantation. J. Biomed. Mater. Res. 27:183–189; 1993.
24. Miura, Y.; O'Driscoll, S. Culturing periosteum in vitro: The influence of different sizes of explants. Cell Transplant. 7(5):453–457; 1998.
25. Ohgushi, H.; Caplan, A. I. Stem cell technology and bioceramics: From cell to gene engineering. J. Biomed. Mater. Res. Appl. Biomater. 48:913–927; 1999.
26. Ollier, L. Recherches experimentales sur les graffes osseuses. J. Physiol. Homme Animaux 3:88–108; 1860.
27. Ono, I.; Tateshita , T.; Satou, M.; Sasaki, T.; Matsumoto, M.; Kodama, N. Treatment of large complex cranial bone defects by using hydroxyapatite ceramic implants. Plast. Reconstr. Surg. 104(2):339–349; 1999.
28. Perka, C.; Schultz, O.; Spitzer, R. S.; Lindenhayn, K.; Burmester, G. R.; Sittinger, M. Segmental bone repair by tissue-engineered periosteal cell transplants with bioresorbable fleece and fibrin scaffolds in rabbits. Biomaterials 21:1145–1153; 2000.
29. Pittenger, M. F.; Mackay, A. M.; Beck, S. C.; Jaiswal, R. K.; Douglas, R.; Mosca, J. D.; Moorman, M. A.; Simonetti, D. W.; Craig, S.; Marshak, D. R. Multilineage potential of adult human mesenchymal stem cells. Science 284(5411):143–147; 1999.
30. Pitt, C. G. Poly(ε-caprolactone) and its copolymers. In: Chasin, R.; Langer, R., eds. Biodegradable polymers as drug delivery systems. New York: Marcel Dekker; 1990: 71–120.
31. Porter, N. L.; Pillar, R. M.; Grynpas, M. D. Fabrication of porous calcium polyphosphate implants by solid freeform fabrication: A study of processing parameters and in vitro degradation characteristics. J. Biomed. Mater. Res. 56(4): 504–515; 2001.
32. Prabhakar, U.; James, E.; Dodds, R. A.; Lee-Rykacewski, E.; Riemann, D. J.; Lipshutz, D.; Trulli, S.; Jonak, Z.; Tan, K. B.; Drake, F. H.; Gowen, M. A. Novel human bone marrow stroma-derived cell line TF 274 is highly osteogenic in vitro and in vivo. Calcif. Tissue Int. 63:214–229; 1998.
33. Redlich, A.; Perka, C.; Schultz, O.; Spitzer, R. S.; Häupl, T.; Burmester, G. R.; Sittinger, M. Bone engineering on the basis of periosteal cells cultured in polymer fleeces. J. Mater. Sci. Mater. Med. 10:767–772; 1999.
34. Sittinger, M.; Bujía, J.; Rotter, N.; Reitzel, D.; Minuth, W. W.; Burmester, G. R. Tissue engineering and autologous transplant formation: Practical approaches with resorbable biomaterials and new cell culture techniques. Biomaterials 17:237–242; 1996.
35. Thomson, R. C.; Yaszemski, M. J.; Powers, J. M.; Mikos, A. G. Fabrication of biodegradable polymer scaffolds to engineer trabecular bone. J. Biomater. Sci. Polym. Ed. 7: 23–38; 1995.
36. Tonna, E. A.; Cronkite, E. P. Cellular response to fracture studied with tritiated thymidine. J. Bone Joint Surg. 43: 352–362; 1961.
37. Uchida, A.; Nade, S. M. L.; McCartney, E. R.; Ching, W. J. The use of ceramics for bone replacement. A comparative study of three different porous ceramics. J. Bone Joint Surg. Br. 66(2):269–275; 1984.
38. Vacanti, C. A.; Vacanti, J. P. Bone and cartilage reconstruction. In: Lanza, R.; Langer, R.; Chick, W., eds. Principles of tissue engineering. New York: R. G. Landes Co.; 1997:619–631.
39. Vander, A. J.; Shermann, J. H.; Luciano, D. S. Human physiology. New York: McGraw-Hill; 1985:341–366.
40. Vert, M.; Li, M. S.; Spenlehauer, G.; Guerin, P. Bioresorbability and biocompatibility of aliphatic polyesters. J. Mater. Sci. 3:432–446; 1992.
41. Wake, M. C.; Patrick, C. W.; Mikos, A. G. Pore morphology effects on the fibrovascular tissue growth in porous polymer substrates. Cell Transplant. 3:339–343; 1994.
42. White, E.; Shors, E. C. Biomaterial aspects of Interpore-200 porous hydroxyapatite. Dent. Clin. North Am. 30:49; 1984.
43. Yoshikawa, T.; Ohgushi, T.; Nakajiima, H.; Akahane, M.; Tamai, S.; Ichijima, K. A. Long term implantation of cultured bone in porous hydroxyapatite. Bioceramics 10: 117–146; 1997.
44. Young, J. H.; Teumer, J.; Kemp, P. D.; Parenteau, N. L. Approaches to transplanting engineered cells and tissues. In: Lanza, R.; Langer, R.; Chick, W., eds. Principles of tissue engineering. Austin, TX: R. G. Landes Co.; 1997: 297–307.

TISSUE ENGINEERING
Volume 8, Number 3, 2002

EXHIBIT 6

In Vivo Mesenchymal Cell Recruitment by a Scaffold Loaded with Transforming Growth Factor β1 and the Potential for *in Situ* Chondrogenesis*

Q. HUANG, M.D., M.Sc.,[1] J.C.H. GOH, Ph.D.,[1]
D.W. HUTMACHER, M.Biomed.Eng., Ph.D., M.B.A.,[2] and E.H. LEE, M.D., F.R.C.S.[1]

ABSTRACT

The objectives of this study were (1) to develop a biphasic implant made of a bioresorbable polymeric scaffold in combination with TGF-β1-loaded fibrin glue for tissue-engineering applications, and (2) to determine whether the implant made of a polycaprolactone (PCL) scaffold and TGF-β1-loaded fibrin glue could recruit mesenchymal cells and induce the process of cartilage formation when implanted in ectopic sites. Twenty-four 6-month-old New Zealand White rabbits were used. Scaffolds loaded with various doses of TGF-β1 in fibrin glue were implanted subcutaneously, intramuscularly, and subperiosteally. The rabbits were killed and implants were removed at 2, 4, and 6 weeks postoperatively. The specimens were subjected to various staining techniques for histological analysis. Light microscopic examination of all specimens revealed that the entire pore space of the scaffolds was filled with various tissues in each group. The entire volume of the scaffolds in the groups loaded with TGF-β1 and implanted intramuscularly and subcutaneously was populated with mesenchymal cells surrounded with an abundant extracellular matrix and blood vessels. The scaffold loaded with TGF-β1 and implanted subperiosteally was found to be richly populated with chondrocytes at 2 and 4 weeks and immature bone formation was identified at 6 weeks. We conclude that scaffolds loaded with TGF-β1 can successfully recruit mesenchymal cells and that chondrogenesis occurred when this construct was implanted subperiosteally.

INTRODUCTION

ARTICULAR CARTILAGE is crucial to the normal function of synovial joints, because its presence enables the articulating bones to transmit high loads while maintaining contact stresses at an appreciably low level, and to move relatively onto each other with little friction. However, localized articular cartilage le-

[1]Department of Orthopedic Surgery, National University Hospital, National University of Singapore.
[2]Laboratory for Biomedical Engineering (LBME), Department of Mechanical Engineering National University of Singapore.
*This study was performed at the Department of Orthopedic Surgery, National University of Singapore, and presented at the 10th International Conference on Biomedical Engineering, Singapore, December 6–9, 2000.

sions have been found in 30 to 60% of acute and chronic knee injuries in humans and these occurred in a variety of injuries such as blunt trauma, fractures, and dislocations.[1] It is well established that injured articular cartilage has limited potential for healing on its own.[2]

In the last three decades clinical and basic scientific investigations have shown that implantation of artificial matrices, growth factors, perichondrium, and periosteum can stimulate the formation of cartilaginous tissue in osteochondral and chondral defects in synovial joints.[3] However, the results vary considerably among individuals, and the tissues that form after these treatments do not duplicate the composition, structure, and mechanical properties of normal articular cartilage.[3–5] In response to this, tissue engineering has emerged as a potential new therapy in which synthetic materials, seeded with appropriate cell populations, are grown *in vitro* and subsequently implanted in patients.[6–9] A number of research groups have shown that cartilage-like tissue can be grown in porous scaffolds made of collagen, collagen and hyaluronan, hydroxyapatite, or polyglycolic and polylactic acid.[10–15]

The current limitations of *in vitro* tissue engineering method are 2-fold: first, it requires an appropriate cell culture technique, which is technically demanding and has the potential risk of disease transmission due to cell culture supplements of bovine origin. Second, the tissues must be obtained from the patient, typically from a biopsy. This may be practical in laboratory animals, but might present problems in patients. *In vivo* tissue engineering has potential because it can be performed arthroscopically. This would allow surgeons to apply this treatment in outpatient clinics. Operative morbidity from the donor sites could be diminished significantly and the total duration of hospitalization greatly reduced. Maximum reconstructive cost efficiency could then be realized, with improved rehabilitation results and hence better quality of life.

Classic histologists postulated that cells existing in adult loose connective tissue retain the multipotentiality of embryonic mesenchymal cells. These cells were called undifferentiated mesenchymal cells. Such cells would give rise to differentiated cells that would be utilized for large-scale repair and formation of new tissue, such as new blood vessels or new or ectopic bone and cartilage and were isolated from periosteum, muscle, and granulation tissue.

Transforming growth factor β1 (TGF-β1) has been used to recruit mesenchymal stem cells in a great number of studies because of its potent chemotactic effect.[16–20] The objectives of the present study were as follows: (1) to develop a biphasic biodegradable implant to recruit mesenchymal cells *in vivo*, (2) to determine whether a PCL scaffold loaded with TGF-β1 in combination with fibrin glue can recruit mesenchymal cells and induce the process of cartilage formation when implanted in ectopic sites, and (3) to histologically assess the composition and morphology of the constructs 2, 4, and 6 weeks postoperatively.

MATERIALS AND METHODS

Study design

Twenty-four 6-month-old New Zealand White rabbits, weighing 2.5–3.0 kg, were used in this study. Implantation experiments were carried out in both hind limbs of each rabbit and at three anatomically distinct sites in each hind limb, giving a total of 48 limbs and a sample size of 144 implants ($n = 144$). A scaffold made of poly(caprolactone) (PCL), in the geometric form of a cylinder (5 mm diameter [Ø5] × 6 mm) was loaded with two different doses of TGF-β1 (Sigma, St. Louis, MO) in combination with fibrin glue (Immun AG, Vienna, Austria) and implanted subcutaneously, intramuscularly, and subperiosteally. As controls nonloaded PCL scaffolds were included in each group.

There were four groups at each anatomical site in this study (Table 1). In group 1 ($n = 36$), the scaffolds were empty; in group 2 ($n = 36$), the scaffolds were loaded only with fibrin glue; and in group 3 ($n = 36$) and group 4 ($n = 36$), the scaffolds were loaded with TGF-β1 (100 and 200 ng per scaffold, respectively) in fibrin glue. Each group was further divided into three subgroups ($n = 12$) according to the implantation sites.

Implant preparation

Polycaprolactone scaffolds were fabricated by fused deposition modeling (FDM) described in detail by Hutmacher et al.[4,21] Briefly, specimens were fabricated with filaments made of polycaprolactone (Sigma-

TABLE 1. EXPERIMENTAL GROUPS

	Implants			
Site	*Scaffold only*	*Scaffold + fibrin glue*	*Scaffold + fibrin glue + TGF-β1 (100 ng)*	*Scaffold + fibrin glue + TGF-β1 (200 ng)*
Subcutaneous (SC)	Group (SC1)	Group (SC2)	Group (SC3)	Group (SC4)
2-week period	4	4	4	4
4-week period	4	4	4	4
6-week period	4	4	4	4
Intramuscular (IM)	Group (IM1)	Group (IM2)	Group (IM3)	Group (IM4)
2-week period	4	4	4	4
4-week period	4	4	4	4
6-week period	4	4	4	4
Subperiosteal (SP)	Group (SP1)	Group (SP2)	Group (SP3)	Group (SP4)
2-week period	4	4	4	4
4-week period	4	4	4	4
6-week period	4	4	4	4

Aldrich, Milwaukee, WI) on an FDM 3D modeler rapid prototyping system from Stratasy (Eden Prairie, MN). Scaffolds of Ø5 × 6 mm with 65 ± 4% porosity and a laydown pattern of 0/60/120° were fabricated for the experiment. The pore morphology, measured on the basis of scanning electron microscopy (SEM) micrographs, fell within the range of 380 × 430 × 590 μm (Fig. 1). The fibrin glue was prepared from a TISSEEL kit (Immuno AG). Lyophilized TISSEEL was reconstituted with the aprotinin solution at 3000 KIU/mL, using a Fibrintherm (a combined warming and stirring device), and for preparing the thrombin solution the contents of the vial containing calcium chloride solution were transferred into the vial containing lyophilized thrombin 500 μL (quick solidification), swirled briefly to dissolve the lyophilized material, and then kept at 37°C until use. Lyophilized TGF-β1 (2 μg) was dissolved in 0.5 mL of thrombin solution to prepare TGF-β1 solution (2000 ng/500 μL). Sequential applications of 50 μL of TISSEEL solution and 50 μL of thrombin solution in group 2, 50 μL of TISSEEL solution and 25 μL of thrombin plus TGF-β1 solution in group 3, and 50 μL TISSEEL solution and 50 μL of thrombin plus TGF-β1 solution in group 4 were performed and loaded onto each scaffold to prepare them as implants. When we conducted the implant preparation, TISSEEL solution was injected first with a pipette and the solution was allowed to contact the pores of the scaffold, and then thrombin solution containing TGF-β1 was added. As the high thrombin concentration led to rapid solidification of fibrin glue, TGF-β1 was fixed into the implant. All implants were used within 2 h of preparation.

Surgical procedures for implantation and retrieval

All operations were performed with sterile technique under general anesthesia. Both sides of the lower extremity were approached through a longitudinal medial parapatellar incision over the anteromedial aspect of the distal femur and the proximal tibia. The scaffolds were implanted in three locations, subperiosteally after the periosteum of proximal tibia was incised and raised, intramuscularly in a quadriceps muscle pouch, and subcutaneously at the distal lateral aspect of the thigh. All implants were fixed to adjacent tissues with sutures to keep them in place. The rabbits were killed and the implanted specimens were removed at 2 weeks ($n = 4$, in each subgroup), four weeks ($n = 4$, in each subgroup), or 6 weeks ($n = 4$, in each subgroup) postoperatively. The specimens were fixed in 10% formalin immediately after removal. Subsequently, the specimens were embedded in paraffin, sectioned (5-mm thickness), and stained with hematoxylin and eosin, safranin O, toluidine blue, and Masson's trichrome for histological studies. The animal protocol was reviewed and approved by the National University of Singapore Animal Care Advisory Committee. Animals were housed and cared for at the Animal Holding Unit of the National University of Singapore.

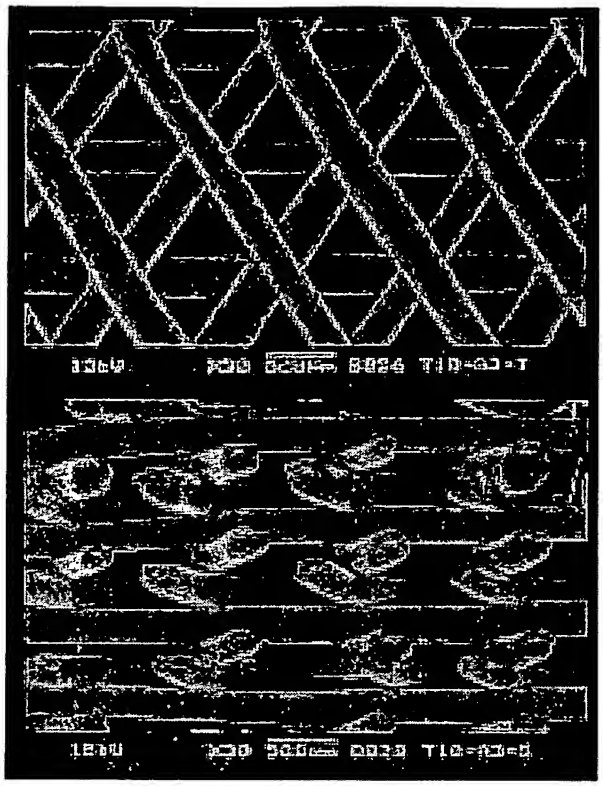

FIG. 1. Scanning electron micrograph of freeze-fractured surfaces of a PCL scaffold with a 0/60/120° lay-down pattern and a porosity of 61% (left top view and right side view). Side view of the scaffold architecture in the -z direction of the FDM build process, showing a completely interconnected honeycomb pattern with triangular pores.

Analysis

Specimen appearance was compared among the four study groups. Histological features and matrix production were assessed by hematoxylin and eosin staining. In addition, safranin O, toluidine blue, and Masson's trichrome were used. Safranin O was used to detect the presence of glycosaminoglycans, which are

FIG. 2. A subperiosteal specimen 4 weeks after implantation in group 3.

differentiated products of chondrocytes and stained red with safranin O stain, toluidine blue to confirm the presence of a well-developed cartilaginous matrix with proliferating cells in the samples, and Masson's trichrome to confirm the presence of collagen.

RESULTS

At 2, 4, and 6 weeks postoperatively, the implants were easily visualized at the sites of implantation (Fig. 2). Gross morphological examination revealed a thin fibrous capsule surrounding the subcutaneous implants. In contrast, no capsule was identified at the intramuscular and subperiosteal implant sites.

Light microscopic examination of all specimens revealed that in each group the entire scaffold architecture was filled with various tissues (Table 2). (Note that PCL scaffolds were dissolved in the process of histological preparation of the specimens, leaving a void within the tissue; Fig. 12). The pore space of the scaffolds in all the groups without TGF-β1 was loosely filled with collagen and sparsely distributed mes-

TABLE 2. HISTOLOGICAL CHARACTERISTICS OF THE GROUPS

Time point (weeks)	*Groups*	*Histological findings*
2	SC1, SC2, IM1, IM2, SP1, SP2	The pore space of scaffolds was loosely filled with collagen and sparsely distributed mesenchymal cells and macrophages
4	SC1, SC2, IM1, IM2, SP1, SP2	Similar histological findings as those at 2 weeks, except higher collagen content could be detected
6	SC1, SC2, IM1, IM2, SP1, SP2	Similar histological findings as those at 4 weeks, except higher collagen content could be detected
2	SC3, SC4, IM3, IM4	The pores of scaffold were populated with mesenchymal cells and blood vessels
4	SC3, SC4, IM3, IM4	More collagen and fewer blood vessels were seen
6	SC3, SC4, IM3, IM4	Newly formed tissue was characterized by fibroblasts surrounded by abundant collageneous extracellular matrix
2	SP3, SP4	Embryonic hyaline cartilage was the dominant feature with round and small chondrocytes in lacunae packed closely together with minor intervening homogeneously staining matrix
4	SP3, SP4	Hypertrophic cartilage was identified by its typical morphology of round cells embedded in extensive extracellular matrix
6	SP3, SP4	Immature bone characterized by failure to display an organized lamellated appearance and, on the basis of collagen fiber arrangement, designated as nonlamellar; relatively more cells per unit area than mature bone; randomly arranged cells

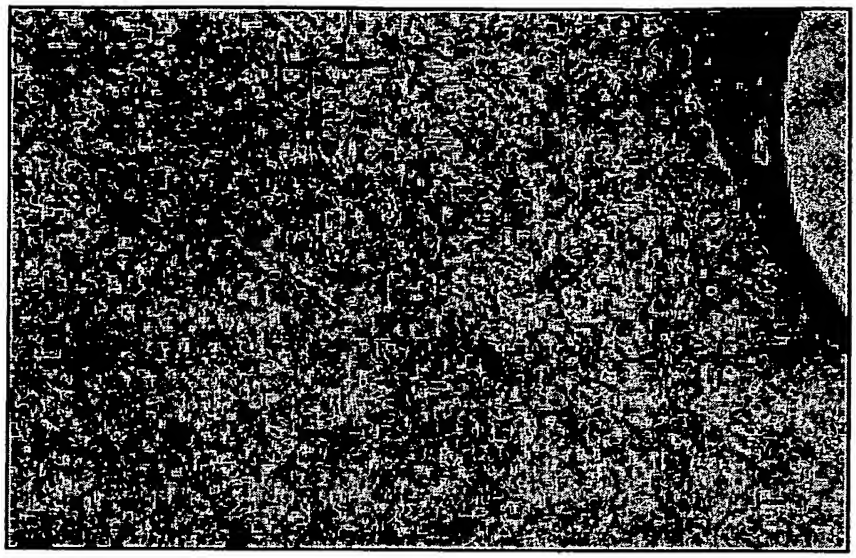

FIG. 3. Pore space loosely filled with mesenchymal cells and macrophages in the matrix of a PCL scaffold-only implant, 2 weeks after subcutaneous implantation. (Safranin O stain; original magnification, ×400.

enchymal cells and macrophages at 2 weeks (Fig. 3). Histological characteristics remained unchanged at 4 and 6 weeks except that higher collagen content could be detected (Figs. 4 and 5).

In comparison, the scaffolds that were implanted intramuscularly and subcutaneously in groups 3 and 4 were populated with mesenchymal cells and blood vessels at 2 weeks (Fig. 6). More collagen and fewer blood vessels were seen at 4 weeks (Fig. 7), and at 6 weeks the newly formed tissue was characterized by fibroblasts surrounded by an abundant collagenous extracellular matrix (Fig. 8). There was no new cartilage formation in these specimens.

In groups 3 and 4, the specimens implanted subperiosteally showed a nodular pattern in combination with hypercellular cartilage. Bone formation was identified 6 weeks after implantation. The mesenchymal cells, embryonic cartilage, hypertropic cartilage, and immature bone were intermingled partly or wholly in the pores and their distribution at different periods of time are as shown in Fig. 9. At 2 weeks the embryonic

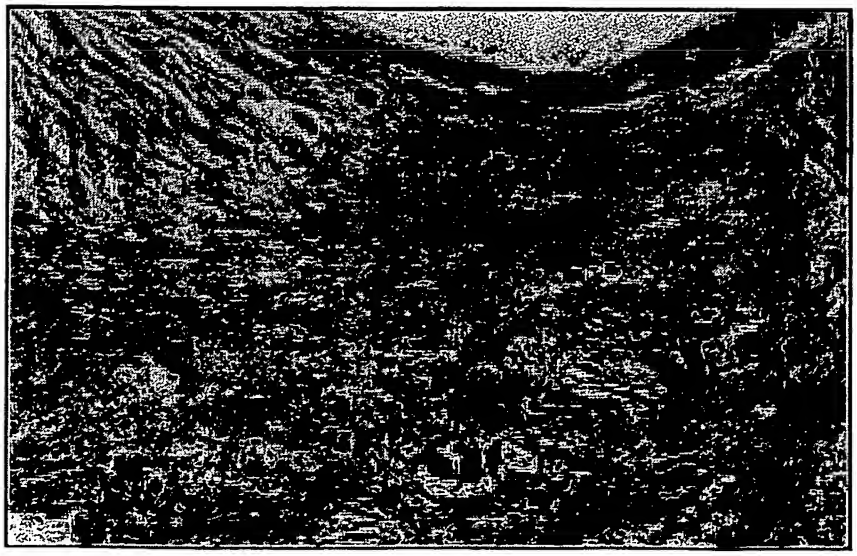

FIG. 4. Pore space loosely filled with mesenchymal cells and macrophages in the matrix of a PCL scaffold–fibrin glue implant, 4 weeks after subcutaneous implantation. (H&E; original magnification, ×400.)

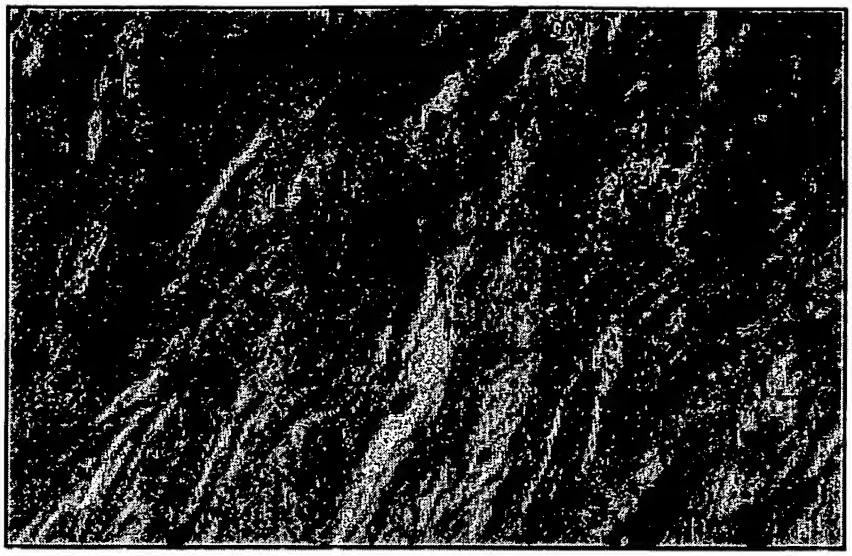

FIG. 5. A PCL scaffold–fibrin glue implant, 6 weeks after subcutaneous implantation. The section shows a high level of collagen content with sparsely distributed cells. (H&E; original magnification, ×400.)

hyaline cartilage was the dominant feature, with round and small chondrocytes in lacunae packed closely together with a minor, intervening homogeneously staining matrix (Fig. 10). Hypertrophic cartilage was identified at 4 weeks by its typical appearance consisting of round cells embedded in an extensive extracelluar matrix demonstrated with toluidine blue staining, collagen visualized with Masson's trichrome staining, and glycosaminoglycan visualized with safranin O staining (Fig. 11). At 6 weeks, immature bone was seen. Immature bone does not display an organized lamellated appearance and, on the basis of collagen fiber arrangement, such bone is designated as nonlamellar. Immature bone contains relatively more cells per unit area than mature bone. The cells in immature bone tend to be randomly arranged (Figs. 12 and 13).

Qualitatively, there was no difference in the morphological characteristics of the specimens between group 3 and group 4 and between group 1 and group 2 at all the time points studied after implantation.

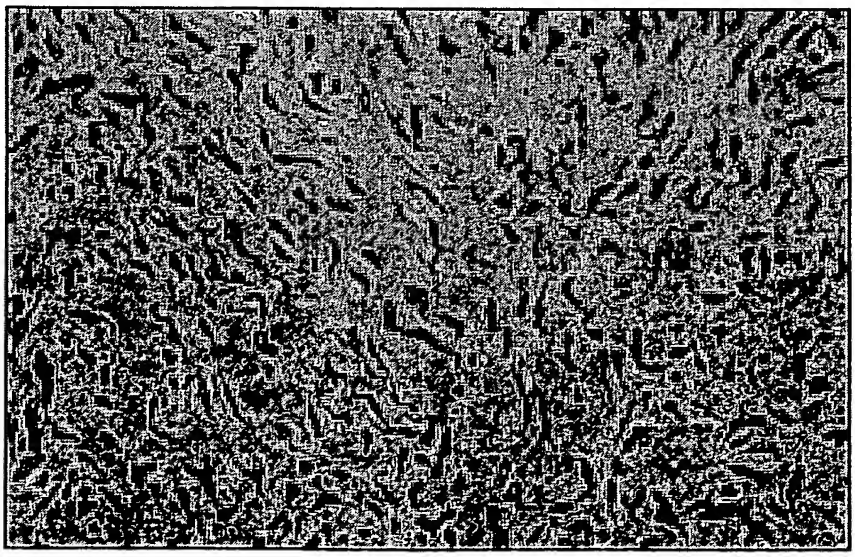

FIG. 6. PCL scaffold–fibrin glue–TGF-β1 (100 ng), 2 weeks after subcutaneous implantation. Proliferation of mesenchymal cells is apparent, but there is no marked evidence of collagen. (Masson's trichrome stain; original magnification, ×400.)

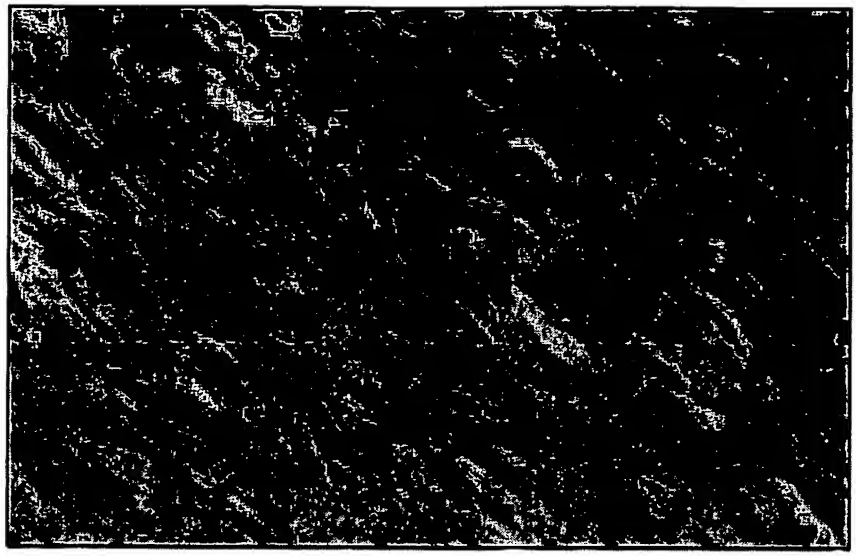

FIG. 7. PCL scaffold–fibrin glue–TGF-β1 (200 ng), 4 weeks after intramuscular implantation. Proliferation of mesenchymal cells with ingrowths of blood vessels is seen. (H&E; original magnification, ×400.)

DISCUSSION

The regeneration of injured or excised tissues requires at the site of injury the presence of progenitor cells with the ability to proliferate and differentiate into the appropriate phenotypes to restore the damaged or missing tissue.[22] When these progenitor cells are absent, scarce, or exposed to an inappropriate microenvironment, reparative scar tissue is formed at the site of injury. This scar tissue reestablishes tissue continuity but it is a poorly organized structure lacking the functional characteristics of the original tissue.[23,24] There are two approaches to obtaining sufficient numbers of reparative cells at the site of injury: cytokines and growth factors can be introduced as recruitment agents to attract the reparative cells to the site,[16,25] or in a more direct approach, cells that induce tissue repair can be directly introduced into the damaged area.[26,27]

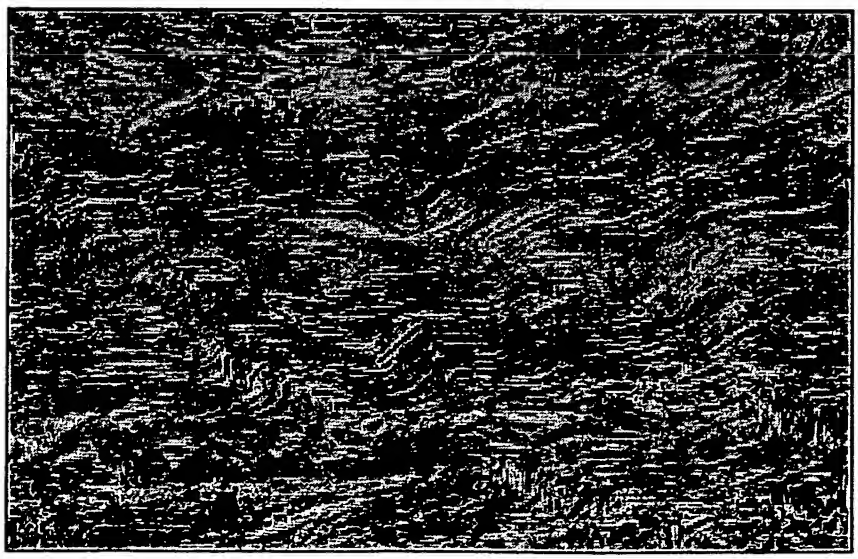

FIG. 8. PCL scaffold–fibrin glue–TGF-β1 (100 ng), 6 weeks after subcutaneous implantation. Fibroblasts with a high level of collagen are evident. (Toluidine Blue stain; original magnification, ×400.)

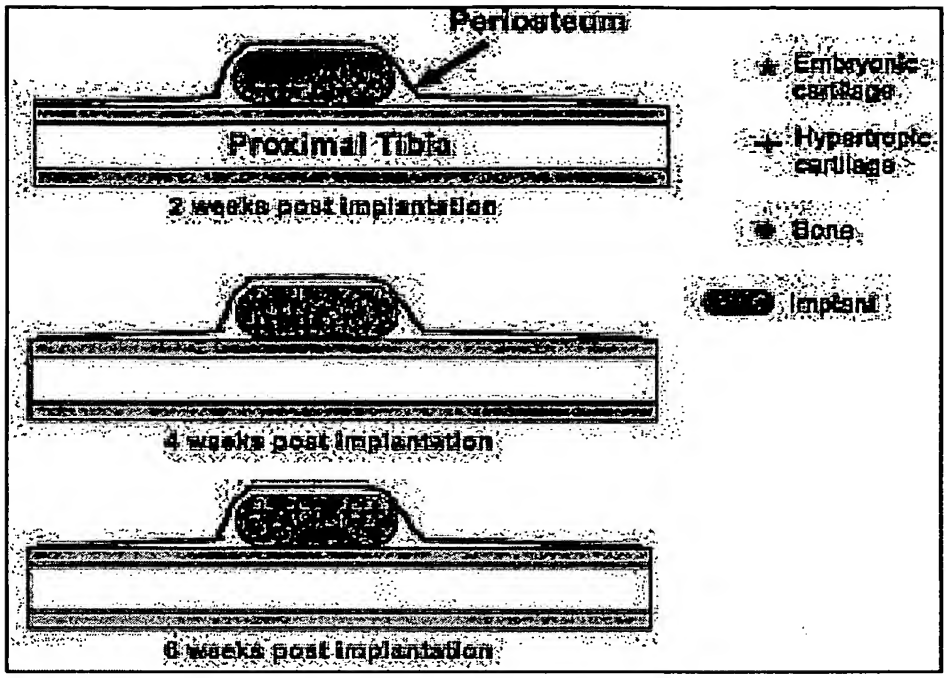

FIG. 9. Distribution of embryonic cartilage, hypertropic cartilage, and immature bone at different time points.

Cartilage regeneration is a challenging task because articular cartilage is walled off from the subchondral bone marrow by calcified tissue, which allows no access to the macrophages, endothelial cells, and mesenchymal cells that reside therein.[28–31] Shapiro et al. confirmed in their study that the repair of full-thickness defects of articular cartilage was mediated wholly by the proliferation and differentiation of mesenchymal cells of the bone marrow.[32]

A great number of surgical treatment strategies have been applied, with varying success in animal stud-

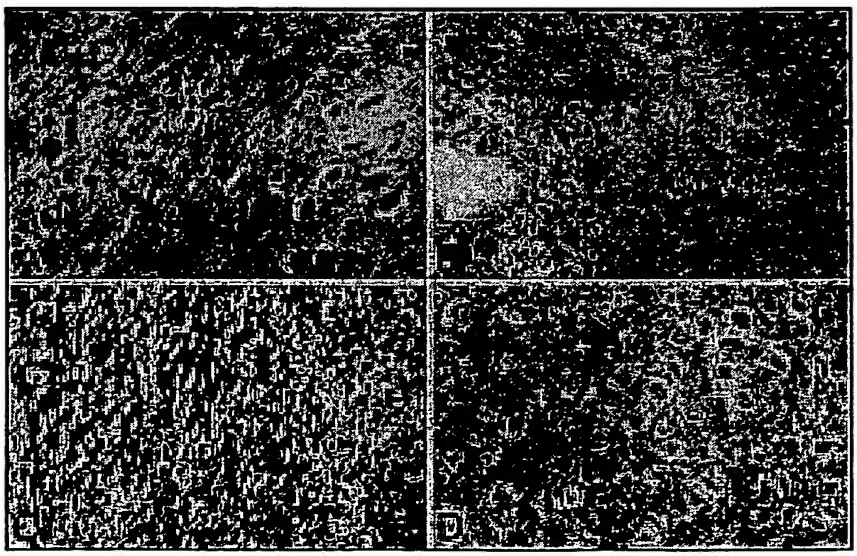

FIG. 10. PCL scaffold–fibrin glue–TGF-β1 (200 ng), 2 weeks after subperiosteal implantation. Mesenchymal cells differentiated into chondrocytes are evident. (**A**) Embryonic cartilage. (H&E; original magnification, ×400.) (**B**) Low glycoaminoglycan content. (Safranin O stain; original magnification, ×400.) (**C**) Underdeveloped cartilaginous matrix. (Toluidine blue stain; original magnification, ×400.) (**D**) Low collagen content. (Masson's trichrome stain; original magnification, ×400.)

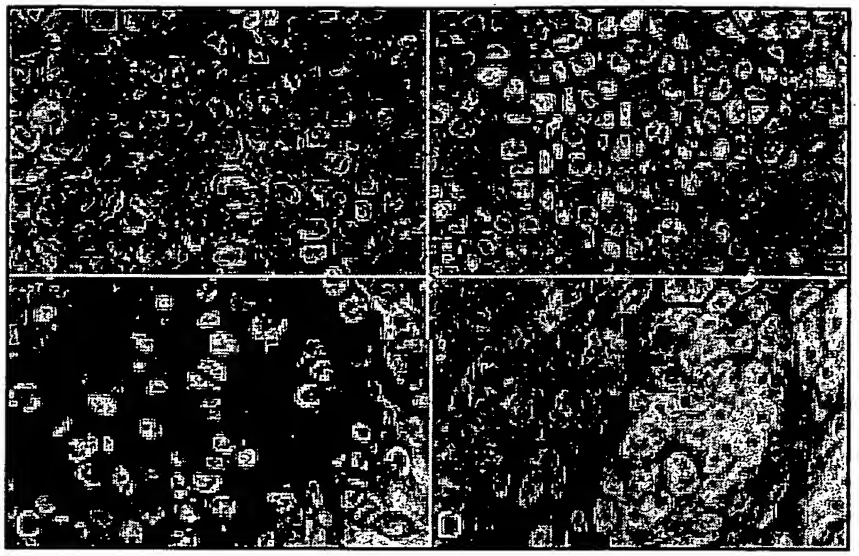

FIG. 11. PCL scaffold–fibrin glue–TGF-β1 (200 ng), 4 weeks after subperiosteal implantation. Hyaline cartilage is formed. (**A**) Hypertrophic chondrocytes. (H&E; original magnification, ×400.) (**B**) Presence of glycoaminoglycan. (Safranin O stain; original magnification, ×400.) (**C**) Well-developed cartilaginous matrix. (Toluidine blue stain; original magnification, ×400.) (**D**) Presence of collagen. (Masson's trichrome stain; original magnification, ×400.)

ies and clinical trials, to repair degenerated or damaged articular cartilage and subchondral bone.[33–38] Tissue engineering has emerged as a potentially new therapy in which synthetic materials, seeded with appropriate cell populations, are grown *in vitro* and subsequently implanted in patients. Investigators have found that cartilage can be tissue engineered into porous scaffolds made of collagen, collagen and hyaluronan, hydroxyapatite, or polyglycolic acid and polylactic acid.[13–15]

The purpose of the current study was to determine whether mesenchymal cells could be induced to proliferate and completely fill the pore space of a scaffold *in vivo* to make a graft similar to those created by *in vitro* tissue-engineering methods.

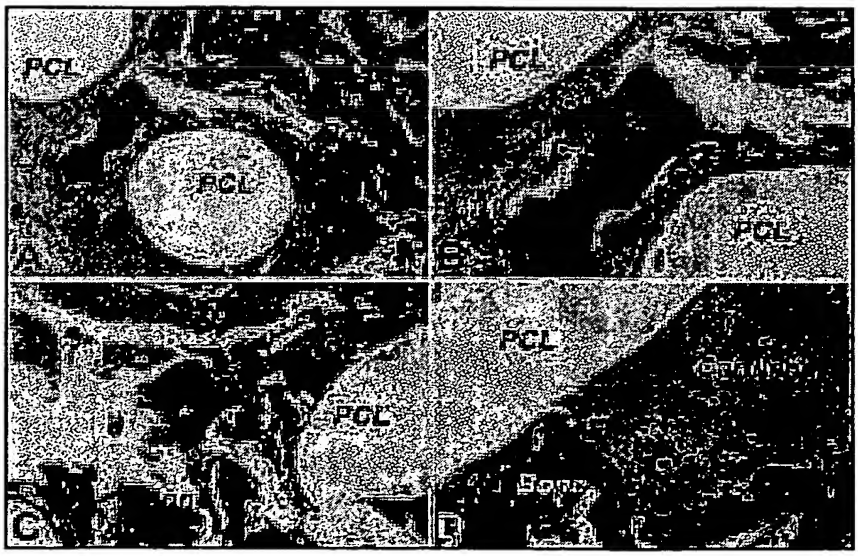

FIG. 12. PCL scaffold–fibrin glue–TGF-β1 (100 ng), 6 weeks after subperiosteal implantation. Immature bone is seen in the pore space. (**A–D**) H&E. Original magnification: (**A**) ×100; (**B,C**) ×200; (**D**) ×400. The PCL scaffold was dissolved in the process of histological preparation and voids were left.

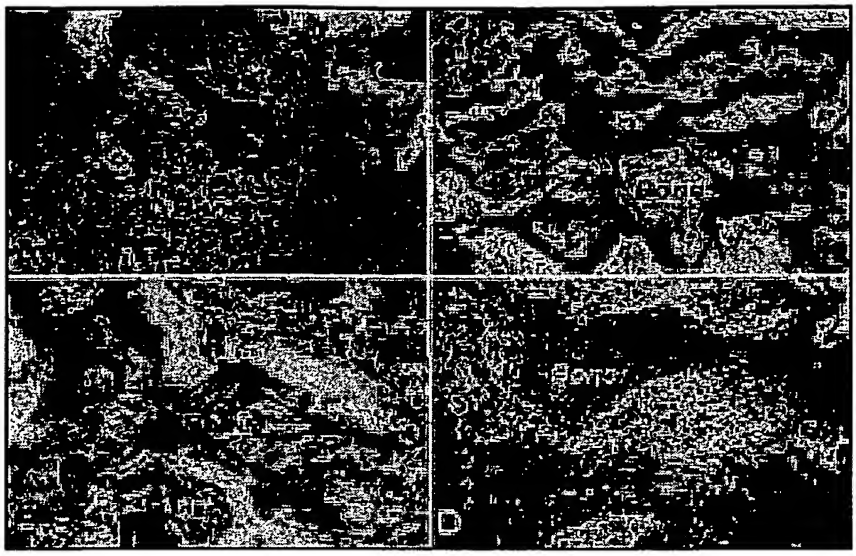

FIG. 13. PCL scaffold–fibrin glue–TGF-β1 (200 ng), 6 weeks after subperiosteal implantation. Immature bone is evident. Staining: **(A)** H&E; **(B)** safranin O; **(C)** Masson's trichrome; **(D)** toluidine blue. Original magnification: **(A–D)** ×400.

Traditionally, TGF-β1 has been regarded as a cartilage-inducing factor as well as a bone-inducing factor.[16–20] However, in our study cartilage did not form in the pore space of a scaffold loaded with TGF-β1 and implanted intramuscularly or subcutaneously, even after 6 weeks. Instead, fibrous tissue consisting of collagen fibrils occupied the pore space. One of the reasons for this may be the lack of other elements in the biochemical and biomechanical environment; it has been shown that mesenchymal cells differentiate into chondrocytes and cartilage when subjected to compression and low oxygen tension. Another reason may be the sources of mesenchymal cells.

Joyce et al.[39] injected TGF-β1 or TGF-β2 beneath the femoral periosteum in a rat model. The result was that periosteal cells differentiated into chondrocytes, proliferated to create a mass of subperiosteal cartilage, and subsequently underwent orderly endochondral ossification. These data showed that mesenchymal precursor cells located in the periosteum might be stimulated by TGF-β to proliferate and differentiate. In our study this process occurred in biphasic implants loaded with TGF-β1 and implanted subperiosteally.

Qualitative analysis revealed that there was no significant difference in the histological appearance of implants loaded with TGF-β1 at 100 and 200 ng/scaffold. The doses and concentrations of TGF-β1 used in different studies were quite variable,[16,17,40,41] and its effect on tissues and cells is influenced by multiple factors such as carrier properties, different recipient sites, and so on. We believe that doses of 100–200 ng/scaffold could create effective concentrations *in situ* to recruit mesenchymal cells; of course, further studies must be performed to evaluate in detail the dose dependency of the response.

The critical properties of a tissue-engineered construct to be used in orthopedic surgery include degree of strength retention over time, and structural and mechanical equivalence to cartilage. The PCL scaffold is designed to maintain an interconnected pore network for at least 6 months[4,21] and in this way, the neocartilage would have sufficient time to mature without biomechanical overload. However, the host tissue reaction up to the complete resorption of the scaffold matrix must be studied from a biocompatibility point of view.

The concept of a two-phase scaffold (collagen matrix and copolymer) containing growth factors or chondrocytes for the healing of articular defects has been investigated. The objective is to separately influence the restoration of the subchondral bone and the cartilage.[42,43] Athanasiou et al. studied the potential benefit of combining local delivery of TGF-β1 with implantation of a two-phase biodegradable scaffold, with a stiffer phase in the region of the subchondral bone and a softer phase for interfacing with the cartilage.[42] In our study, a PCL scaffold loaded with fibrin glue offers another form of biphasic implant. The PCL scaffold does not biodegrade rapidly,[4,21] and therefore the structural geometry of the material could last for

months, whereas the fibrin glue is an organic material derived from human plasma. A previous study with mice suggested that fibrin had a remarkably synergistic effect on bone morphogenic protein (BMP) activity, inasmuch as the composite produced significantly more new bone yield than did BMP alone. It was shown that fibrin enhanced cell proliferation, which would increase the cell population of undifferentiated mesenchymal cells or prechondroblasts preceding new bone formation.[44] This effect of fibrin alone on cell proliferation was not evident in this present study. In comparing groups 1 and 2, there was no marked increase in cells in scaffolds loaded only with fibrin glue. As such, fibrin glue may act to stabilize TGF-β1 locally, improve contact between TGF-β1 and the surrounding cells, and control the release of TGF-β1. This may be attributed to the synergistic effect of fibrin on TGF-β1. Clinically, fibrin glue is relatively nonantigenic and should be a good biodegradable distributor–carrier for TGF-β1.

Our initial study objective was to determine whether the loaded biphasic implant could recruit mesenchymal cells and induce the process of cartilage formation when implanted in ectopic sites; therefore the analysis methods used were mainly to identify the characteristics of cartilage formation. Further studies are required to examine the effects of longer term implantation of this implant on bone formation and to apply more analysis methods to identify bone formation and maturation.

The results from this study demonstrated that implants made of a PCL scaffold in combination with TGF-β1-loaded fibrin glue and removed from subperiosteum at different time intervals could potentially be used as cartilage or bone grafts. Future studies will be undertaken to evaluate the feasibility of transplanting these *in vivo* tissue-engineered grafts at the optimal period of time into cartilage defects and to compare their efficacy with *in vitro*-engineered scaffold–chondrocyte or mesenchymal stem cell constructs.

ACKNOWLEDGMENTS

The authors thank Mr. S.C. Yong, Miss J. Chan, Mr. B.K. Tan, and Miss S.W. Chong for technical assistance.

REFERENCES

1. Clancy, W.G., Shelbourne, K.D., Zoellner, G.B., Keene, J.S., Reider, B., and Rosenberg, T. Treatment of knee joint instability secondary to rupture of the posterior cruciate ligament. J. Bone Joint Surg. **65,** 310, 1983.
2. Hunter, W. On the structure and diseases of articulating cartilage. Phil. Trans. **B9,** 267, 1943.
3. Buckwalter, J.A., and Mankin, H.J. Articular cartilage. II. Degeneration and osteoarthrosis, repair, regeneration, and transplantation. J. Bone Joint Surg. **79,** 612, 1997.
4. Hutmacher, D.W. Polymeric scaffolds in tissue engineering bone and cartilage. Biomaterials **21,** 2529, 2000.
5. Ohgushi, H., and Caplan, A.I. Stem cell technology and bioceramics: from cell to gene engineering. J. Biomed. Mater. Res. **48,** 913, 1999.
6. Bruder, S.P., Fink, D.J., and Caplan, A.I. Mesenchymal stem cells in bone development, bone repair, and skeletal regeneration therapy. J. Cell Biochem. **56,** 283, 1994.
7. Fitzsimmons, J.S., and O'Driscoll, S.W. Technical experience is important in harvesting periosteum for chondrogenesis. Trans. Orthop. Res. Soc. **23,** 914, 1998.
8. Gallay, S.H., Miura, Y., Commisso, C.N., Fitzsimmons, J.S., O'Driscoll, S.W. Relationship of donor site to chondrogenic potential of periosteum in vitro. J. Orthop. Res. **12,** 515, 1994.
9. Miura, Y., Fitzsimmons, J.S., Commisso, C.N., Gallay, S.H., and O'Driscoll, S.W. Enhancement of periosteal chondrogenesis in vitro: dose-response for transforming growth factor-β-1 (TGF-β1). Clin. Orthop. **301,** 271, 1994.
10. Chu, C.R., Coutts, R.D., Yoshioka, M., Harwood, F.L., Monosov, A.Z., and Amiel, D. Articular cartilage repair using allogeneic perichondrocyte-seeded biodegradable porous polylactic acid (PLA): a tissue-engineering study. J. Biomed. Mater. Res. **29,** 1147, 1995.
11. Grande, D.A., Halberstadt, C., Naughton, G., Schwartz, R., and Manji, R. Evaluation of matrix scaffolds for tissue engineering of articular cartilage grafts. J. Biomater. Mater. Res. **34,** 211, 1997.
12. Puelacher, W.C., Kim, S.W., Vacanti, J.P., Schloo, B., Mooney, D., abd Vacanti, C.A. Tissue-engineered growth of cartilage: the effect of varying the concentration of chondrocytes seeded onto synthetic polymer matrices. Int. J. Oral Maxillofac. Surg. **23,** 49, 1994.

13. Brittberg, M., Lindahl, A., Nilson, A., Ohlsson, C., Isaksson, O., and Peterson, L. Treatment of deep cartilage defects in the knee with autologous chondrocyte transplantation. N. Engl. J. Med. **331,** 889, 1994.
14. Freed, L.E., Marquis, J.C., Nohria, A., Emmanual, J., Mikos, A., and Langer R. Neocartilage formation in vitro and in vivo using cells cultured on synthetic biodegradable polymers. J. Biomed. Mater. Res. **27,** 11, 1993.
15. Noguchi, T., Oka, M., Fujino, M., Neo, M., and Yamamuro, T. Repair of osteochondral defects with grafts of cultured chondrocytes. Comparison of allografts and isografts. Clin. Orthop. **302,** 251, 1994.
16. Hunziker, E.B., and Rosenberg, L.C. Repair of partial-thickness defects in articular cartilage: cell recruitment from the synovial membrane. J. Bone Joint Surg. **78,** 721, 1996.
17. Ripamonti, U., Duneas, N., Van Den Heever, B., Bosch, C., and Crooks, J. Recombinant transforming growth factor-β-1 induces endochondral bone in the baboon and synergizes with recombinant osteogenic protein-1 (bone morphogenetic protein-7) to initiate rapid bone formation. J. Bone Miner. Res. **12,** 1584, 1997.
18. Centrella, M., Horowitz, M.C., Wozney, J.M., and Mccarthy, T.L. Transforming growth factor-β gene family members and bone. Endocr. Rev. **15,** 27, 1994.
19. Massague, J., Cheifetz, S., Laiho, M., Ralph D.A., Weis, F.M., and Zentella, A. Transforming growth factor-β. Cancer Surv. **12,** 81, 1992.
20. Seyedin, S.M., Thomas, T.C., Thompson, A.Y., Rosen, D.M., and Piez, K.A. Purification and characterization of two cartilage-inducing factors from bovine demineralized bone. Proc. Natl. Acad. Sci. U.S.A. **82,** 2267, 1985.
21. Hutmacher, D.W., Zein, I., Teoh, S.H., Ng, K.W., Schantz, J.T., and Leady, J.C. Design and fabrication of a 3D scaffold for tissue engineering bone. In: Agrawal, C.M., Parr, J.E., and Lin, S.T., eds. Synthetic Bioabsorbable Polymers for Implants. West Conshohocken, PA: American Society for Testing and Materials, 2000, pp. 152–167.
22. Witte, M.B., and Barbul, A. General principles of wound healing. Surg. Clin. North Am. **77,** 509, 1997.
23. Mutsaers, S.E., Bishop, J.E., McGrouther, G., and Laurent, G.J. Mechanisms of tissue repair: from wound healing to fibrosis. Int. J. Biochem. Cell Biol. **29,** 5, 1997.
24. Weber, K.T. Metabolic response of extracellular matrix in tissue repair. Ann. Med. **29,** 333, 1997.
25. Sellers, R.S., Peluso, D., and Morris, E.A. The effect of human recombinant bone morphogenetic protein-2 (rhBMP-2) on the healing of full-thickness defects of articular cartilage. J. Bone Joint Surg. **79,** 1452, 1997.
26. Wakitani, S., Goto, T., Pineda, S.J., Young, R.G., Mansour, J.M., Caplan, A.I., and Goldberg, V.M. Mesenchymal cell-based repair of large, full-thickness defects of articular cartilage. J. Bone Joint Surg. **76,** 579, 1994.
27. Vacanti, C.A., Kim, W., Schloo, B., Upton, J., and Vacanti, J.P. Joint resurfacing with cartilage grown in situ from cell-polymer structures. Am. J. Sports Med. **22,** 485, 1994.
28. Bennett, G.A., Bauer, W., and Maddock, S.J. A study of the repair of articular cartilage and the reaction of normal joints of adult dogs to surgically created defects of articular cartilage, "joint mice" and patellar displacement. Am. J. Pathol. **8,** 499, 1932.
29. DePalma, A.F., McKeever, C.D., and Subin, D.K. Process of repair of articular cartilage demonstrated by histology and autoradiography with tritiated thymidine. Clin. Orthop. **48,** 229, 1966.
30. Harada, K., Oida, S., and Sasaki, S. Chondrogenesis and osteogenesis of bone marrow-derived cells by bone-inductive factor. Bone **9,** 177, 1988.
31. Mankin, H.J. The reaction of articular cartilage to injury and osteoarthritis (first of two parts). N. Engl. J. Med. **291,** 1285, 1974.
32. Shapiro, F., Koide, S., and Glimcher, M.J. Cell origin and differentiation in the repair of full-thickness defects of articular cartilage. J. Bone Joint Surg. **75,** 532, 1993.
33. Magnuson, B.P. Joint debridement: surgical treatment of degenerative arthritis. Surg. Gynecol. Obstet. **73,** 1, 1941.
34. Insall, N.J. Intra-articular surgery for degenerative arthritis of knee. J. Bone Joint Surg. **48,** 211, 1967.
35. Mitchell, N., and Shepard, N. The resurfacing of adult rabbit articular cartilage by multiple perforations throughout the subchondral bone. J. Bone Joint Surg. **58,** 230, 1976.
36. Henche, H.R. Patellar shaving (indications, technique, results) in the knee. In: Hastings, D., ed. Ligament and Articular Cartilage Injury. New York: Springer-Verlag, 1967, pp. 157–164.
37. Meachim, G., and Roberts, C. Repair of the joint surface from subarticular tissue in the rabbit knee. J. Anat. **109,** 317, 1971.
38. Altman, R.D., Kates, J., Chun, L.E., Dean, D.D., and Eyre, D. Preliminary observations of chondral abrasion in a canine model. Ann. Rheumat. Dis. **51,** 1056, 1992.
39. Joyce, M.E., Roberts, A.B., Sporn, M.B., and Bolander, M.E. Transforming growth factor-β and the initiation of chondrogenesis and osteogenesis in the rat femur. J. Cell Biol. **110,** 2195, 1990.
40. Nicoll, S.B., Radin, S., Santos, E.M., Tuan, R.S., and Ducheyne, P. In vitro release kinetics of biologically active transforming growth factor-β-1 from a novel porous glass carrier. Biomaterials **18,** 853, 1997.
41. Tielinen, L., Manninen, M., Puolakkainen, P., Pihlajamaki, H., Pohjonen, T., Rautavuori, J., et al. Polylactide pin with transforming growth factor-β-1 in delayed osteotomy fixation. Clin. Orthop. **355,** 312, 1998.

42. Athanasiou, K.A., Korvick, D., and Schenck, R. Biodegradable implants for the treatment of osteochondral defects in a goat model. Tissue Eng. **3,** 363, 1995.
43. Frenkel, S.R., Toolan, R.C., Menche, D., Pitman, M.I., and Pachience, J.M. Chondrocyte transplantation using a collagen bilayer matrix for cartilage repair. J. Bone Joint Surg. **79,** 831, 1997.
44. Kawamura, M., and Urist, M.R. Human fibrin is a physiologic delivery system for bone morphogenetic protein. Clin. Orthop. **235,** 302, 1988.

Address reprint requests to:
E.H. Lee, M.D., F.R.C.S.
Department of Orthopedic Surgery
National University of Singapore
10 Kent Ridge Crescent
Singapore 119260
E-mail: meddean@nus.ed.sg

This article has been cited by:

1. Isabelle Catelas , Joseph F. Dwyer , Sam Helgerson . 2008. Controlled Release of Bioactive Transforming Growth Factor Beta-1 from Fibrin Gels In Vitro. *Tissue Engineering Part C: Methods* **14**:2, 119-128. [Abstract] [PDF] [PDF Plus]
2. James Melrose, Christine Chuang, John Whitelock. 2008. Tissue engineering of cartilages using biomatrices. *Journal of Chemical Technology & Biotechnology* **83**:4, 444-463. [CrossRef]
3. Isabelle Catelas , Joseph F Dwyer , Sam Helgerson . Controlled Release of Bioactive Transforming Growth Factor Beta-1 from Fibrin Gels In Vitro. *Tissue Engineering Part C: Methods*, ahead of print. [Abstract] [PDF] [PDF Plus]
4. Marc M. Thibault , Caroline D. Hoemann , Michael D. Buschmann . 2007. Fibronectin, Vitronectin, and Collagen I Induce Chemotaxis and Haptotaxis of Human and Rabbit Mesenchymal Stem Cells in a Standardized Transmembrane Assay. *Stem Cells and Development* **16**:3, 489-502. [Abstract] [PDF] [PDF Plus]
5. Rachel Rivkin , Alon Ben-Ari , Ibrahim Kassis , Lior Zangi , Elena Gaberman , Lilia Levdansky , Gerard Marx , Raphael Gorodetsky . 2007. High-Yield Isolation, Expansion, and Differentiation of Murine Bone Marrow-Derived Mesenchymal Stem Cells Using Fibrin Microbeads (FMB). *Cloning and Stem Cells* **9**:2, 157-175. [Abstract] [PDF] [PDF Plus]
6. C. L. Bliss, J. A. Szivek, B. C. Tellis, D. S. Margolis, A. B. Schnepp, J. T. Ruth. 2007. Sensate scaffolds can reliably detect joint loading. *Journal of Biomedical Materials Research Part B Applied Biomaterials* **81b**:1, 30. [CrossRef]
7. Vincenzo Guarino, Filippo Causa, Luigi Ambrosio. 2007. Bioactive scaffolds for bone and ligament tissue. *Expert Review of Medical Devices* **4**:3, 405. [CrossRef]
8. Seung-Jae Lee, Hyun-Wook Kang, Tae-yeun Kang, Byung Kim, Geunbae Lim, Jong-Won Rhie, Dong-Woo Cho. 2007. Development of a scaffold fabrication system using an axiomatic approach. *Journal of Micromechanics and Microengineering* **17**:1, 147. [CrossRef]
9. Fernando G. Torres, Aldo R. Boccaccini, Omar P. Troncoso. 2007. Microwave processing of starch-based porous structures for tissue engineering scaffolds. *Journal of Applied Polymer Science* **103**:2, 1332. [CrossRef]
10. Seok-Jung Kim, Jae-Deog Jang, Seung-Koo Lee. 2007. Treatment of long tubular bone defect of rabbit using autologous cultured osteoblasts mixed with fibrin. *Cytotechnology* **54**:2, 115. [CrossRef]
11. P. Behrens, P.C. Kreuz. 2007. Knochenmarkstimulierende Techniken zur Knorpeldefektbehandlung: gestern, heute und morgen. *Trauma und Berufskrankheit* **9**:4, 242. [CrossRef]
12. Chris P. Geffre, Cody L. Bliss, John A. Szivek, Donald W. DeYoung, John T. Ruth, David S. Margolis. 2007. Sensate scaffolds coupled to telemetry can monitorin vivo loading from within a joint over extended periods of time. *Journal of Biomedical Materials Research Part B Applied Biomaterials* . [CrossRef]
13. Xinxin Shao , James C.H. Goh , Dietmar W. Hutmacher , Eng Hin Lee , Ge Zigang . 2006. Repair of Large Articular Osteochondral Defects Using Hybrid Scaffolds and Bone Marrow-Derived Mesenchymal Stem Cells in a Rabbit Model. *Tissue Engineering* **12**:6, 1539-1551. [Abstract] [PDF] [PDF Plus]
14. Dr. J. Elisseeff , A. Ferran , S. Hwang , S. Varghese , Z. Zhang . 2006. The Role of Biomaterials in Stem Cell Differentiation: Applications in the Musculoskeletal System. *Stem Cells and Development* **15**:3, 295-303. [Abstract] [PDF] [PDF Plus]

15. Stephen J. Curran , Rui Chen , Judith M. Curran , John A. Hunt . 2005. Expansion of Human Chondrocytes in an Intermittent Stirred Flow Bioreactor, Using Modified Biodegradable Microspheres. *Tissue Engineering* **11**:9-10, 1312-1322. [Citation] [PDF] [PDF Plus]

16. Pieter J. Emans , Don A.M. Surtel , Eric J.J. Frings , Sjoerd K. Bulstra , Roel Kuijer . 2005. In Vivo Generation of Cartilage from Periosteum. *Tissue Engineering* **11**:3-4, 369-377. [Abstract] [PDF] [PDF Plus]

17. P. Behrens. 2005. Matrixgekoppelte Mikrofrakturierung. *Arthroskopie* **18**:3, 193. [CrossRef]

18. J Elisseeff, C Puleo, F Yang, B Sharma. 2005. Advances in skeletal tissue engineering with hydrogels. *Orthodontics and Craniofacial Research* **8**:3, 150. [CrossRef]

19. A.L. Darling, Wei Sun. 2005. Free-form fabrication and micro-CT characterization of poly-ε -caprolactone tissue scaffolds [EMBS 2003 Student Paper Finalists]. *IEEE Engineering in Medicine and Biology Magazine* **24**:1, 78. [CrossRef]

20. Jeffrey M. Karp, Feryal Sarraf, Molly S. Shoichet, John E. Davies. 2004. Fibrin-filled scaffolds for bone-tissue engineering: Anin vivo study. *Journal of Biomedical Materials Research* **71a**:1, 162. [CrossRef]

21. A. L. Darling, W. Sun. 2004. 3D microtomographic characterization of precision extruded poly-ε-caprolactone scaffolds. *Journal of Biomedical Materials Research* **70b**:2, 311. [CrossRef]

22. Dietmar W. Hutmacher , Michael Sittinger . 2003. Periosteal Cells in Bone Tissue Engineering. *Tissue Engineering* **9**:supplement 1, 45-64. [Abstract] [PDF] [PDF Plus]

23. Jeffrey M. Karp, Kathy Rzeszutek, Molly S. Shoichet, John E. Davies. 2003. Fabrication of Precise Cylindrical Three-Dimensional Tissue Engineering Scaffolds for In Vitro and In Vivo Bone Engineering Applications. *Journal of Craniofacial Surgery* **14**:3, 317. [CrossRef]

EXHIBIT 7

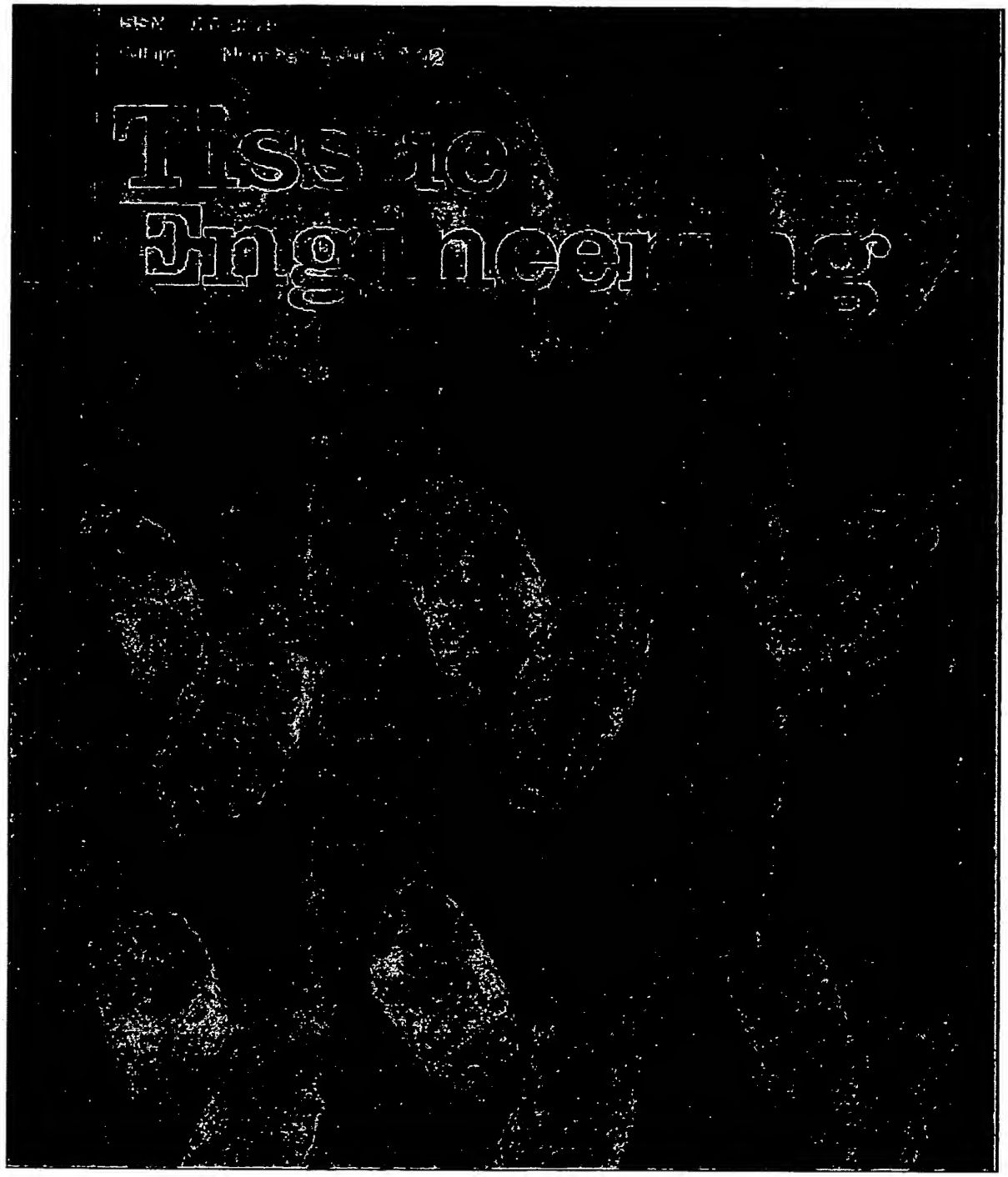

EXHIBIT 8